Shear Strengthening of Prestressed Concrete Beams with Ultra-High Performance Fibre Reinforced Concrete

Numerical Analysis by ATENA Model

By

Nikhil Jayananda

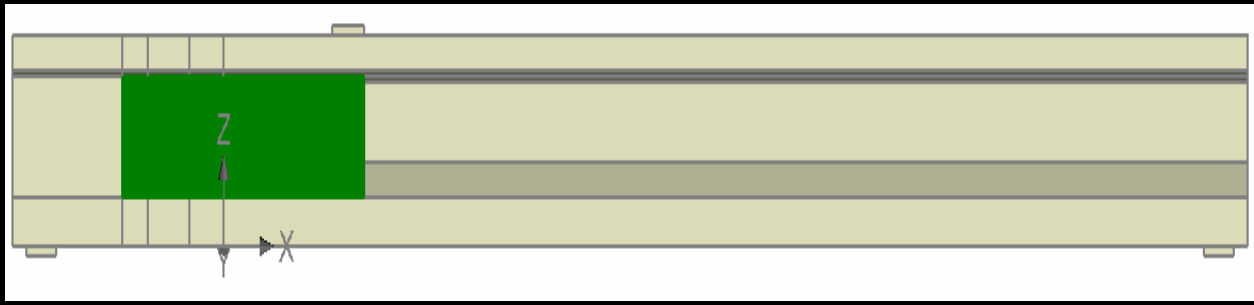

TU Delft

Shear Strengthening of Prestressed Concrete Beams with Ultra High-Performance Fiber Reinforced Composite (UHPFRC) – Numerical analysis by ATENA model.

by
Nikhil Jayananda

Supervised by
Dr.ir. M. Luković

Assessment Committee
Prof.dr.ir D.A. Hordijk
Dr.ir. S Grünewald
Dr.ir. M Roosen
Prof.dr.ir. E Schlangen

A thesis submitted in partial fulfillment for the
degree of Master of Science.

Faculty of Civil Engineering and Geosciences (CEG). Delft University of Technology.

August 2018

Abstract

The growing need for strengthening of concrete structures to improve their structural performance challenges structural engineers to come up with strengthening techniques that is most suitable and effective for a structural system in its deteriorated state. Although there are quite a few techniques in practice for strengthening of concrete structures -reinforced or prestressed, various factors limit their efficiency and performance. Use of novel concrete-based materials such as Ultra High Performance Fibre Reinforced Composite (UHPFRC) can lead to an effective strengthening system due to the exceptional material properties of UHPFRC. In particular, the strain hardening behavior of UHPFRC in tension and its excellent durability. Out of the two main mechanisms of failure in concrete elements namely flexure failure and shear failure, shear failure is the most critical due to the abrupt nature of its mechanisms that leads to complete collapse of the structures with no sign of warning. This makes shear strengthening of prestressed concrete structures, that typically form the supporting elements in large infrastructural units such as bridges, a very essential course of action. To investigate the effectiveness of using UHPFRC in shear strengthening of prestressed concrete elements, the post-tensioned T girders of Helperzoom bridge, Groningen, Netherlands are chosen as reference beams which are strengthened with UHPFRC. The reference beams are subjected to a 3-point bending test to determine their failure mechanism and structural capacity. The reference beam is modelled, and tests are simulated by finite element analysis using ATENA. Since the simulated beam failure in shear compression rather than shear tension by localization of the shear tension crack. In order to understand this behavior and the failure mechanism and to check if the results from the simulations are reasonable, a detailed analysis is performed. The influence of shear reinforcement and prestressing, active in the critical shear region, on the shear capacity and the final failure mode are investigated. The results from the numerical analysis are compared to the results from experimental shear tests performed on existing post-tensioned girders which exhibit a similar mode of failure as observed in the reference T beams. The shear capacity of the reference T beam is also calculated from the Flexural Shear Crack Model proposed by Huber et.al [1] and it is seen that the shear capacity from the numerical analysis from ATENA is in close match to that obtained from the analytical model. The contribution of the arching effect to the shear capacity calculated from the model is between 77% and 87% for the beams tested in this research and the contribution is between 28% and 58% in the beams tested in the experiment. In the last step, the effectiveness of strengthening the reference beam with UHPFRC is determined. The results show that the effect of strengthening with UHPFRC is maximum in the reference beam without stirrups and prestressing both in terms of shear capacity and ductility.

Acknowledgement

"Success in not final, failure is not fatal: It is the courage to continue that counts."

- *Sir Winston Churchill*

The last two years at Delft University of Technology will forever be in my heart. This period taught me lessons in life that I will carry for the rest of my life. For someone who had taken everything in life as a given, TU Delft showed me the true value of things that I was negligent about before coming here. Thank you, TU Delft for not just making me a better engineer but also a better person overall.

When I begin to thank individuals, I cannot look beyond Dr. Mladena Lukovic. Mladena, you have been an ideal supervisor to me in all ways. You are always approachable, you have answers to literally everything that I ask. I could not have done this without your help and guidance. I am truly inspired by not just how knowledgeable you are but also by the work ethic that you carry. You are truly amazing. And Congrats to you on Luka!! I hope you have a wonderful journey as a mother.:).

My next thank you must go to Prof. Dr. Dick Hordijk. For someone in a position that you are in, you are truly a special person. In spite of your busy schedule, you were always ready to help and guide me and you pushed me for the right reasons. I am grateful to you for this. Next, I want to thank Dr. Marco Roosen and Prof. Dr. Cor van der Veen for their support and guidance in Mladena's absence. The discussions we had helped me to a great amount. My thanks to Dr. Steffen Grünewald. The mixing sessions we had were quite fun. I also want to thank Prof. Dr. Erik Schlangen for agreeing to be a part of my assessment committee.

I want to thank my classmates and friends with whom I had a wonderful time for the last two years. The love and blessings from my parents cannot be be understated and I hope I have made them proud. Last but not the least, I want to thank my fiancée Chandana Jois. Without you none of this would have been possible. You stood by me in my most difficult times, supported me and motivated me. I hope I have made you proud as well. My gratitude and love to you.

Contents

List of Figures

List of Tables

List of Abbreviations

AAR	Alkali Aggregate Reaction
ACI	American Concrete Institute
CFRP	Carbon Fibre Reinforced Polymer
CTRM	Carbon Textile Reinforced Mortar
ECC	Engineered Cementitious Composite
FRP	Fibre Reinforced Polymer
GFRP	Glass Fibre Reinforced Polymer
NSC	Normal Strength Concrete
OECD	Organization for Economic Co-operation and Development
UHPC	Ultra-High-Performance Concrete
UHPFRC	Ultra-High-Performance Fibre Reinforced Composite
UHSC	Ultra-High-Strength Concrete
RC	Reinforced Concrete
RWS	Rijkwaterstaat (Dutch Ministry of Infrastructure and Transport)
TRC	Textile Reinforced Composite
TRM	Textile Reinforced Mortar

1 Introduction.

1.1 Research Background and Scope.

Reinforced Concrete (RC) has been applied as a structural material for more than 150 years now. Regardless of the experience and knowledge gained on the domain in this period, structures made of reinforced concrete may require repair/strengthening because of ageing (degradation), increased loading conditions and as a consequence of human errors in construction.

A significant number of infrastructural facilities were constructed during the second half of the 20^{th} century using reinforced or prestressed concrete. Many of these structures are reaching or have already reached the end of their planned design service period and deterioration in the form of corrosion of steel, spalling of concrete and concrete cracking is sometimes observed. Apart from this, many buildings that originally were constructed for a specific use now are being considered to be renovated or upgraded for a different application that may require higher load-carrying capacity [2].

As a result of these higher load demands, existing structures need to be reassessed and may require strengthening to meet higher load requirements. In short, the need for strengthening of existing civil engineering structures can be summarized by the following reasons:

- Load increased due to higher live loads, increased wheel loads, installation of heavy machinery, or vibrations.
- Damage to structural parts due to aging of construction materials or fire damage, corrosion of steel reinforcement, and/or impact of vehicles.
- Improvements in suitability for use due to limitation of deflections, reduction of stress in steel reinforcement and/or reduction of crack widths.
- Modification of structural system due to elimination of walls/columns and/or openings cut through slabs, or change in the application of the structure
- Errors in planning or construction due to insufficient design dimensions and/or insufficient reinforcing steel.
- Obligations to comply with new, more stringent design codes and/or seismic upgrade which generally require a higher structural capacity [3].

Because of these factors, structural engineers are faced with the challenge of selecting and evaluating the best method of repair or strengthening for a specific structural element which is not only effective in terms of structural performance but also cheap and that involves a relatively easy and fast method of execution.

There is no single solution that offers a simple, straightforward method for all repair and strengthening projects. Further, the processes of repair and retrofit of existing structures are

complicated because most of these structures are occupied, and much of the mainstream construction community's expertise is centered on new construction and not on dealing with existing construction. Success can be achieved if the repair and strengthening systems are tailored to serve a structure's intended use without interfering with its occupants or function. The key to success is a combination of the different design skills and application techniques—assessing the current state of the structure and eventually proposing the best method for structural strengthening necessary for such projects. As such, engineers must rely on their expertise in using mechanical and structural behavior principles to develop a comprehensive retrofit solution.

Figure 1.1 Shows how (e.g. in case of design fault, increased demands, etc.). strengthening can accommodate the ever-increasing demand for better performance of civil engineering structures. Typically, challenges arise because of unknown factors associated with the structural state—such as continuity, load path, and material properties—as well as the size and locations of existing reinforcement or pre-stressing. The degree to which the upgrade system and the existing structural elements share the loads also must be evaluated and addressed properly in the upgrade design, detailing, and implementation procedure. The importance of detailing and its direct effects on the effectiveness and durability of structural upgrades cannot be overemphasized. In fact, inadequate detailing is one factor that can lead to the total failure of a structural repair system.

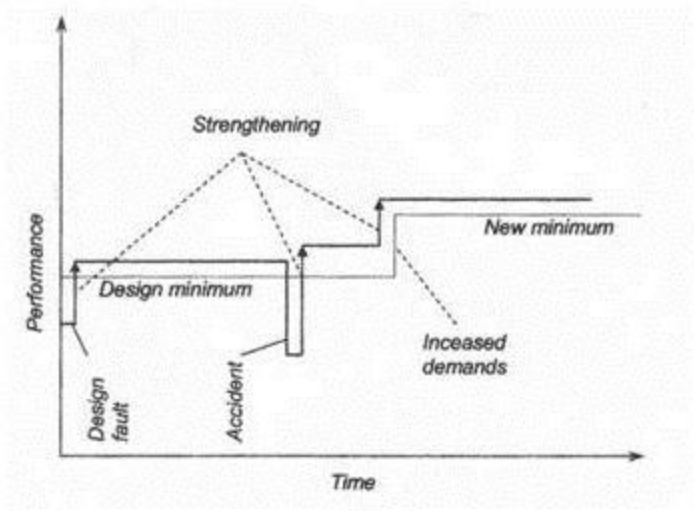

Figure 1.1 Performance history of a structure [3].

1.1.1 Overview of the need for strengthening of existing structures in the Netherlands and rest of the world.

Infrastructure forms one of the most important assets of the Netherlands' economy. About 50% of the national gross wealth comes from this sector [4]. Among many other, bridges and viaducts for transportation form a crucial part of the infrastructural facilities.

Current demands and interests of Rijkwaterstaat (RWS) as an organization responsible for design, construction, management and maintenance of the main infrastructure facilities in the Netherlands, with the focus on the main road network, concern both maintenance and extension of the service life (i.e. rehabilitation and strengthening) of existing structures, as well as the construction of new structures. Most existing viaducts in the Netherlands and worldwide (Figure1.2) are built in the 1960s and 1970s and are exceeding, or have already exceeded, their design service life [5].

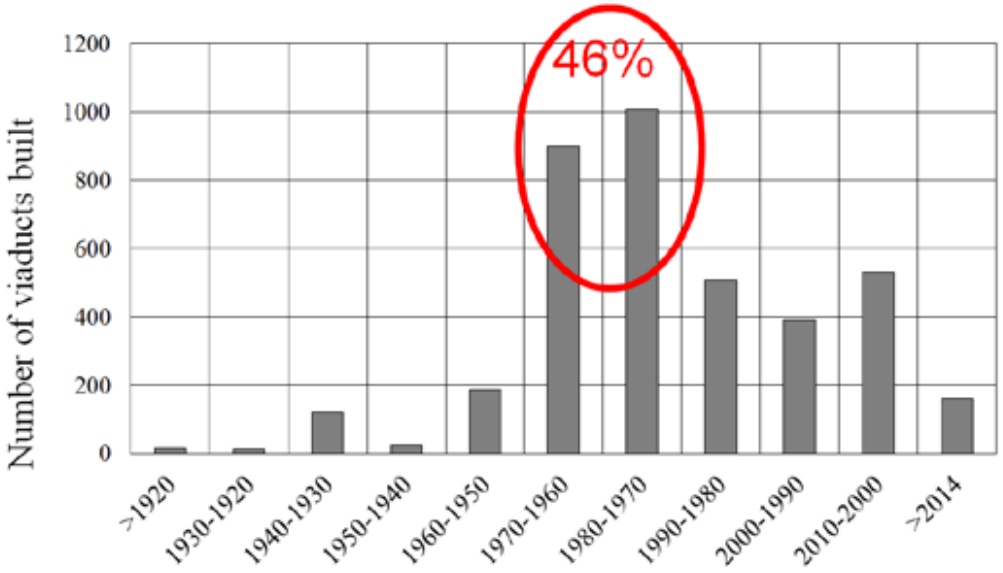

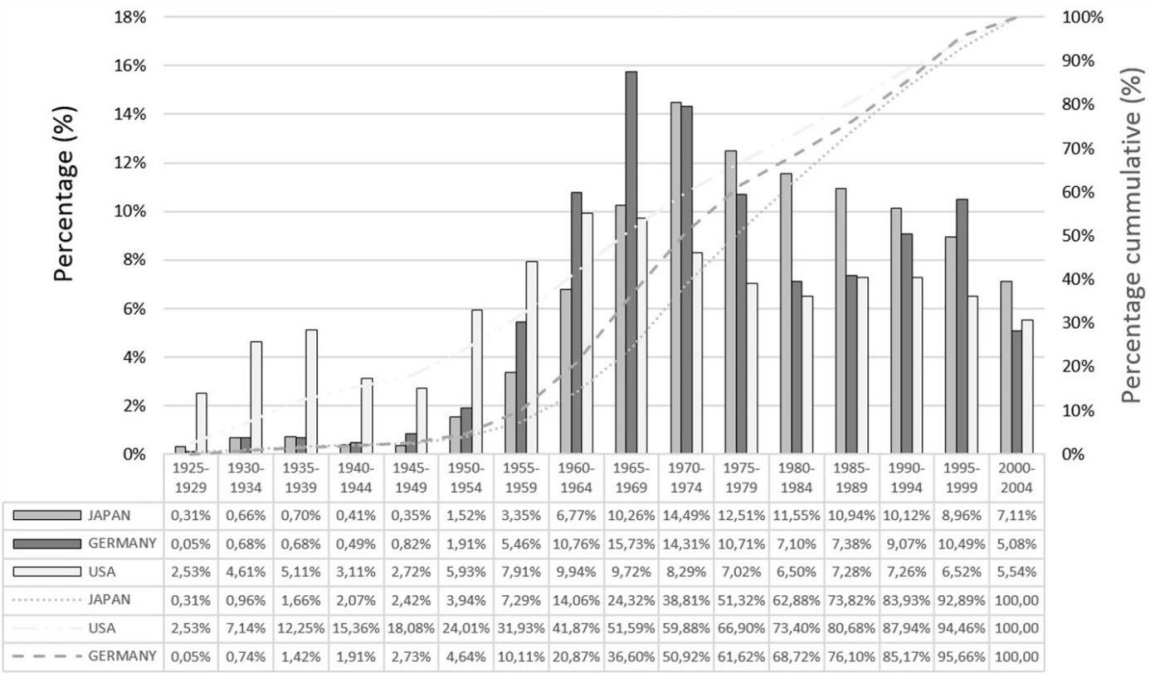

	1925-1929	1930-1934	1935-1939	1940-1944	1945-1949	1950-1954	1955-1959	1960-1964	1965-1969	1970-1974	1975-1979	1980-1984	1985-1989	1990-1994	1995-1999	2000-2004
JAPAN	0,31%	0,66%	0,70%	0,41%	0,35%	1,52%	3,35%	6,77%	10,26%	14,49%	12,51%	11,55%	10,94%	10,12%	8,96%	7,11%
GERMANY	0,05%	0,68%	0,68%	0,49%	0,82%	1,91%	5,46%	10,76%	15,73%	14,31%	10,71%	7,10%	7,38%	9,07%	10,49%	5,08%
USA	2,53%	4,61%	5,11%	3,11%	2,72%	5,93%	7,91%	9,94%	9,72%	8,29%	7,02%	6,50%	7,28%	7,26%	6,52%	5,54%
JAPAN	0,31%	0,96%	1,66%	2,07%	2,42%	3,94%	7,29%	14,06%	24,32%	38,81%	51,32%	62,88%	73,82%	83,93%	92,89%	100,00
USA	2,53%	7,14%	12,25%	15,36%	18,08%	24,01%	31,93%	41,87%	51,59%	59,88%	66,90%	73,40%	80,68%	87,94%	94,46%	100,00
GERMANY	0,05%	0,74%	1,42%	1,91%	2,73%	4,64%	10,11%	20,87%	36,60%	50,92%	61,62%	68,72%	76,10%	85,17%	95,66%	100,00

Figure 1.2 Historical overview of built bridges in the Netherlands (top) and worldwide (bottom) [6].

According to the Organization for Economic Co-operation and Development (OECD) improving the current infrastructure will require an estimated $7 trillion/year USD [7]. In Europe, the annual budget for repair and strengthening of bridges is around £215M [8]. 1500 railways bridges need strengthening, 4500 have to be replaced and an additional 3000 bridge decks need replacing as well [9]. In the US more than 60,000 bridges are structurally deficient and this number reaches 80,000 in China.

Extending the service life of concrete structures with a short service life of repair and strengthening solutions leads to repeated repairs and strengthening's and significantly increased structural life cycle costs, which often reaches several times higher values compared to the initial construction costs [10]. Furthermore, it may have a negative effect on the availability of the infrastructure. Therefore, repair and strengthening certainly require new improved methods and materials to extend their current service life. Usually repairs do not involve any structural improvements in the elements. Whereas for strengthening the end goal is to increase the structural performance typically by increasing the load capacity of the structure.

All the above considerations summarize the importance of not only the need for repair and strengthening of existing structures but also reiterate the complexity involved in the process. Careful evaluation of different techniques of repair/strengthening is therefore a must as we approach this relatively new development in the field of structural engineering.

Although the behavior of concrete elements in both flexure and shear is critically important, this thesis will focus on the shear strengthening of prestressed concrete beams. Flexural failure in beams typically occurs with a certain amount of ductility thus preventing abrupt damage without warning. On the other hand, shear failure is very brittle, can happen without warning signs and can lead to loss of human lives and significant damage. Therefore, this thesis is mainly focused on the brittle shear failure and shear strengthening.

1.2 Shear Capacity

In almost every design, shear failure forms the governing aspect of dimensioning. Shear failure of concrete elements both reinforced and prestressed requires special attention as the failure mechanism comes with low redundancy. The failure occurs abruptly without warnings. As a result, a minimum shear reinforcement is required to be provided. However, many such failures have occurred with reasons ranging from insufficient shear reinforcement to uncertainty in the contribution of the concrete to the shear strength of beams. This is an issue not just in conventional reinforced concrete structures but also in prestressed concrete.

Typically, in bridges, shear failure is a concern near the supporting piers/abutments due to concentration of high shear forces from the support reactions. This is a critical issue for the beams supporting the bridge deck, which are usually prestressed girders.

Figure 1.3 Example of a brittle shear failure (Chada Overpass, Chile). [11]

Three types of shear failure can mainly occur in reinforced and prestressed concrete structures (depending on factors such as, for example, longitudinal reinforcement ratio, shear reinforcement ratio, concrete compressive strength etc.):

1. Diagonal tension also named as flexural Shear Failure (Figure 1.4 (left))
2. Shear compression failure (Figure 1.4 (right))
3. Shear Tension (Figure 1.5)

For a reinforced prismatic beam, two types of failures, namely the flexural shear failure and shear compression failure, are considered as "shear failures". *The flexural shear failure* depicted in Figure 1.4 (left) originates from the flexural cracks nearest to the support (where the shear force is the greatest). The flexural cracks develop into the inclined shear-flexure crack and propagate further till the failure mechanism occurs. Therefore, in the flexural shear failure the opening of the critical diagonal crack results in the collapse of the beam. Shear compression failure also starts with the diagonal crack, but the final failure occurs due to the crushing of the concrete. A splitting crack of concrete strut develops as a secondary effect of failure (Figure 1.4 right).

The third failure mechanism is typical for prestressed T beams and hollow core slabs and is related to shear tension cracking, hence called *the shear tension failure*. This very brittle failure type appears in beams with thin webs in regions where shear force is large compared to bending moment (e.g. a point of contra-flexure or in a vicinity of a support). [12]. This failure occurs in the part of the beam without flexural cracks and where the shear stresses are high (near the supports). In the uncracked region, a large splitting crack initiates from the web region where the principal tensile stresses have exceeded the tensile strength of concrete

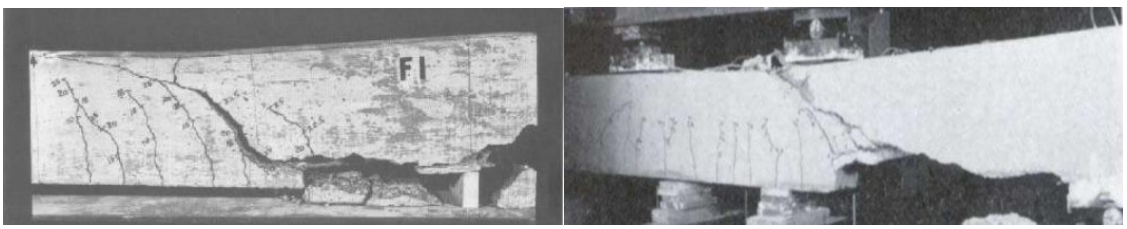

Figure 1.4 Failure mechanism in shear. Flexural shear (left) & Shear Compression (right) [12] [13]

.

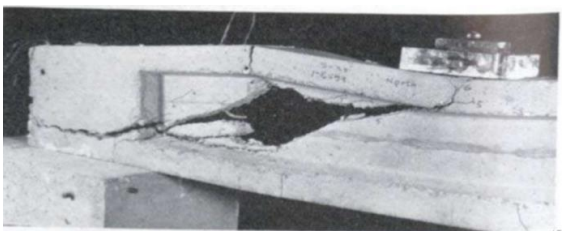

Figure 1.5 Shear tension failure [12].

The principal stresses are defined as the normal stresses on the face oriented in such a way that shear stress vanishes. From figure 1.6 it can be seen that such tensile stresses are a cause of the crack at 45 degrees to the horizontal. It is important to note that cracking occurs when the principal tensile stresses exceed the tensile strength of concrete.

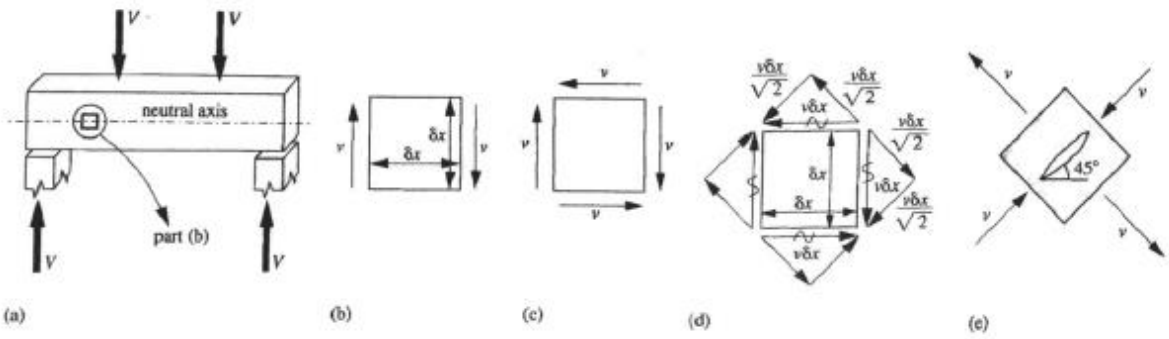

Figure 1.6 Stress in a segment of concrete; a) a beam subjected to four- point bending; b) and c) shear stresses in a concrete segment; d) stress resolution; e)stresses in the principal directions. [14]

Although there are many analytical models and codes to predict the shear capacity of concrete elements with and without shear reinforcement – Eurocode 2 (EC2), fib model code (MC2010), American Concrete Institute (ACI) etc., these codes have been prepared having in mind the design of new robust structures, rather than the assessment of existing constructions. Therefore, they are very conservative and existing structures have to be assessed with refined shear models in order to avoid expensive and often unnecessary strengthening measures.

1.3 Research Aim.

The aim of the research is to investigate, firstly the shear behavior of prestressed concrete beam, its capacity and failure mode, and secondly to investigate the needs and benefits for its shear strengthening using UHPFRC. This is particularly interesting as prestressed beams (mostly with I or T cross-section) form the support structures for many building slabs and bridge decks (Figure 1.7). The performance of these beams in both bending and shear is extremely critical for the structural capacity and safety of the overlaying slabs or decks. Any loss in performance of the beams resulting in the capacity less than the required is detrimental to entire construction. Therefore, in case needed, strengthening of such beams is of vital importance for the integrity and safety of the infrastructure.

Figure 1.7 RC beams supporting bridge decks and slabs [15] [16]

Typically, shear strengthening of prestressed beams is made by increasing the web thickness (figure 1.8).

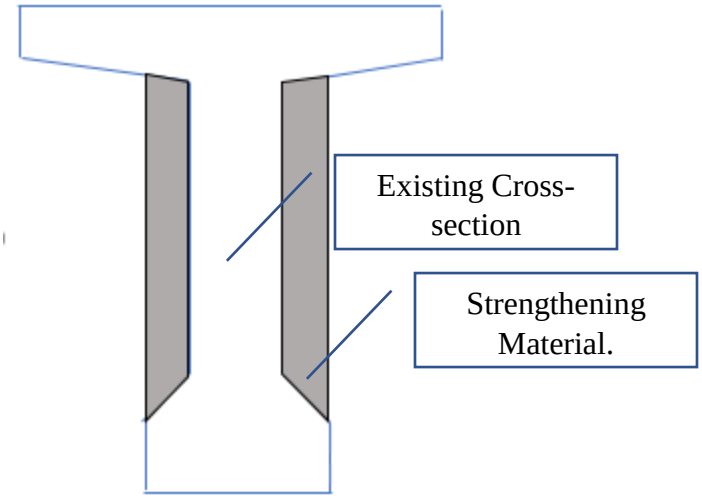

Figure 1.8 Graphical scheme for shear strengthening

1.3.1 Research Objective.

The research focuses on a real scenario of a bridge deck in Groningen, Netherlands (Figure 1.9). The Helperzoom bridge in Groningen area has been dissembled due to safety concerns by the Dutch Ministry of Infrastructure and Environment (Rijkwaterstraat). The post-tensioned T beams supporting the deck will be tested in the TU Delft laboratory to assess its capacity and failure mode.

Figure 1.9 Bridge Deck in Helperzoom, Groningen, Netherlands

The thesis will present numerical simulations of the test by finite element analysis using ATENA. The numerical study will be used first to investigate the possible shear failure mechanism and the ultimate shear capacity of the prestressed beam. Since at the moment of writing this report the experimental study is still not being performed, the results from the numerical analyses will be compared with the results predicted by existing shear models.

In addition to this, numerical modelling of the prestressed T beams strengthened with UPHFRC (Ultra high performance fibre reinforced composite) will be carried out to investigate the behavior and possible increase in bearing capacity of the beams.

The idea to strengthen the T beam with UHPFRC is derived from a more commonly executed method of using NSC with an FRP (Fibre reinforced Polymer) wrap to strengthen concrete girders. In this method, the existing structure (beam) is added with additional concrete which is usually of normal strength. In the next step, FRP sheet is wrapped around the added material to give the system additional strength because of the high stiffness and tensile strength of the fibre polymers. The FRP sheet is then anchored to the existing structure to prevent loss of bond between the added concrete and FRP (Figure 1.10).

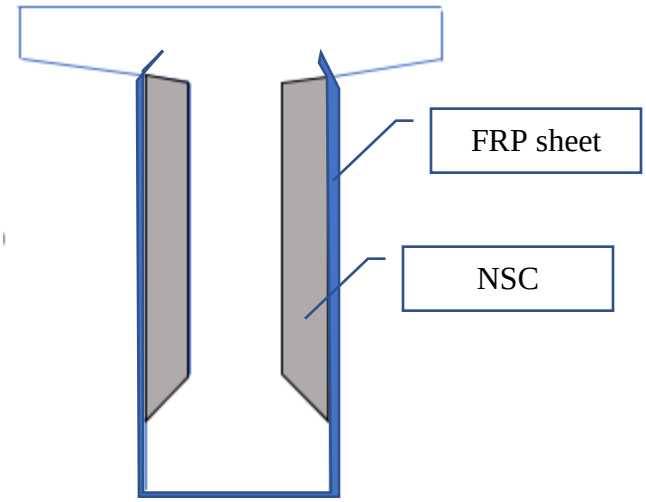

Figure 1.10 Strengthening with NSC and FRP wrapping.

One of the common failure modes in structures strengthened in such a manner, is the premature debonding of the FRP sheet from the added material. This is because of the large differences in stiffness and tensile strength between the added concrete and FRP. As result of debonding, complete usage of the high stiffness and strength of FRP cannot be achieved [17].

An alternate approach to this is to strengthen the beams with UHPFRC, which is a type of concrete but with a slightly higher tensile strength compared to NSC. But the beneficial aspect of UHPFRC is its strain hardening behavior in tension, which is a contribution of the steel fibers. Also, the high durability and permeability of UHPFRC can be added values to structures strengthened with UHPFRC

1.3.2 Research Questions.

The thesis will be able to answer the following questions:

1. ***Is the existing beam expected to fail in shear? If not, which are the main mechanism contributing to its shear capacity?***

2. ***What is the contribution of the added UHPFRC to the structural capacity of the post-tensioned T beam in which the shear capacity is critical?***

1.3.3 The overview of the thesis

Chapter 1 gives the introduction and research aim, **Chapter 2** focuses on state of the art of strengthening methods. As a strengthening solution in this research, UHPFRC layer applied on the webs of the T beam is chosen. **Chapter 3** gives the overview of main UHPFRC properties and its applications for strengthening. **Chapter 4** presents the methodology of research. **Chapter 5** gives the discusses the results obtained from the numerical analyses by ATENA. **Chapter 6** gives the conclusions and recommendations.

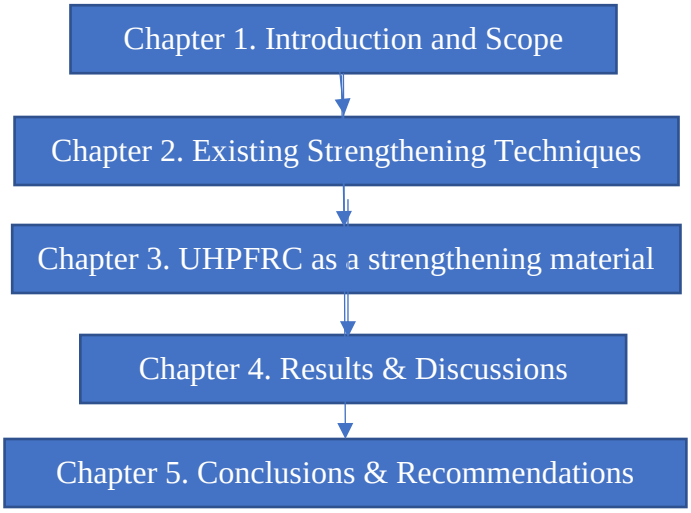

Figure 1.11 Overview of thesis.

2 Strengthening Techniques.

Many aspects must be addressed when evaluating a specific technique used for strengthening. One of the main problems faced in this aspect is the speed at which the strengthening process can be completed. This is critical as one of primary objectives of strengthening is increasing the structural performance by causing minimal obstruction to the functionality of the structure. Also, concerns with regard to existing materials, often in deteriorated condition, loads during strengthening and to existing geometry prevail when strengthening of structures is carried out. In some cases, it can also be difficult to reach the area of the structure that needs to be strengthened.

When concrete structural strengthening is to be undertaken, all failure modes must be evaluated. Strengthening a structure for flexure may lead to shear failure instead of giving the desired increased load bearing capacity. It should also be noted that not only the failure mode of the strengthened member is important. If a critical member of a structure is strengthened, another member can become the critical one. Because of changed stiffness in a statically undetermined structural system the whole structure must be investigated. The strengthening should also be designed with consideration to minimize the maintenance and repair needs in the future.

When a strengthening solution is designed the consequences from loss of strengthening effectiveness by fire, vandalism, collision etc. must also be considered.

In the current practice, quite a few methods have been established for strengthening of concrete structures. Each technique has its own benefits as well as disadvantages. A brief account of the different techniques is made in this section.

A distinction is made between the conventional techniques that are traditionally applied and innovative methods of strengthening that have been recently developed.

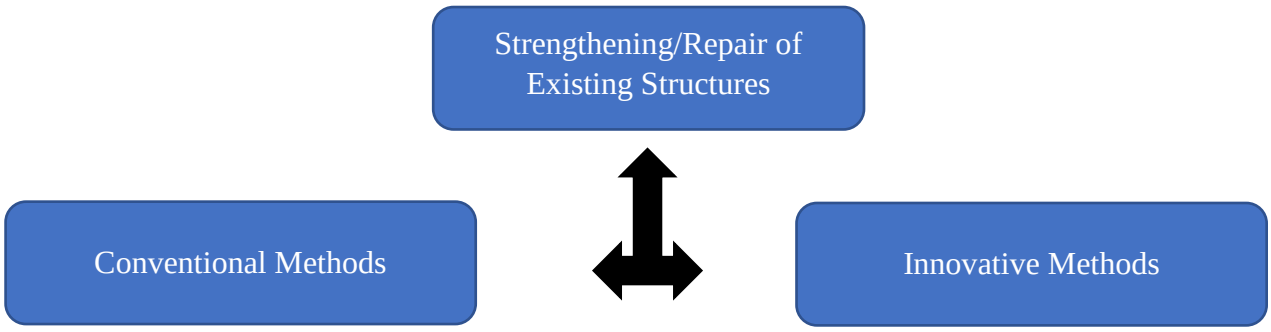

2.1 Conventional Techniques.

Although this thesis deals with shear strengthening of the prestressed T beam, in this chapter the general overview of strengthening methods which are applied both with reinforced and prestressed concrete beams is given. In addition, apart from shear strengthening, also flexural strengthening is addressed.

2.1.1 Section Enlargement (Jacketing).

As the name suggests, the main idea of this method of strengthening is to increase the load-carrying capacity and stiffness of an element by increasing its cross-sectional dimensions. [18]. The method comprises many steps such as temporarily supporting the element that needs strengthening and then with the help of additional formwork the new layer of concrete is casted against the existing deteriorating layer. Prior to the application of a new layer of concrete, the underlying concrete layer has to be prepared to ensure proper bonding with the repair material. Also, the new reinforcement needs to be anchored into the existing cross-section. Any deformation in the form of concrete spalling or corrosion of steel must be treated before the application of the strengthening layer. Figure 2.1 shows a typical example of a section enlargement performed on a prestressed beam.

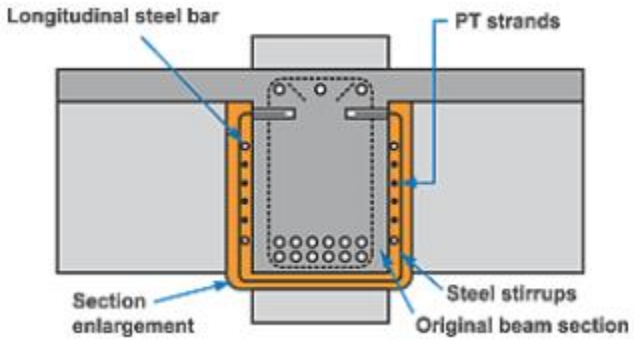

Figure 2.1 Cross section of a prestressed beam strengthened by Section Enlargement Technique [19].

The obvious disadvantage of this method of strengthening is the increase of the structural dimensions of the element which may diminish the functionality and add to the dead load of the element. Another disadvantage is the use of extra formwork which further increases the costs and hinder caused by the strengthening operation.

2.1.2 External Post Tensioning.

Both reinforced concrete and pre-stressed elements can be strengthened using this technique which is effective in increasing the flexural as well as the shear capacity. External post-tensioning is particularly appropriate for box girders or in general structural elements having a high static height as typically found in bridges. The post tensioning forces are delivered using either standard pre-

stressing tendons or high strength steel bars located outside the concrete section (Figure 2.2). A major advantage of this technique is that strengthening is realized with barely any increase in the self-weight of the beam.

Figure 2.2 Strengthening by external post-tensioning in bridge decks [20]

Although this might seem as an economical solution for the strengthening of large concrete sections such as bridge decks, there is an added cost required for tensioning and anchoring the cables/steel bars. Further, any damage to tendons due to direct exposure will significantly reduce the efficiency of strengthening.

2.1.3 Shotcrete.

Shotcrete is one of the oldest techniques used to repair and strengthen reinforced concrete structures. Concrete is applied with or without additional reinforcement using a high-pressure nozzle (Figure 2.3). The problems with such a method of strengthening is not only the significant increase in the dead load of the structure but also the relatively weak bond of shotcrete with the underlying concrete surface.

Figure 2.3 Strengthening by reinforced shotcrete [18].

2.1.4 Strengthening with externally bonded plates and lamellas.

a) Steel Plates.

Steel plates are usually bonded with the concrete surface to realize a composite action between the two materials whereby increasing the load bearing capacity of the concrete element substantially (Figure 2.4). This technique may be highly efficient in case of beams subjected to bending. Steel plates are typically bonded with epoxy-based adhesives to the prepared concrete surface or installed in grooves in the concrete and anchored at their ends. The adhesives require specific ambient conditions for optimal curing and strength. The concrete substrate has to be even and provide sufficient adhesive strength, typically > 1.5*MPa*. The position and the concrete cover of the existing reinforcing bars have to be considered. Special attention is paid to the corrodibility of the steel plates before and after the application. Since the fire resistance of the adhesive and the steel plates is very limited, respective load cases and fire proofing measures have to be accounted for [21].

Figure 2.4 Shear Strengthening of RC beams by the addtion of steel plates [18].

b) Fiber Reinforced Polymer (FRP) lamellas and sheets.

Strengthening by the addition of layers of FRP is the most commonly used method of strengthening in practice. Typically used fibers are carbon fibers (CFRP). Recently, use of glass fibers (GFRP) has also seen an increase in application. Execution is similar to that in the case of steel plates where the lamella is bonded to surface prepared concrete layer. In contrast to the steel plates, the FRP lamellas are much lighter and provide a higher tensile strength (1500 – 3200 MPa). As a result, the thickness can be limited to 1 – 2mm. Due to this, handling becomes easier. FRP lamellas are also known for their corrosion resistance leading to a durable structure. Due to its high versatility, this method has wider range in terms of application. For flexural strengthening of concrete beams, the FRP lamellas or sheets are applied generally at the tension side. In case of combined bending and shear strengthening, U shaped lamellas are applied which are bonded to both the bottom and sides of the beam cross – section.

Strengthening Techniques.

Figure 2.5 Bending strengthening of RC beams using CFRP lamellas (left) and shear strengthening of RC beams (right) using U-shaped CFRP jackets [22] [23].

In addition to the lamellas, strengthening using FRP can also be made by spraying with a special vinyl ester resin applied on the concrete surface.

A major disadvantage of this technique is the deterioration of material and bond properties of FRP sheets due to increase in temperature (fire) [24]. Also, the decrease in shear capacity of beams strengthened using FRP sheets under fire conditions is significant [25].

2.2 Novel types of Concrete for Strengthening.

In recent times a lot of research efforts have been put towards development of special concrete types, specifically designed to meet certain requirements (sustainability, durability, aesthetics, etc.), or a certain property (high strength, high ductility, low permeability, low weight). Use of such novel material composites can be a viable option for strengthening of existing civil engineering structures due to use of fiber in the cement matrix which increase the strength of composite considerably. These materials can be listed as follows:

1.UHPFRC (Ultra-High Performance Fibre Reinforced Concrete), also known as UHPC (Ultra-High-Performance Concrete), or UHSC (Ultra-High Strength Concrete).

2. SHCC (Strain-Hardening Cementitious Composites), also referred to as ECC (Engineered Cementitious Composite) or bendable concrete.

3. TRC (Textile Reinforced Composite) or TRM (textile reinforced mortar).

All the above listed material composites can be used for strengthening of existing civil engineering structures. The choice of material to be used depends on the purpose of the application and other aspects related to execution and economy.

Despite their benefits, the application of such innovative material composites is very limited. This is due to various reasons listed below [5].

- Lack of design codes and guidelines.
- High scatter of material properties (especially in mixes with fibers) and uncertainties related to lab vs. field testing.
- Gap in knowledge between material properties and structural behavior.
- Lack of experience/confidence.
- Insufficiently trained labor.
- Advanced production technology that needs to be implemented.
- Potential high (financial) risk.
- Difficulties in acquisition of building permissions.
- High price.

The first step in overcoming the above limitations should be to gain substantial knowledge about these materials and their suitability in different areas of applications. Although, quite a few researches have been carried out on these composites and behavior, it is still not sufficient to arrive at a state of large scale application of these composites in a new construction or for strengthening of existing structures. This makes for the motivation to carry of the current research.

Many applications have been carried out by making using of the high strength and stiffness properties along with the addition of extra concrete layers for strengthening structures. (1.3.1). But if it is to be proven that just by the application of high strength concrete such as UHPFRC without the FRP sheet, can improve the structural performance, mainly the capacity, then it would be a significant step in answering some of the questions that concern applications of novel based concrete materials in strengthening structures.

3 UHPFRC as a strengthening material.

3.1 Ultra-High-Performance Fiber Reinforced Composite. (UHPFRC)

Among the many types listed in previous chapter, the one that interests the most is the Ultra High-Performance Fiber Reinforced composite (UHPFRC). This section gives a broad picture of the composite -its composition, material properties and some examples of real-life applications in strengthening of existing concrete structures.

UHPFRC form a novel material developed over the last three decades. A set of special traits, such as durability, outstanding material properties, and ease of application, render UHPFRC particularly attractive for the improvement (rehabilitation, strengthening) of concrete structures. Also, due to the high strength and ductility of the composite as strengthening material, the cross-section of the element to be strengthened does not need to be increased significantly. Therefore, the increase in self-weight is minimal.

3.1.1 General Properties.

The brittleness associated with high strength concrete is overcome in UHPFRC via addition of steel fibers. As a result, the composite shows excellent material and durability properties. With a characteristic compressive strength ranging between 150 – 250 MPa, UHPFRC also behaves exceptionally in tension in comparison with conventional normal strength concrete (NSC). The characteristic properties used to identify this material include either strain softening or strain hardening behavior in tension, high ductility, toughness and fracture energy [26]. All these attributes are particularly beneficial in strengthening of concrete structures.

3.1.2 Material Composition.

The composition of UHPFRC is characterized by a dense cement matrix and fine particle distribution with relatively high binder content. UHPFRC mixes typically contain 650 to 900 kg/m^3 of cement as well as micro-silica and fine particles (quartz, basalt, etc.) with a maximum grain size generally not exceeding 1 mm, or 2 mm. The water/binder ratio is between 0.13 and 0.17. The components are mixed using a superplasticizer to obtain an ultra-compact matrix. More recently limestone filler is used to replace a significant amount of cement and to improve workability, leading to more economic and environmentally friendly UHPFRC [27].

The matrix is generally strengthened with straight steel fibers of 13 to 15 mm length and an aspect ratio of more than 65, with a dosage of up to 3% in volume (or 240 kg/m3), in order to obtain high tensile strength and significant tensile strain hardening behavior, a most important property for applications, especially in strengthening using composite action – RC – UHPFRC [28].

UHPFRC as a strengthening material.

Figure 3.1 Steel fibers in UHPFRC mix [29]

3.1.3 Material Properties

Compression.

The characteristic compressive strength of UHPFRC usually ranges between 150 - 250 MPa showing a rather linear stress -strain relationship until the yield strength (Figure 3.2).

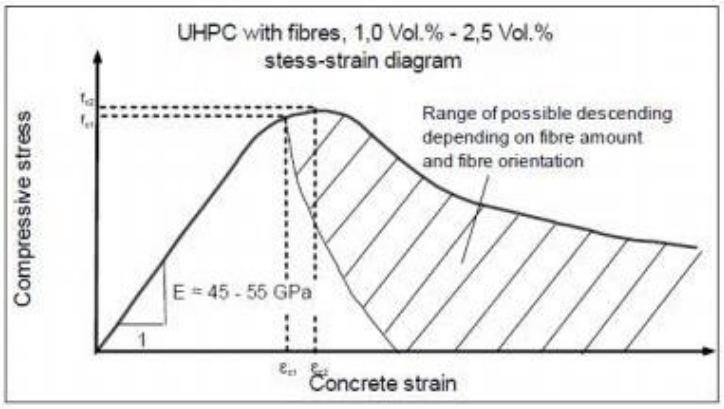

Figure 3.2 Characteristic Compressive Behaviour of UHPFRC [30].

Tension.

The tensile behavior of UHPFRC is characterized by a higher tensile capacity in comparison to NSC. Also, the fibers in the composite attribute to the tensile hardening behavior of UHPFRC.

The tensile behavior of UHPFRC is illustrated in Figure 3.3.

The characteristic tensile behavior of UHPFRC into 3 phases [28].

1. The elastic phase – with a limiting yield stress f_{Ute}, typically ranging between 7 to 11 MPa.

2. The strain hardening phase as result of fiber activation which is characterized by multiple fine micro – cracking of the matrix; the material still behaves like a continuum. Significant

strain hardening behavior is only obtained with (straight) steel fibers having an aspect ratio larger than 65 and a fiber content of upto 3% in volume. Strain hardening domain shall reach strains ε_U more than 2‰ and while the (uniaxial) tensile strength f_{Ut} reaches values ranging from 9 to 15MPa.

3. The third phase starts upon the formation of a discrete macro-crack at ultimate resistance and strain softening begins. The maximum crack opening $w_{Ut,max}$ equals about half of the fiber length, i.e. 6 to 8mm. At these crack openings, no more tensile stress is transferred.

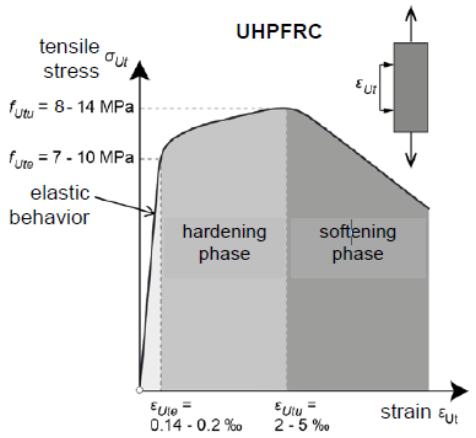

Figure 3.3 Characteristic Tensile behavior of UHPFRC [28].

The tensile hardening and softening behavior of UHPFRC depends on the bond, aspect ratio, content and random orientation of the straight steel fibers [31] [32]. The specific fracture energy of UHPFRC typically ranges from 20 to 30kJ/m2 [28]. Specific fracture energy is defined as the total energy required to open a crack of unit area.

Elastic Modulus and Stiffness.

The elastic modulus of UHPFRC is slight higher than that of NSC. Typically, the stiffness of UHPFRC ranges between 50 – 80 GPa. In the tensile strain hardening domain, UHPFRC shows reducing apparent modulus of elasticity with increasing hardening strain.

Shrinkage and Creep.

Evolution of shrinkage and creep of UHPFRC is similar to other cement-based materials, but by thermal treatment at early age, creep and shrinkage of UHPFRC is considerably reduced.

Also, shrinkage develops rapidly and about 60 to 90 % of total shrinkage has completed already after 50 days. This is because the largest part of shrinkage of UHPFRC results from endogenous shrinkage and a smaller part from drying shrinkage [33] [34].

UHPFRC as a strengthening material.

Fatigue.

UHPFRC has a fatigue endurance limit of 50-60% of its strength in both compression and tension. Above this limit significant damage occurs and fatigue strength is relatively low [35].

Durability and Permeability.

UHPFRC is typically characterized by extremely low air/water permeability and very high resistance against freeze-thaw-cycles, sulfates and AAR (Alkali aggregate reaction). In addition, increased resistance against acid liquids has been determined. This performance is explained by the extremely dense matrix showing a very low number of capillary pores making UHPFRC impermeable for liquids, even under high tensile strains up to about 1.5 ‰ [36].

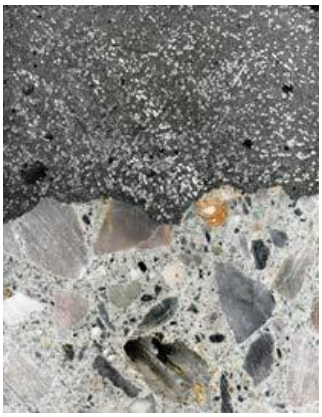

Figure 3.4 Difference in matrix density of UHPFRC (upper) and NSC (lower) [28].

Resistance against abrasion.

In comparison to the other cement composites, UHPFRC has found to have a very high resistance to mechanical and hydro – abrasion [37].

Fire Resistance.

The fire resistance of UHPFRC is similar to other cement composites. Increase in resistance to fire can be achieved by the addition of polypropylene (PP) fibers to the composite.

All the above material properties indicate to a high suitability of UHPFRC in strengthening applications. The most important property of the UHPFRC is its high strength in compression and its strain hardening feature in tension. The high durability and low permeability also make the composite a very suitable choice as a strengthening material.

UHPFRC as a strengthening material.

3.2 State of the Art of UHPFRC applications for strengthening.

In the last decade, quite a few applications of UHPFRC both as a strengthening/repair and in new construction have been made. Some of the applications are briefly mentioned below.

- **Improvement of Chillon Viaducts, Switzerland.**

Located in Switzerland, the Chillon viaducts are two parallel posttensioned concrete highway bridges built in the late 1960s. The concrete decks of the viaduct needed strengthening as a result of reduced structural safety caused by (AAR). To increase the structural performance of the deck slab under increasing traffic demands, reinforced UHPFRC was added to the existing deck slab with a thickness of 45mm. The R-UHPFRC acted as external reinforced for both the deck slab and main girder [38].

Figure 3.5 Chillon viaducts along Lake Geneva and the geometry of the box girders cross-section [38].

By casting one layer of R-UHPFRC on the deck slab, the following beneficial effects were achieved:

- increase the deck slab's ultimate resistance in the transverse direction in bending and shear
- increase the deck slab's stiffness to improve the serviceability of the slab and the fatigue safety of the steel rebars in the existing concrete in view of future higher traffic loading
- increase the hogging bending moment resistance and the stiffness in the longitudinal direction of the box girder
- provide waterproofing to protect the existing concrete of the slab from ingress of water (and chloride ions), thus limiting further development of the AAR
- limit duration of the intervention [38].

Figure 3.6 Application of R-UHPFRC on the decks of Chillon Viaduct [28]

UHPFRC as a strengthening material.

- **Rehabilitation of Bridge Pier using prefab UHPFRC shell elements.**

A 40-year old bridge pier made of reinforced concrete near a busy highway has been protected against further deterioration by the addition of a 4mm thick prefab UHPFRC shell element. Due to the relatively impermeable UHPFRC ingress of chloride ions through the transverse cracks of the pier can be prevented thereby improving the long-term durability of the pier. The UHPFRC element requires no further maintenance which is particularly beneficial since the pier is not easily accessible next to the highway due to heavy traffic.

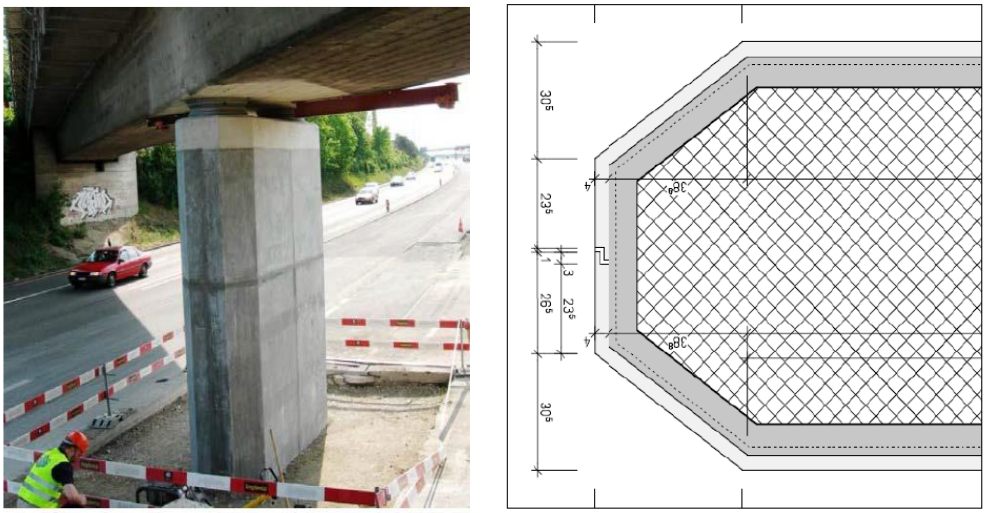

Figure 3.7 Cross section and general view of the rehabilitated bridge pier [38].

- **UHPFRC protection layer on a crash barrier wall.**

A crash wall barrier of reinforced concrete in a highway has been strengthened with a 3cm layer of UHPFRC. Due to its high strength and low permeability, UHPFRC acts as an effective strengthening material in the application.

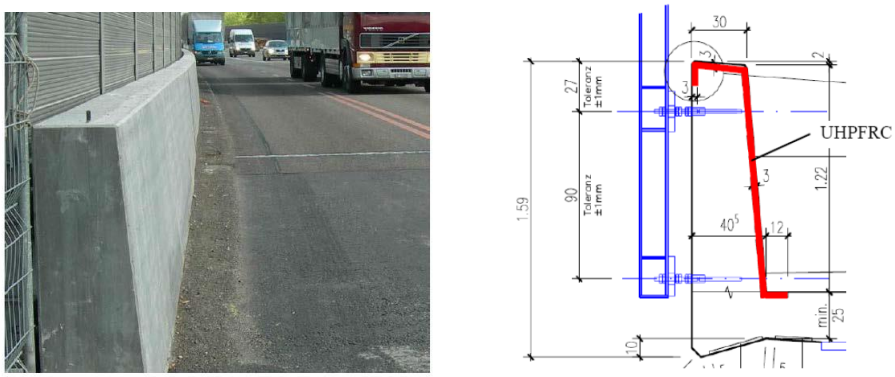

Figure 3.8 Typical cross section of the crash barrier wall and view after rehabilitation [38].

UHPFRC as a strengthening material.

- **Strengthening of an Industrial Floor.**

The 50-year old drivable reinforced concrete floor of a fire brigade building had insufficient load carrying capacity in view of heavier future fire engines. The concept to increase the load carrying capacity of the existing slab of 720 m^2 area was to pour a 4cm thick UHPFRC layer on top of the existing RC slab, as a replacement of the existing cementitious non-load carrying overlay. The UHPFRC layer leads to a thicker load carrying slab which provides (1) a better distribution of local wheel loads, (2) an increase in static height and (3) a high strength material to resist both compression or tension stresses [39].

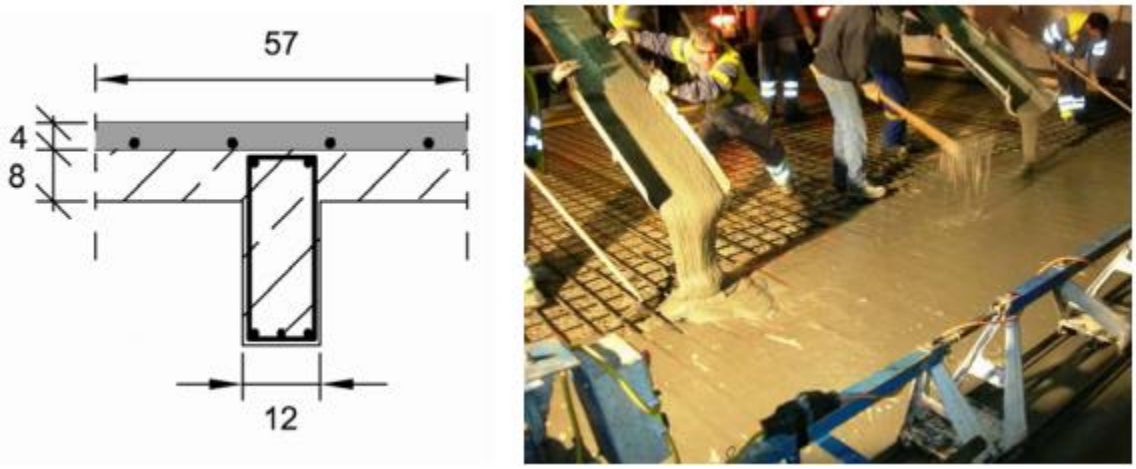

Figure 3.9 Cross section of floor and the application of R-UHPFRC on an industrial flooring [39].

- **Shear strengthening of I girders with Carbon Textile Reinforced Mortar (CTRM)** [40]

CTRM is a type of composite which consists of two layers of an epoxy-resin impregnated carbon grid and a high-performance mortar. The carbon grid consists of fibers with a high tensile strength close to 2400 MPa. The CTRM layers are added to the web of I girders to improve their shear capacities (Figure 3.10).

UHPFRC as a strengthening material.

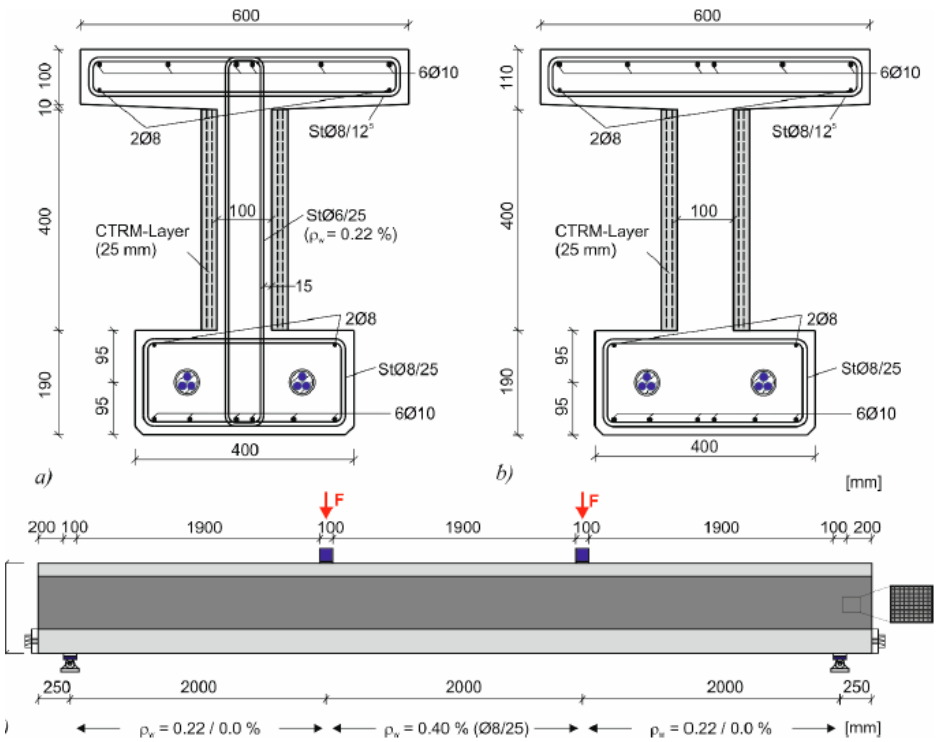

Figure 3.10 Shear strengthening of prestressed I girders with CTRM [40].

Two I girders were tested to determine the contribution of CTRM layer to the shear capacity. One beam with shear reinforcement and the other without. In the I girder with shear reinforcement an increase of 40% in shear capacity was achieved by the addition of the CTRM layer and in the beam without shear reinforcement the increase was 30%.

3.3 Summary

Strengthening using UHPFRC also advantages over the other techniques explained in section 2.1. UHPFRC results in a significant increase in ultimate resistance of the strengthened member with a relatively lower increase in dead load in comparison to the section enlargement technique. Since the material has exceptional properties in both compression and tension compared to NSC, UHPFRC elements of relatively smaller thickness and size can be used in strengthening. The corrosion and fire resistance of UHPFRC is higher than that the steel plates and externally post tensioned steel cables resulting in a much more robust solution for strengthening in case of extreme environmental conditions. Although the application CFRP/GFRP lamellas constitute an efficient technique for strengthening, the use of the lamellas in the form of U-jackets for shear strengthening increase the amount of material use considerably. On the other hand, UHPFRC acting as strengthening material for beams of conventional concrete could possibly enhance the performance not just in bending but also in shear with less amount of material (UHPFRC) use. [41].

UHPFRC can be used as a strengthening material in both cast-in situ and prefabricated applications. Prefabricated laminates lead to an increase in execution speed, and therefore,

reduction of out of use periods of structures, which forms one of the most critical concerns in the strengthening process. Irrespectively of its execution, UHPFRC can be used for increasing the flexural or shear capacity.

This thesis will focus on numerical modelling of the application UHPFRC for shear strengthening.

4 Research Methodology.

The behavior of the post tensioned T beam strengthened using UHPFC is investigated for possible improvements in its shear performances through numerical analysis in ATENA model.

4.1 Programme Used for Simulation: ATENA

ATENA is a finite element software used in this research to numerically model the post-tensioned T beam and the beam with the UHFRC layer and investigate their performance under three point bending test. ATENA is a specialized software for detailed reinforced and prestressed concrete analysis. The emphasis was always on 2D/3D analysis using continuum-based elements, which were enhanced by specialized 3D beam and shell elements. The programme is based on continuum approach and can perform both linear and non-linear analysis. It is constructed by Cervanka Consulting, Czech Republic. For more information see www.cervanka.cz.

The input parameters for ATENA are the material properties of the prestressed concrete beam, the loading/supporting plates and the reinforcement.

The geometry of the model is defined first and then material properties are assigned to the appropriate elements. Three types of elements are defined:

1. Regular concrete beam or composite beam (consisting of regular concrete strengthened with UHPFRC).
2. Steel Plates for loading/support.
3. Reinforcement (shear and longitudinal reinforcement).
4. Prestressing Cables.

4.1 Post -Tensioned T beam.

The beam is subjected to 3-point bending load with a shear span ratio (a/d) of 3.0. The test set-up is adopted as per the experimental setup on which the beams will be tested in the laboratory.

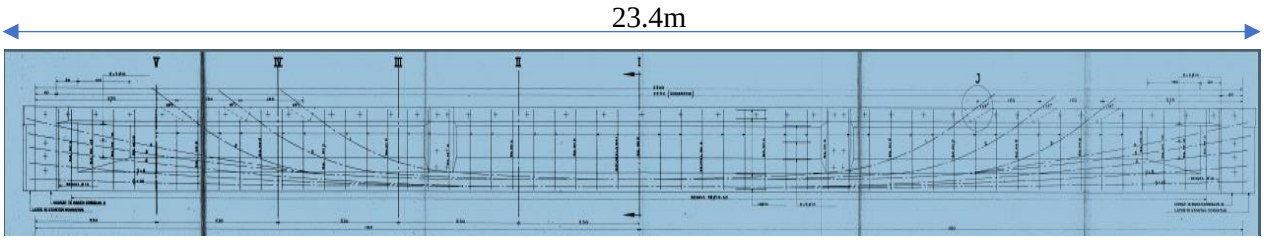

Figure 4.1 Post-Tensioned T Beam supporting Helperzoom bridge deck

The girder has a span of 23.4 m. For the experimental study, only half the span of the beam will be used (Figure 4.2). The length of the beam used for the test will be 11.7 m and the span between the supports will be 11.15 m. The beam consists of 7 post-tensioned cables spanning through the

length of the beam and 3 cables acting as continuous prestressing cables. Additionally, the beam has longitudinal steel reinforcement and web steel reinforcement of 10 mm diameter. The web reinforcement follows the shape of the cross-section. The cross-section has a constant T shape for 9.7 m and then starts to taper outwards until it reaches a full cross-section near the right-hand support. For more information Appendix 1 can be referred.

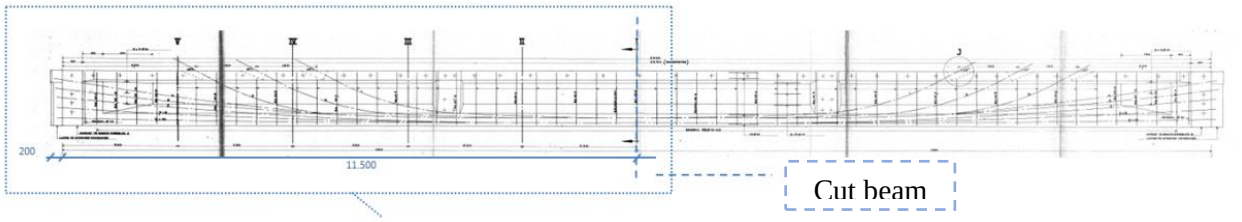

Figure 4.2 Part of the beam sawn for the experiments

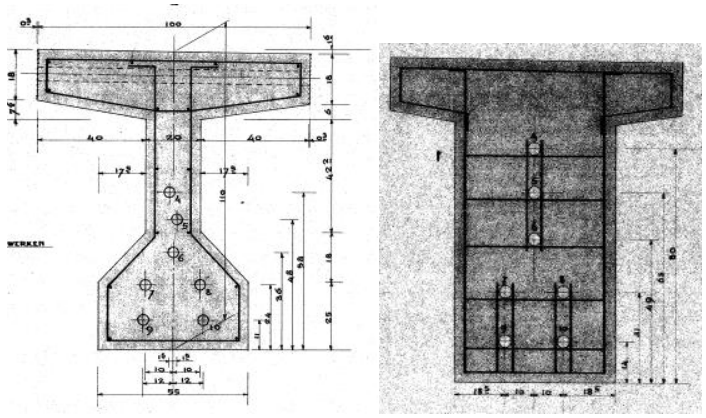

Figure 4.3 Nominal cross-section (left) and cross-section with increased web thickness (right) of T beam.

4.2 Simulation Set-up.

The half girder with a span of 11.7m is subjected to a 3-point bending load with the point load acting at 2.903 m from the right-hand support (Figure 4.4). Other details such as the concrete compressive strength and prestressing cables specifications will be explained in the coming sections.

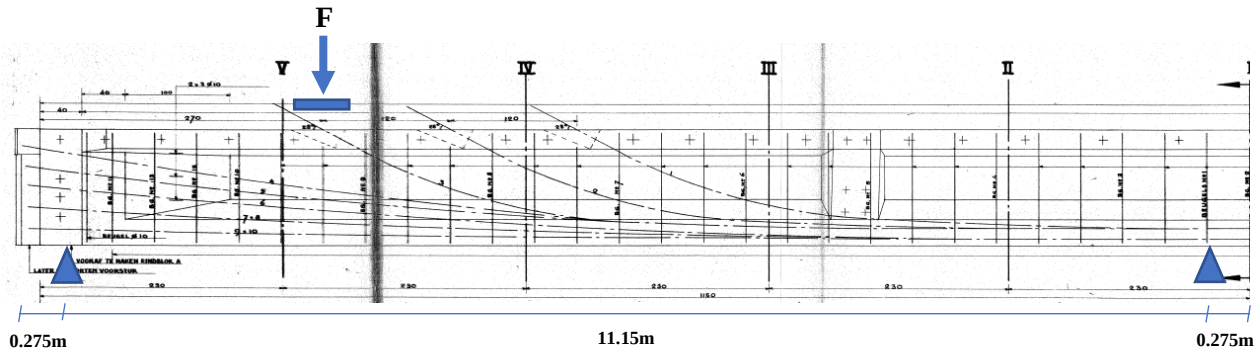

Figure 4.4 Experimental Set-up of 3- point bending test

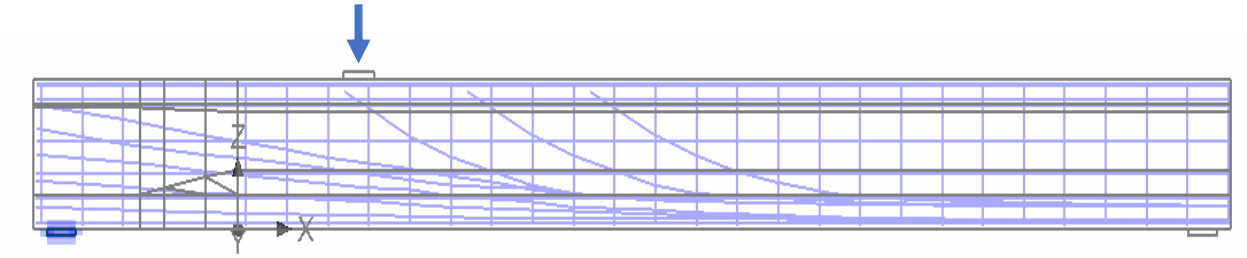

Figure 4.5 Numerical Test-setup of 3-point bending test.

4.3 Modeling input

The test setup is modelled in ATENA to investigate the shear capacity of the prestressed T girder. Before the external load is applied, the geometry of the beam, prestressing cables and reinforcements are modelled, and the respective material properties are assigned.

4.3.1 Geometry.

The geometry of the T girder is quite complex. The cross-section has a constant web thickness of 200 mm for the large part of the girder's span. This cross-section begins at 2 m from the right end of the girder and continues till the left end. At the right end of the beam the thickness of the web is 550 mm and then it continues to reduce linearly until it reaches the cross-section with constant web thickness of 200 mm (Figure 4.6).

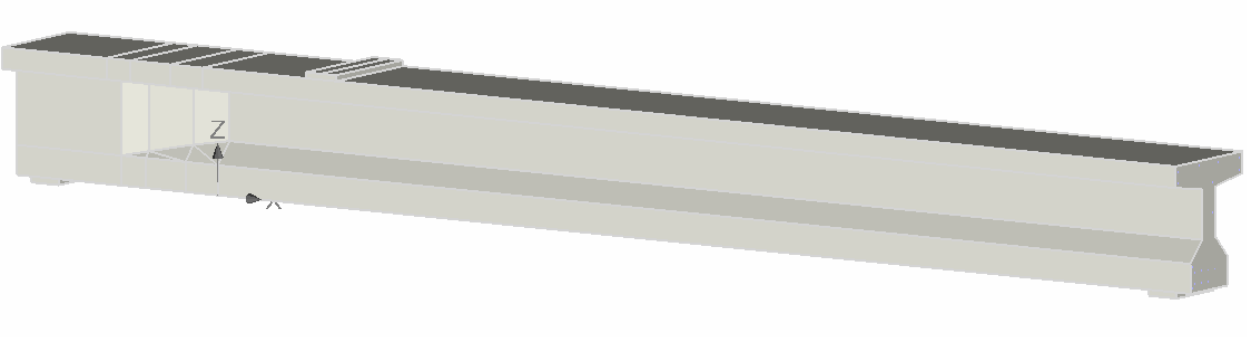

Figure 4.6 Geometry of post-tensioned T Beam

4.3.2 Material properties.

i. Concrete

Concrete class C53/65 is used in the beam with a mean compressive strength of (f_{cm}) 60 MPa and tensile strength (f_t) of 4 MPa.

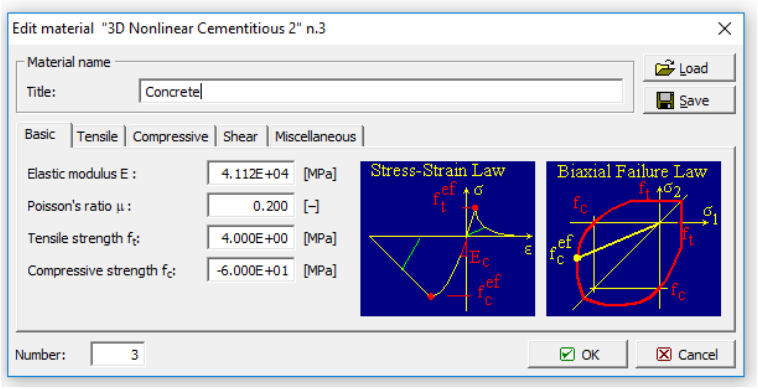

Figure 4.7 Compressive properties of concrete

ii. Reinforcement Steel.

Both longitudinal and shear reinforcement is provided with Ø 10 mm steel bars with a mean yield strength f_{ym} of 440 MPa. The steel is assumed to have ideally plastic behavior after reaching the yield strength. The shear reinforcement has a spacing of 400 mm.

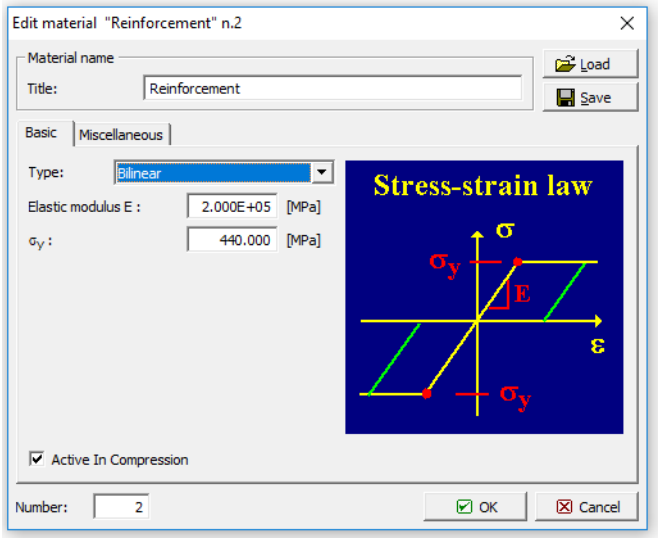

Figure 4.8 Properties of longitudinal reinforcing steel

iii. Prestressing cables.

Internal bonded tendons are used for prestressing. The tendons are post-tensioned and made of 12 wires each of 7 mm in diameter (Freyssinet type 12Ø7). The ultimate strength prestressing steel f_{pu} is 1670 MPa. Area of each tendon A_p is 462 mm^2.

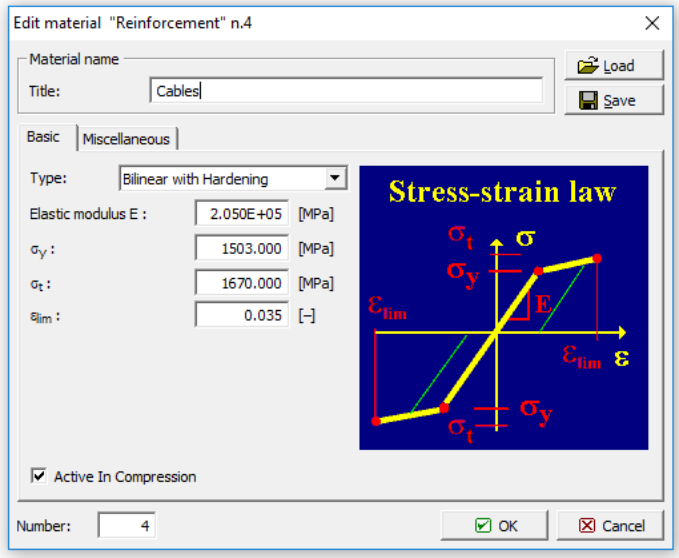

Figure 4.9 Properties of pre-stressing steel.

iv. Loading/Support plates.

Steel plates are used for support and loading platforms. Since the properties of the support and loading plates have a negligible impact on the results, the plates are assumed to be linear elastic isotropic.

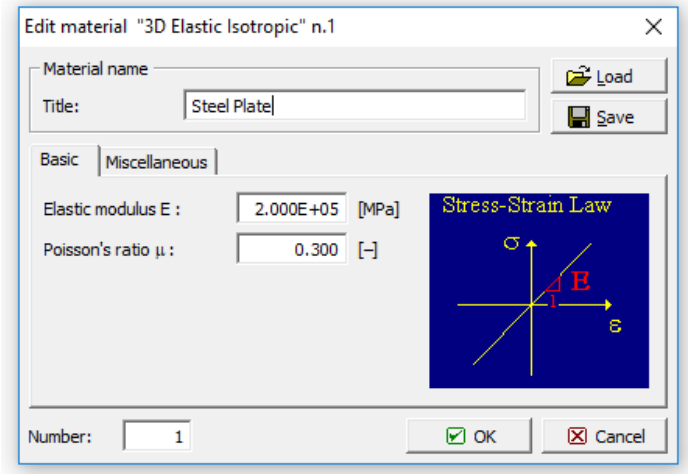

4.3.3 Forces acting on the T beam.

The load than act on the beam are self-weight of the beam, prestressing load and the external point load.

The self-weight is assigned as body forces in the model. The other two forces i.e., load from prestressing and external point load are critical for the tests.

Prestressing Load.

In reality, prestressing on the beams is applied in a post-tensioning manner i.e., after casting of concrete. In ATENA 3D prestressing is applied by defining cables as reinforcement bars with properties of the actual prestressing cables. The prestressing force is essentially defined for those reinforcements bars acting as prestressing tendons. The losses due to friction, wedge-set and time dependent losses are not taken into account in the prestressing force assigned in the model. This makes it a pre-tensioned load. In reality the beams are post-tensioned by stressing from both sides. Therefore, few calculations need to be made to obtain a value of prestressing that can be used in the model. Since the prestressing load in the non-shear region is not of significant importance for the test, using a single value of prestressing load is a fair approximation.

The maximum allowable initial stress is 65% of the ultimate strength of prestressing steel. This is equivalent to a prestressing load P_{mo} of 500 KN (each tendon). After calculating the losses due to friction, wedge-set and time dependent losses, prestressing load that can be used in the model is approximately 380 KN (each tendon). The calculation can be seen in Appendix 2. This prestressing load is applied along with the self-weight in gradual steps/load increments in the model.

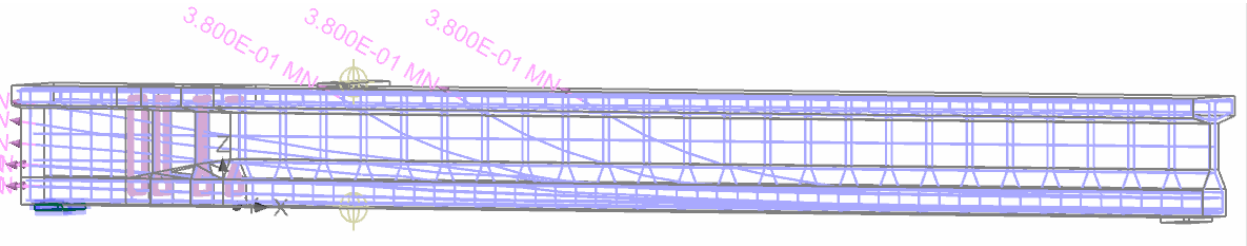

Figure 4.10 Model showing the prestressing forces.

External Point load.

The point load to determine the load bearing capacity of the T beam is applied at 2.903m from the left-hand support. To assess the post-peak behavior of the load-deflection curve, displacement-controlled loading in the model is used. The point load is applied as displacement in steps with increments until a well-defined post-peak region of the load-deflection is obtained. The deflection and load are measured by selection of nodes as monitoring points in ATENA model. Load is measured at the point of application of the load and deflection directly below the load on the bottom fiber of the beam.

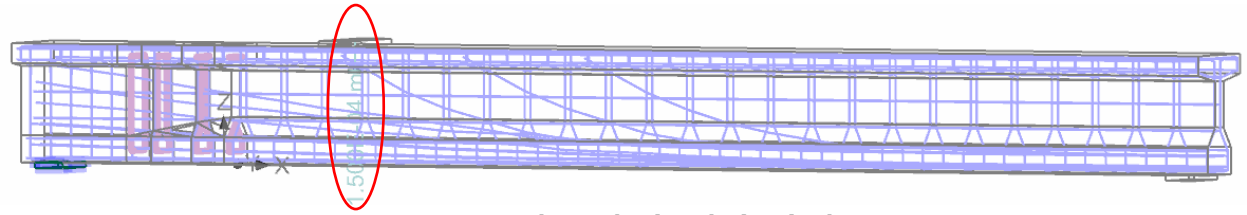

Figure 4.11 External point load applied at displacement.

4.3.4 Mesh Generation

Roughly 5-6 elements per beam thickness is required to accurately capture bending in the ATENA analysis. Therefore, mesh with element size of 200 mm is chosen. Also keeping in mind that as the element size reduces computation speed decreases. Linear tetrahedral elements are used for the mesh (Figure 4.12).

Once the mesh is generated, analysis can be made, and results can be obtained from the post-processor.

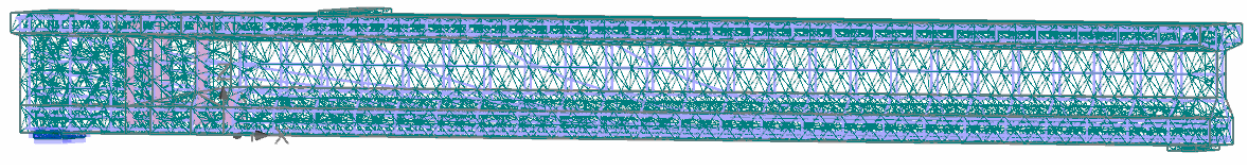

Figure 4.12 Mesh in ATENA model of T beam.

4.4 Test Series

To determine the possible failure mechanism and load capacity of the T beam, 3 - point bending test is used. The reference beam is first tested to determine its failure mechanism – whether a brittle shear failure occurs in the beam. Then UHPFRC is used to strengthen the beam and the strengthened beam is tested under the same loading conditions to determine possible increase in load capacity and improvement in structural behavior.

4.4.1 Reference Beam.

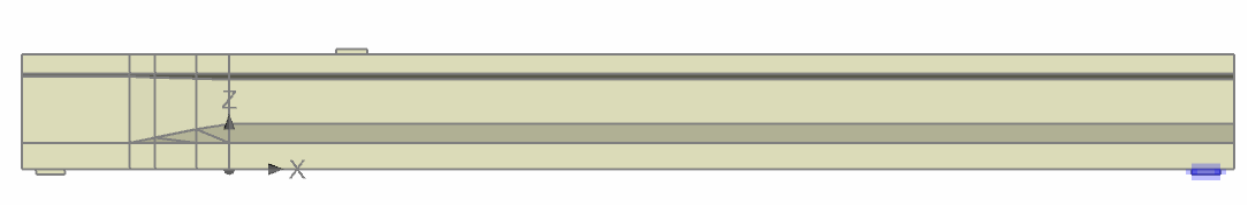

In the numerical simulations, the prestressing load is added along with self-weight in gradual steps with load increments. After the complete prestressing load and self-weight has been applied, the external point load is then applied as displacements in load steps with increment after each step.

4.4.2 Strengthened Beam.

The T beam is strengthened with UHPFRC composite on both sides of the web. The strain hardening property of the UHPFRC material can be effective to prevent brittle shear failure and increase the ultimate capacity. The strain hardening of behavior of UHPFRC is shown in Figure

4.13. The UHPFRC used in the strengthening application have a tensile strength f_t of 7.0 MPa and an ultimate tensile capacity f_{ut} of 8.0 MPa.

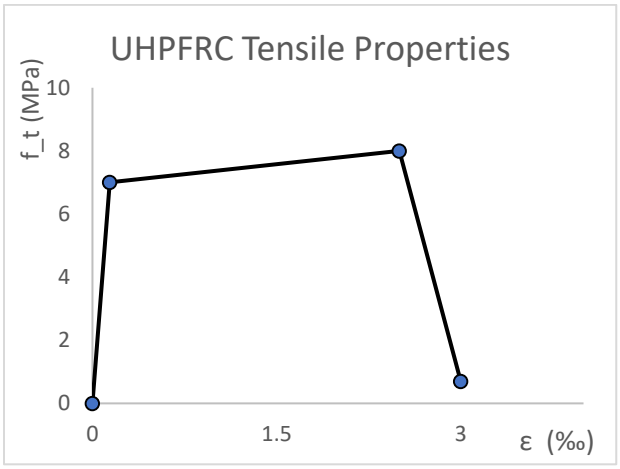

Figure 4.13 Tensile properties of UHPFRC Composite.

The composite is added on both sides of the web by side bonding. A perfect bond is assumed between the concrete and UHPFRC composite. The composite is added in the shear span of the beam, i.e., from 0.96m from the left-hand support till the loading point.

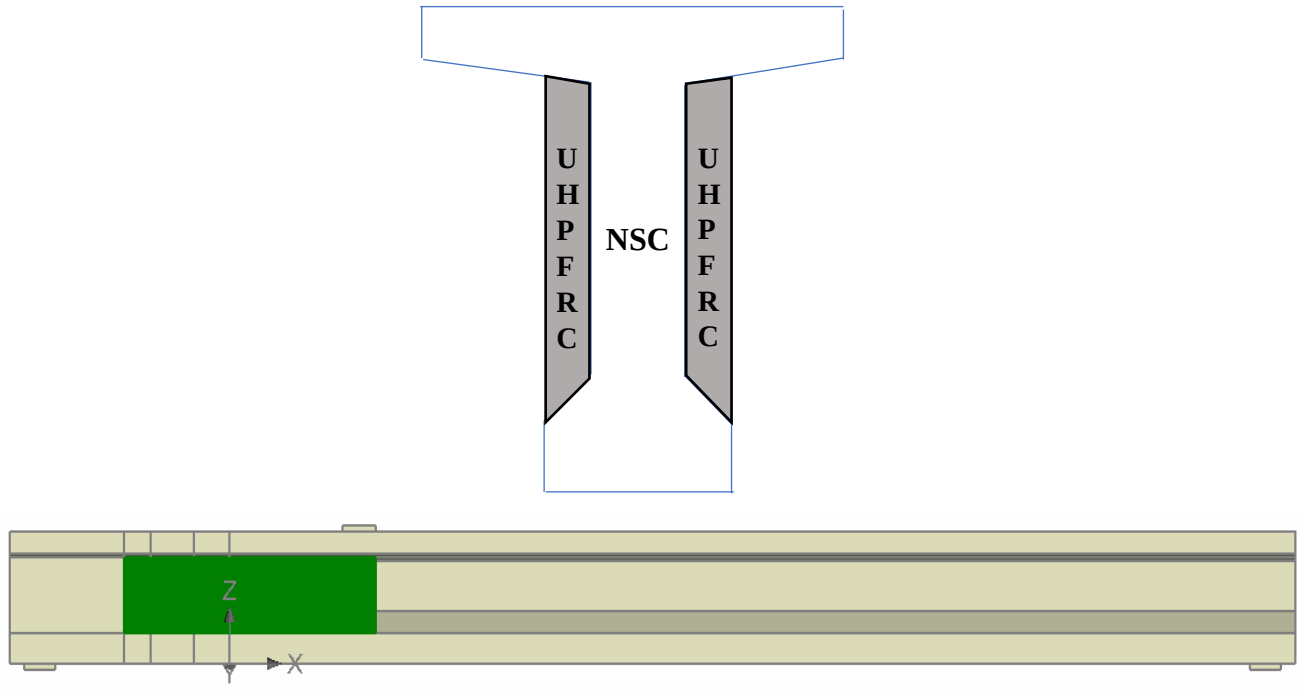

Figure 4.14 Configuration for strengthening of T beam - Cross-section (top) & Span (bottom).

In the ATENA model, the UHPFRC elements are added after the prestressing load has been completely applied. This is done using construction cases available in the ATENA programme [42].

5 Results & Discussions.

In this section the results obtained from the numerical simulation of the 3-point bending test on the T beam are presented and the results are analyzed. The load-deflection curves indicating the ultimate capacities and the crack patterns of the deformed beams are presented and discussed.

Before the results are analyzed, the ATENA model is validated by simple calculations.

5.1 Validation of ATENA model.

The ATENA model is validated by simple calculations for deflection under self-weight. Another check is the deformed shape and stresses at the top and bottom fibre of the T beam resulting from the curvature pressure of the prestressing load.

5.1.1 Deflection of T beam under self-weight.

Since the T beam is simply supported, the maximum deflection (at midspan position) can be easily calculated using formula $\delta = \frac{5qL^4}{384EI}$, where q is the uniformly distributed load due to self-weight. $q = A_c \times \gamma_c$, A_c – cross-sectional area of concrete & γ_c – specific weight of concrete. To make calculations easier A_c is calculated from the nominal cross-section of the T beam which is equal to 0.517 m^2. Specific weight of concrete γ_c = 23 KN/m^3, which gives q = 11.9 KN/m. With span L = 11.15 m, E = 41,100 MPa & I = 0.0747 m^4, deflection at midspan δ = 0.78 mm.

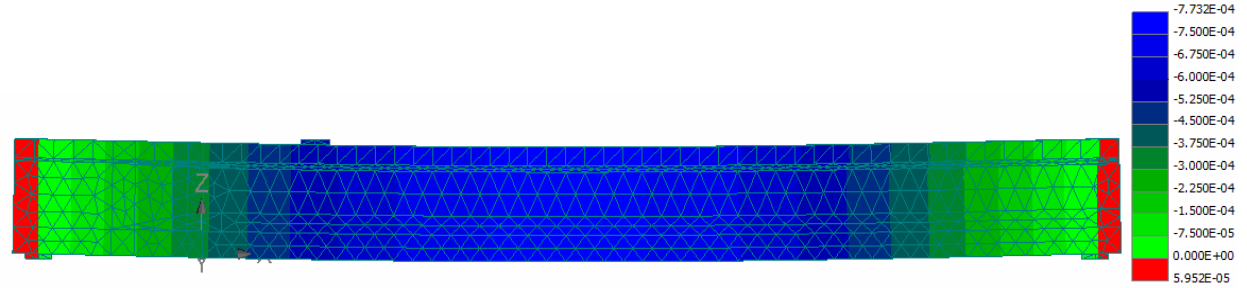

Figure 5.1 Deflection due to self-weight of beam in m

From the ATENA model we have deflection due to self-weight at midspan δ = 0.77 mm.

5.1.2 Check for deformed shape and stresses due to prestressing curvature pressure.

The prestressing cables in the T beam have a curved profile with a downward curvature. The curvature pressure resulting from the cables on the concrete causes a bending moment with an upward curvature on the beam. The stresses on concrete due to this curvature pressure are checked to see if tensile stresses are generated. The stresses are checked at both top and bottom fiber at 2 locations. 1. At the point of application of external load 2. At right hand support position. It should

be noted that the self-weight of beam that causes a downward curvature. Therefore, the stresses are calculated for the combination of both self-weight and curvature pressure due to prestressing. The calculations can be found in Appendix 2.

From the calculations we find that at the loading point, compressive stresses occur at both top and bottom fiber. σ_{ct} = 0 MPa & σ_{cb} = -11.6 MPa. At right hand support position tensile stresses occur at the top fiber and compressive stresses at the bottom fiber. σ_{ct}= +5.65MPa & σ_{cb} = -23.75 MPa. The tensile stresses at the top fiber at right hand support position exceed the tensile strength of concrete (f_t =4.0 MPa) resulting in cracking of concrete.

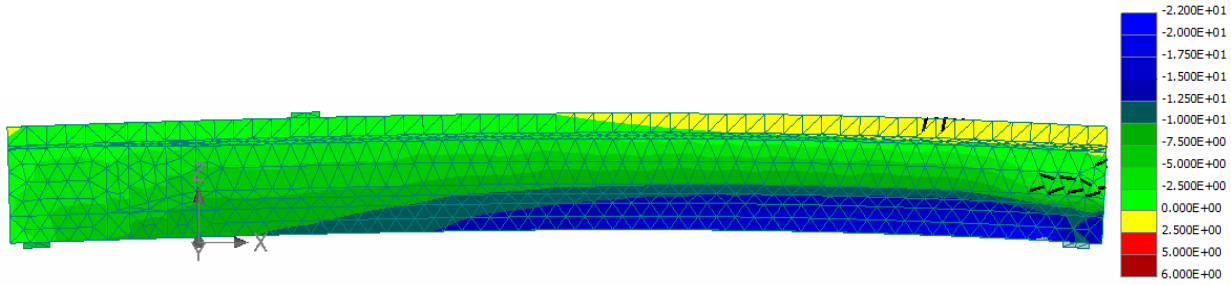

Figure 5.2 Normal Stress σ_{xx} in concrete due to self-weight & prestressing (MPa)

The ATENA model accurately calculates the stresses at all positions except the top fiber at right hand support. Here the stress is +2.5 MPa whereas the calculation gives tensile stress of +5.65 MPa. The difference could be because of the crack formation. Once the crack is opened, the tensile stresses in the concrete are reduced.

From the above two checks it can be that the ATENA model predicts the behavior of the post-tensioned T beam with reasonable accuracy and the model can be used for investigation of the failure mechanism and determination of ultimate load capacity of the T beam subjected to 3-point bending test.

5.2 Reference Beam.

The reference T beam is tested under the 3-point bending load and the load-deflection curves are obtained from the analysis. The beam from now on is referred to as T-R0. The results from the simulations are presented.

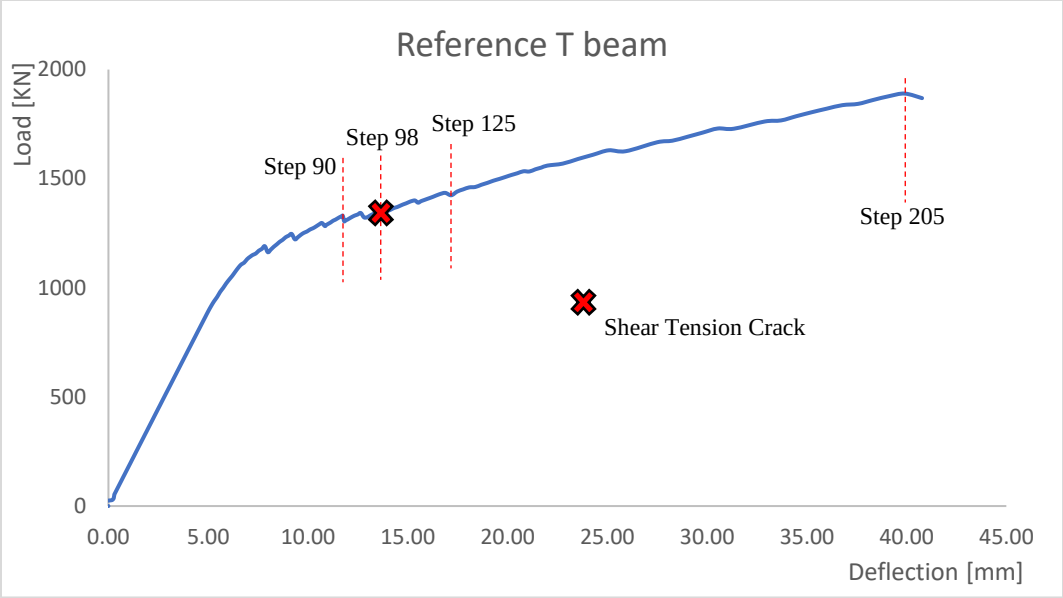

Figure 5.3 Load-Deflection curve for reference T-R0 beam.

The reference T beam has an ultimate capacity of 1890 KN and a maximum deflection of 42 mm. The shear capacity V_u can be calculated from the ultimate capacity (see Figure 5.4).

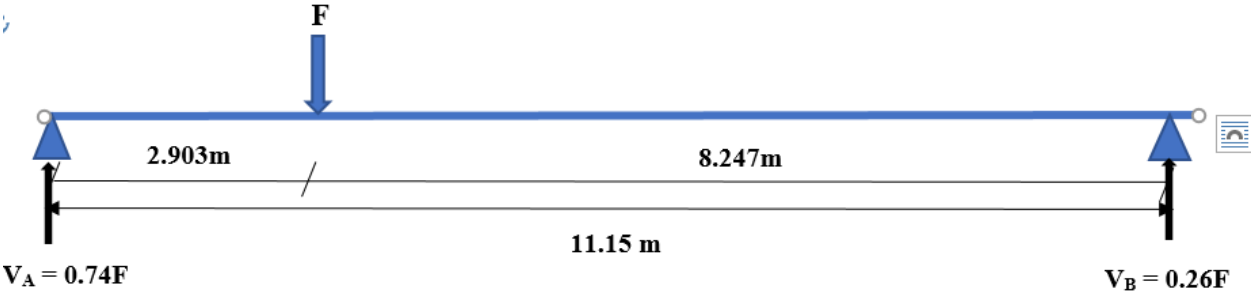

Figure 5.4 Loading scheme in the 3-point bending test.

From Figure 5.4, $V_u = 0.74$. F = 0.74 x 1890 = 1400 kN is the shear capacity of the post-tensioned T beam.

The deformation of the beam is observed at different load intervals to investigate the failure mode and crack patterns. For a certain load interval, a threshold crack width is selected *(threshold crack: only cracks with crack widths larger than this value are seen).* A threshold crack width of 50 micron is chosen.

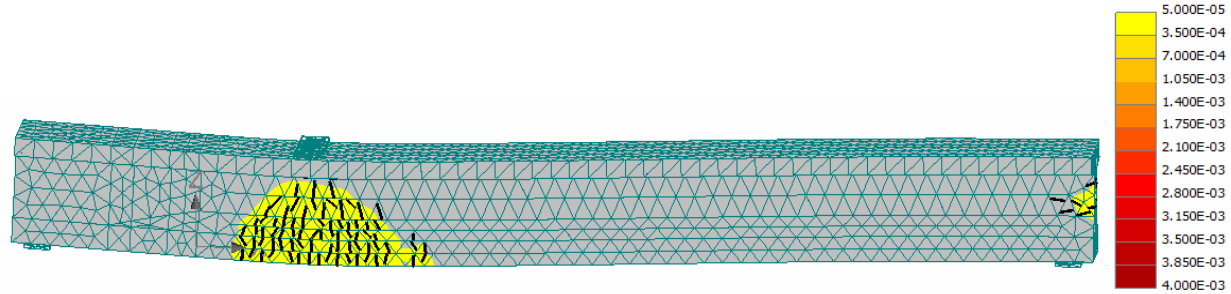

Figure 5.5 Crack Pattern of T-R0 at load = 1330 KN.

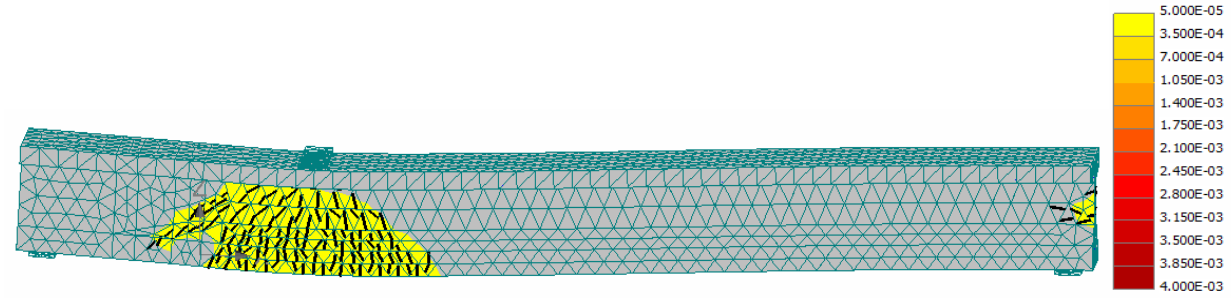

*Figure 5.6 Crack Pattern of T-R0 at Load = 1340 KN (**Shear crack opening**)*

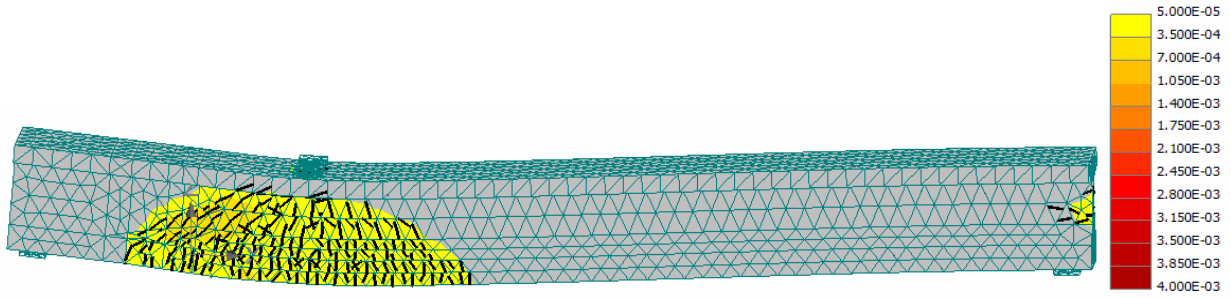

Figure 5.7 Crack pattern of T-R0 at Load = 1440 KN.

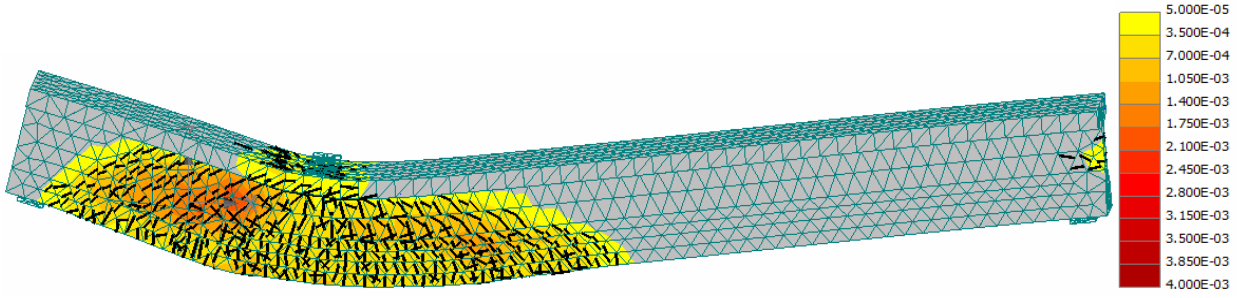

*Figure 5.8 Crack pattern of T-R0 at Load = 1890 KN. (**Failure load**).*

From the deformed shapes presented, it is evident that a shear crack opens at a load level of 1343 kN. Therefore, the cracking shear force V_{cr} = 0.74x1343 =994 kN.

The shear crack is a shear tension crack opening as a result of the principal tensile stresses exceeding the concrete tensile strength. After the formation of the shear tension crack, the load

continues to increase leading to formation of more shear cracks. These cracks are flexural shear cracks that result from flexural cracks and incline inwards due to effect of the shear force acting near the support region.

5.2.1 Shear crack opening.

The opening of shear crack is observed by using monitoring points to determine the shape and difference in crack widths in the shear span before and after opening of the shear crack.

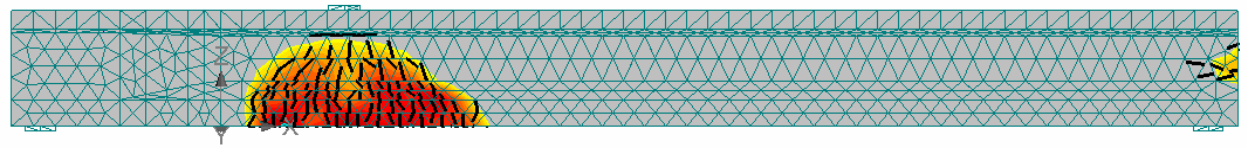

*Figure 5.9 Crack Pattern in T-R0 beam just **before** the shear crack.*

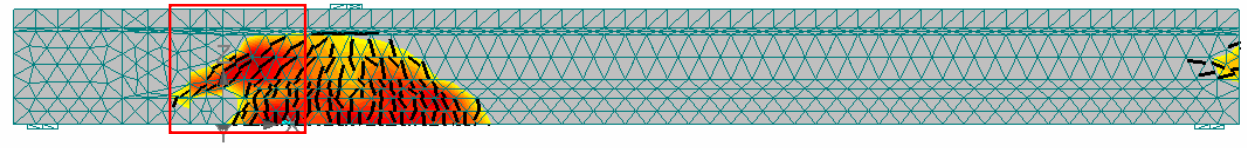

*Figure 5.10 Crack Pattern in T-R0 beam just **after** the shear crack.*

To investigate the opening of the shear crack, the crack width is measured just before and after the opening. The cracks widths are measured over the height of the beam at different locations along the shear span where the crack is expected to occur.

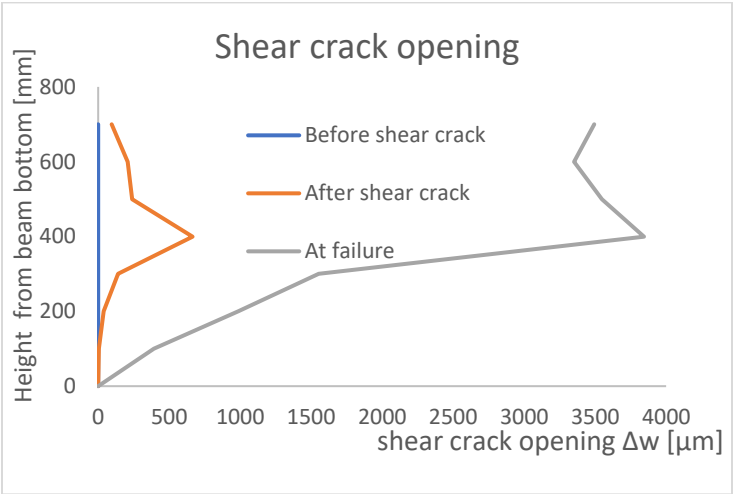

Figure 5.11 Shear tension crack opening in beam T-R0

At the onset of the shear tension crack, the total crack width at a level 400 mm from the bottom of the beam is the largest. This level happens to be close to the centroidal axis of the beam, which is at 618mm from the bottom fiber level.

The crack opened is a shear tension crack with the total crack width at 400 mm level being larger than 600 μm. This is checked against the crack pattern in the model after the shear crack has opened.

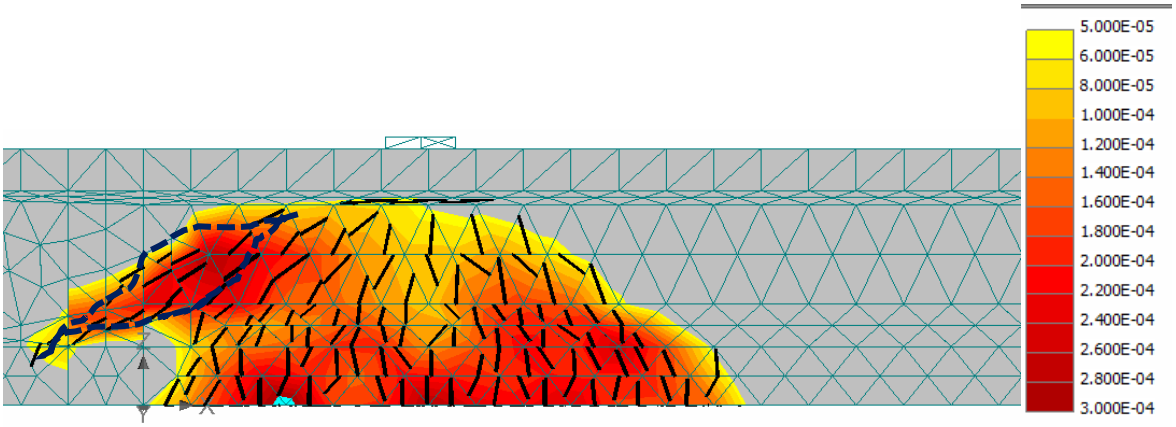

Figure 5.12 Crack width at the onset of shear tension crack in T-R0 (m).

At a height of 400 mm, there are 2 elements cracked, each with a crack width of 300 μm, which makes the total crack width 600 μm.

5.2.2 Failure Mode.

Although a critical shear tension crack opens at a load of 1340 kN, this crack does not develop into a failure mechanism. Due to action of the stirrups, many such cracks are developed, and the beam ultimately fails in compression at the top flange. The failure occurs at a load of 1890 kN. By checking the normal stresses in the beam at failure, it is evident that the compressive stresses in the top flange of the T beam reach the concrete compressive strength (60 MPa). The analysis is aborted once the compression failure occurs.

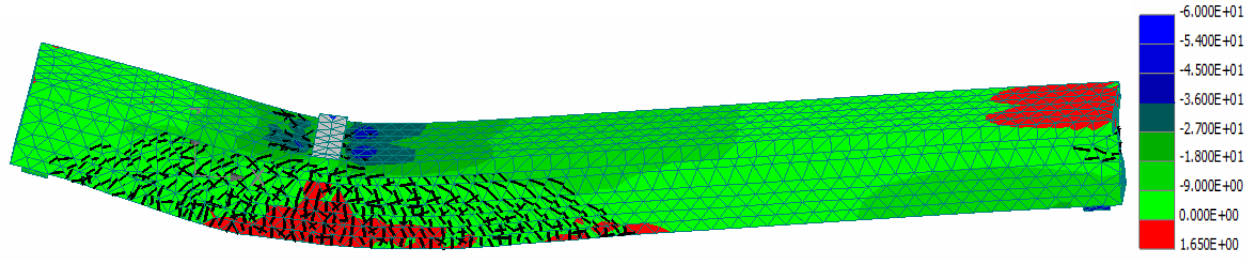

Figure 5.13 Normal stresses σ_{xx} in concrete at failure in T-R0 (MPa).

Figure 5.14 shows the stresses in both longitudinal steel and stirrups. Both longitudinal and transverse reinforcements have yielded at failure. Looking at the stresses in tendons, show that the even the tendons have reached their yield strength at few locations (Figure 5.15).

From calculations of the moment capacity of the beam, the load capacity of the beam in bending $F_{bending}$ is 1935 kN. (Appendix 3). Also, the load bearing capacity of the compressive strut is calculated from the equation $V_{Rd,\,max} = \alpha_{cw}.b_w.z.\upsilon.f_{cd}.\sin\theta.\cos\theta + V_{P,\,\infty}$.

θ is the crack inclination angle and is simplified to 21.8°. $V_{P,\,\infty}$. is the vertical component of prestressing force in the tendons, b_w is the thickness of the web, f_{cd} is the concrete compressive strength, z is the internal lever arm.

The capacity of the concrete compressive strut $V_{Rd,\,max}$ is approximately 1467 kN. This corresponds to a load capacity F of 1980 kN. Although this load capacity has not been reached in the test at failure, the compressive stress has reached the concrete compressive strength of 60 MPa as shown in Figure 5.13.

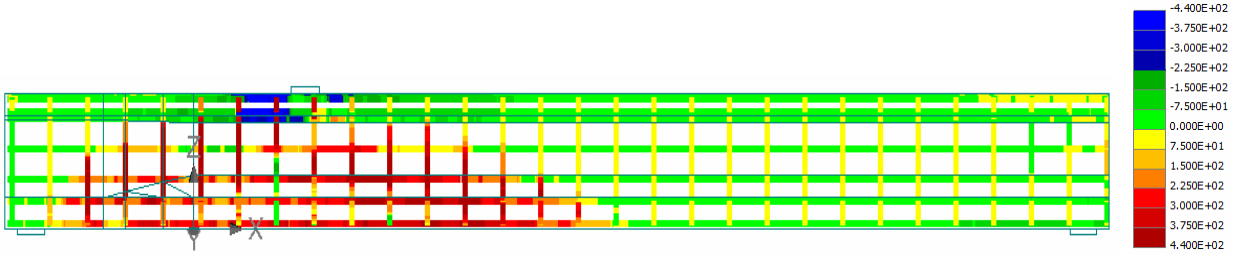

Figure 5.14 Normal stresses σxx in stirrups and longitudinal reinforcement at failure in T-R0 (MPa).

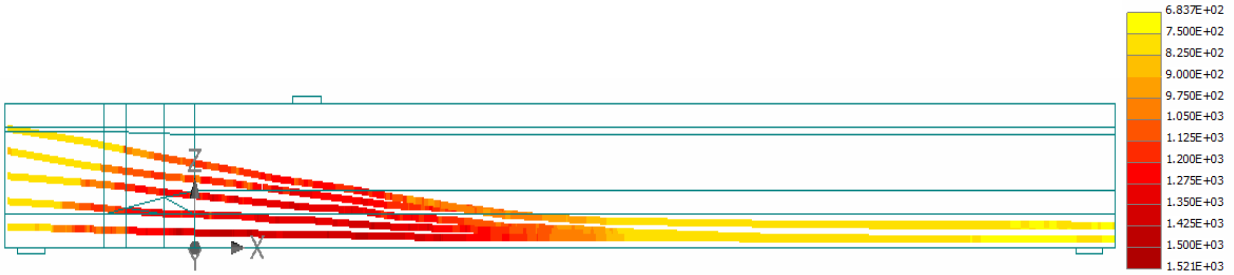

Figure 5.15 Normal stresses σxx in prestressing tendons at failure in T-R0 (MPa).

In summary, the post tensioned T beam does not exhibit a clear shear failure but fails in concrete compression at the top flange after the formation of shear tension and flexural shear cracks. Since the numerical simulations did not show a clear shear failure in the reference beam, the shear reinforcements were removed from the beam in the model to check whether the post tensioned T beam without the stirrups fails in a brittle shear mode.

5.3 Reference beam without stirrups.

The same test set-up is used for the post-tensioned T beam without stirrups to determine its failure mode and ultimate capacity (see Figure 5.16) The beam without stirrups is denoted by T-R1.

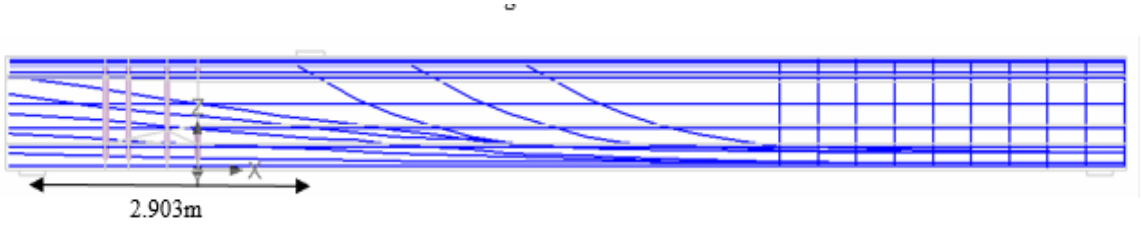

Figure 5.16 Reference T beam without stirrups (T-R1).

The load deflection curve of the T beam without stirrups is very similar to the reference beam T-R0 (with stirrups). However, the ultimate load capacity of the beam without stirrups is slightly lower than T-R0. The T beam without stirrups has a peak load of 1720 kN and a maximum deflection of 36.7 mm. The shear capacity of the beam V_u is equal to 1273 kN.

A shear tension crack is formed at the same load level as it did in T-R0 i.e., 1340 kN. (V_{cr} = 990 kN) Once again, the shear crack did not localize leading to a brittle shear failure even in the absence of stirrups. Normally, in beams without shear reinforcements, it is expected that the shear cracks once formed localize and develop into a failure mode. However, this is not seen in the post-tensioned T beam without stirrups. Here too, the formation of several flexural shear cracks can be seen before the compression failure of concrete in top flange.

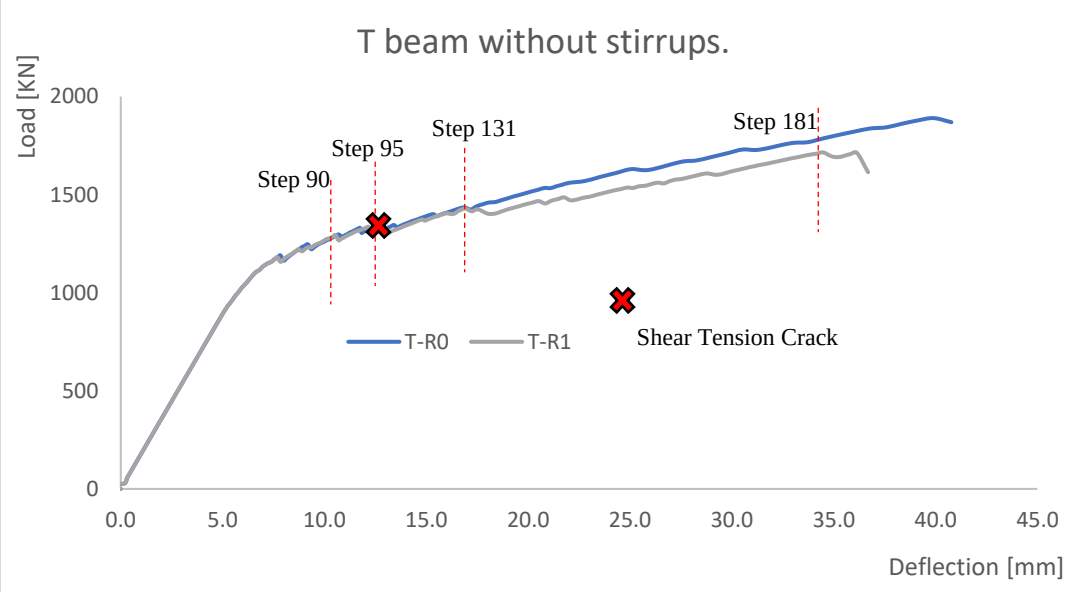

Figure 5.17 Load-deflection curve in beam T-R1.

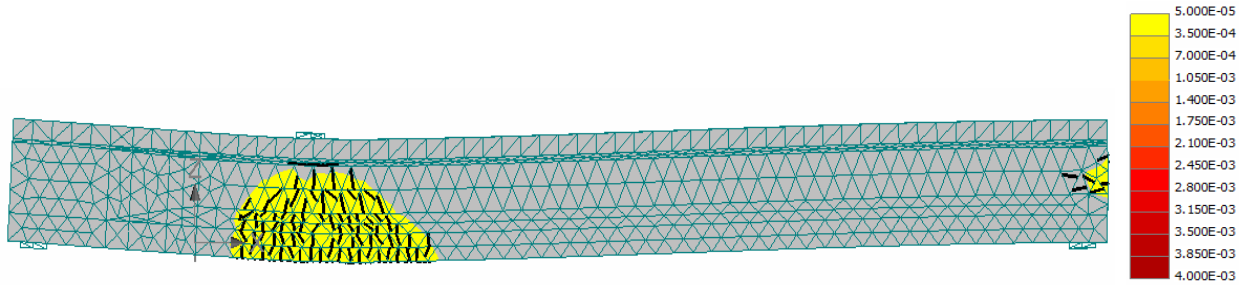

Figure 5.18 Crack Pattern of beam T-R1 at load = 1330 KN.

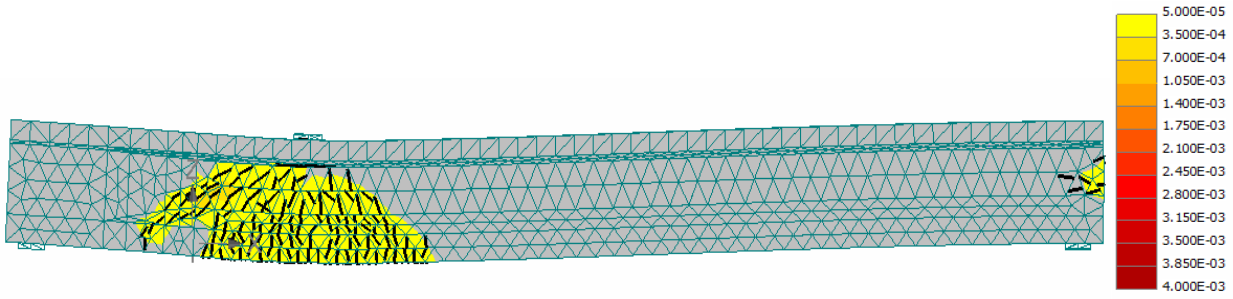

*Figure 5.19 Crack Pattern of beam T-R1 at load = 1340 KN (**shear crack opening**).*

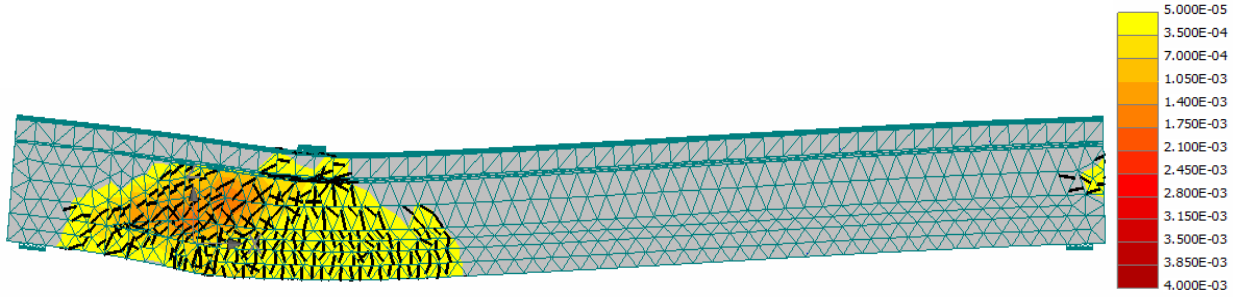

Figure 5.20 Crack pattern of beam T-R1 at Load = 1440 KN.

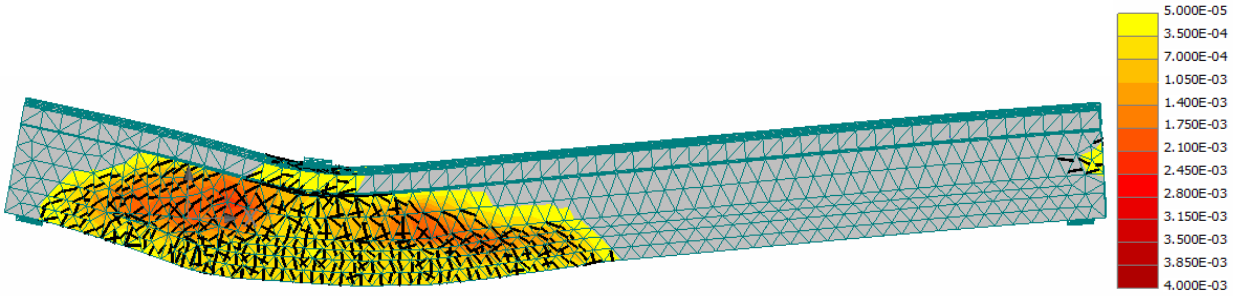

*Figure 5.21 Crack pattern of beam T-R1 at Load = 1720 KN. (**Failure load**).*

5.3.1 Shear crack opening.

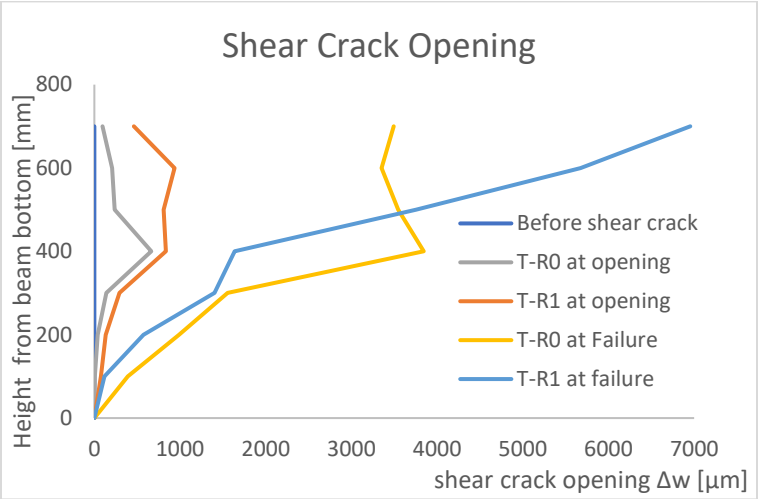

Figure 5.22 Shear tension crack opening in T-R0 and T-R1.

In the absence of stirrups, the crack width of the shear tension crack is larger at the onset of cracking. The crack is the largest near the centroidal axis of the beam. Here the width of the crack is almost 1 mm.

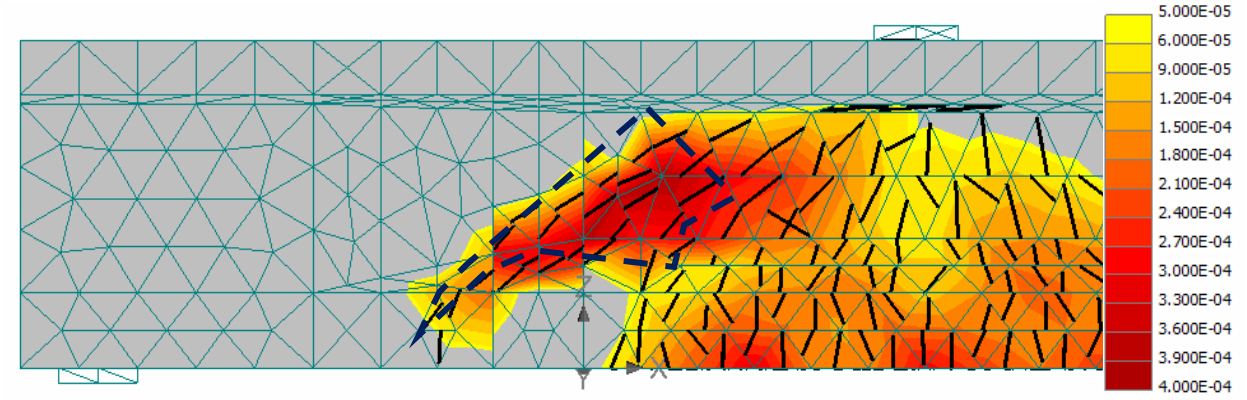

Figure 5.23 Crack width at the onset of shear tension crack in beam T-R1 (m)

5.3.2 Failure Mode

The post-tensioned T beam without stirrup too shows a concrete compression failure at the top flange of the beam.

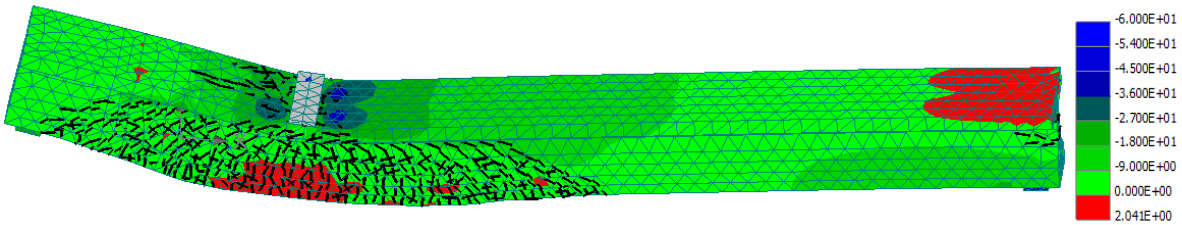

Figure 5.24 Normal stresses σ_{xx} in concrete at failure in T-R1 (MPa).

The stresses in the longitudinal steel reached the yield strength of steel but the prestressing tendons have not yielded yet (Figure 5.25 & 5.26).

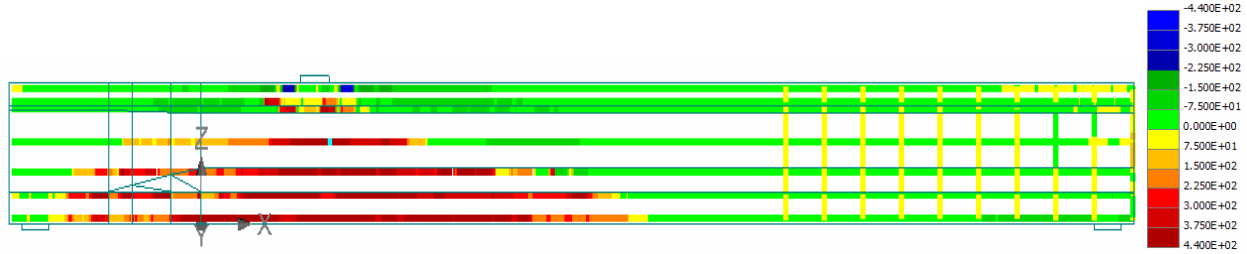

Figure 5.25 Normal stresses σxx in longitudinal steel at failure in T-R1 (MPa).

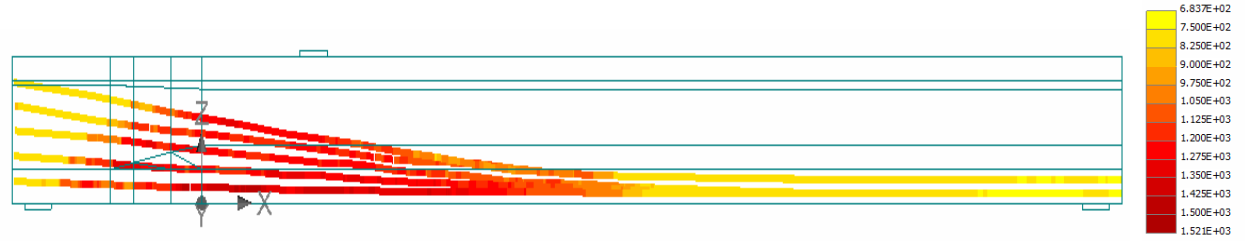

Figure 5.26 Figure 5.26 Normal stresses σxx in prestressing tendons at failure in T-R1 (MPa).

There was no difference in the type of failure modes between beams with and without stirrups. In the next step, the influence of the fracture energy and shear crack stiffness factor of the concrete on the failure mode was investigated. Both parameters were reduced to 10% of their default values in the material model of concrete (Table 5-1). By reducing the fracture energy and shear crack stiffness, the T beam without stirrups is tested to check whether a brittle shear failure can develop immediately after the shear tension crack was opened. This beam is denoted by T-R2.

Table 5-1 Difference between beams T-R1 & T-R2

Beam	Shear Reinforcement	Fracture Energy (N/m)	Shear Crack Stiffness Factor
T-R1	No shear reinforcement	100	20
T-R2	No shear reinforcement	10	2.0

5.4 Reference Beam T-R2.

The post tensioned T beam without stirrups with reduced fracture energy and shear crack stiffness factor was tested under the 3-point bending simulation to investigate whether the reduction can cause a brittle shear failure in the beam.

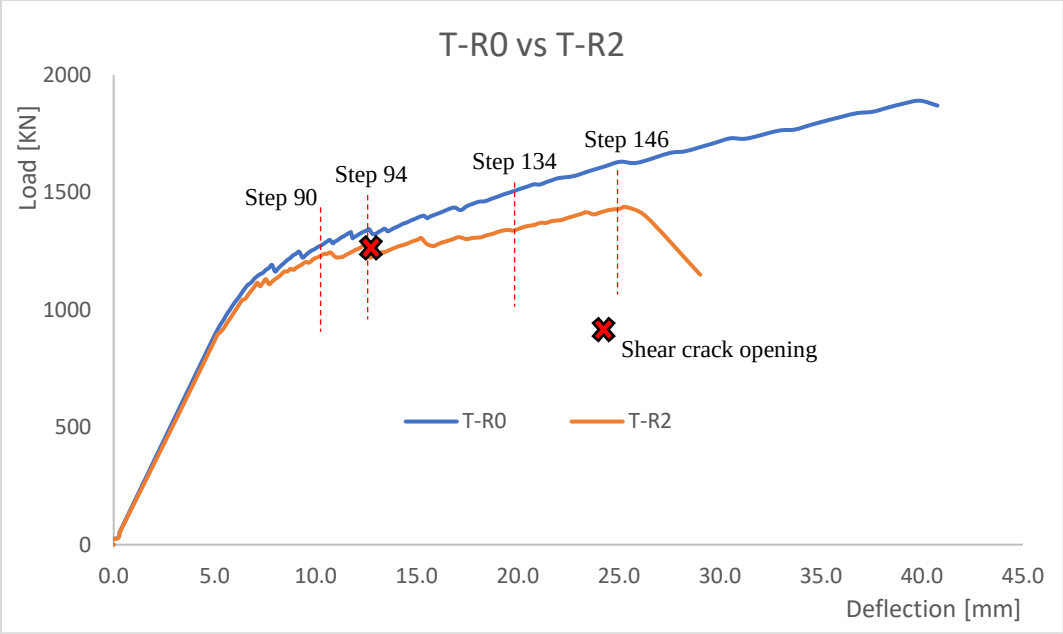

Figure 5.27 Load-deflection curve in beam T-R2.

In this beam, the shear tension cracks forms at a load of 1277 kN, which translates to a cracking shear force V_{cr} of 945 kN. This is at a lower level compared to the previous beam (T-R1). After the formation of the shear crack, the load increases until it reaches a peak load of 1437 kN. (shear strength V_u = 1064 kN). The maximum deflection is 28 mm.

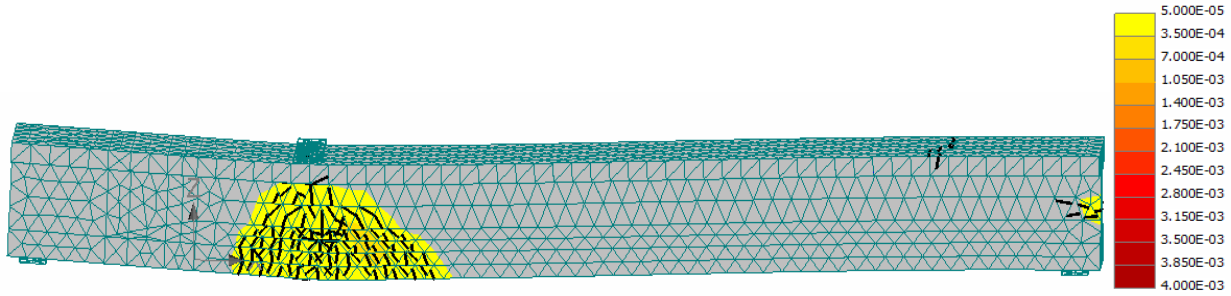

Figure 5.28 Crack pattern of T-R2 at Load = 1260 KN

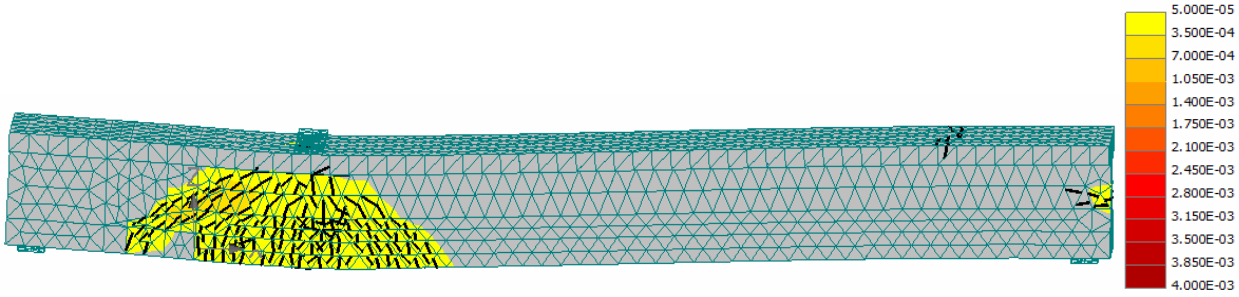

*Figure 5.29 Crack pattern of T-R2 at Load = 1277 KN (**shear crack opening**).*

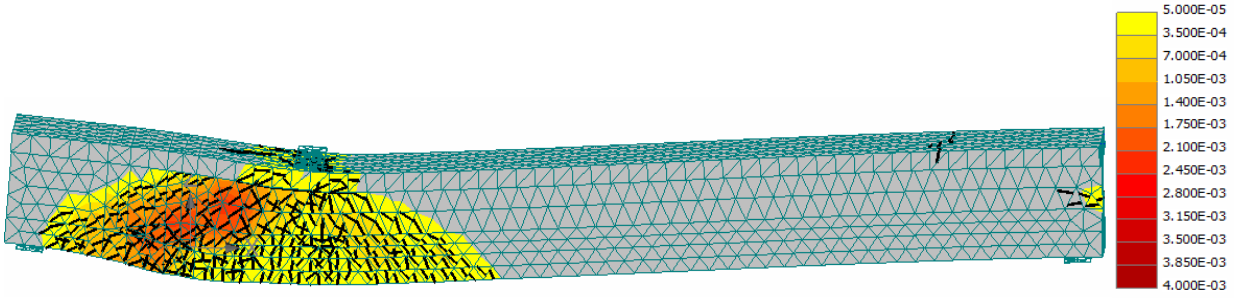

Figure 5.30 Crack pattern of T-R2 at Load = 1370 KN.

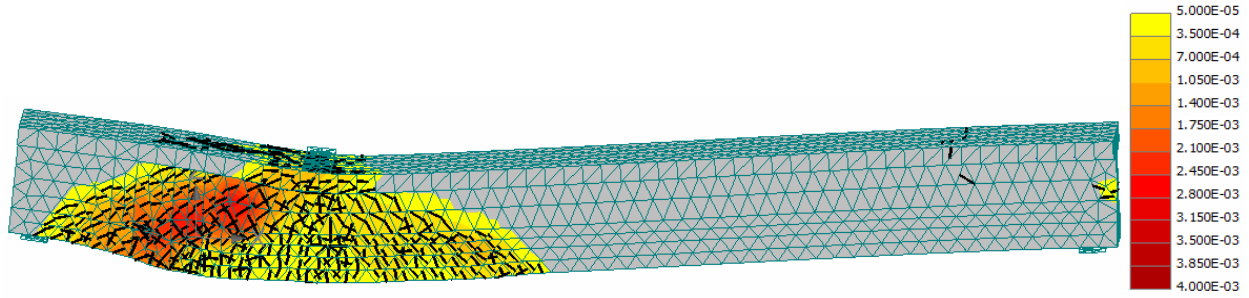

*Figure 5.31 Crack pattern of T-R2 at Load =1437 KN (**Failure load).***

5.4.1 Shear Crack opening

The opening of the shear crack is compared for beam T-R0 and T-R2. The crack width is measured as explained in 5.3.1.

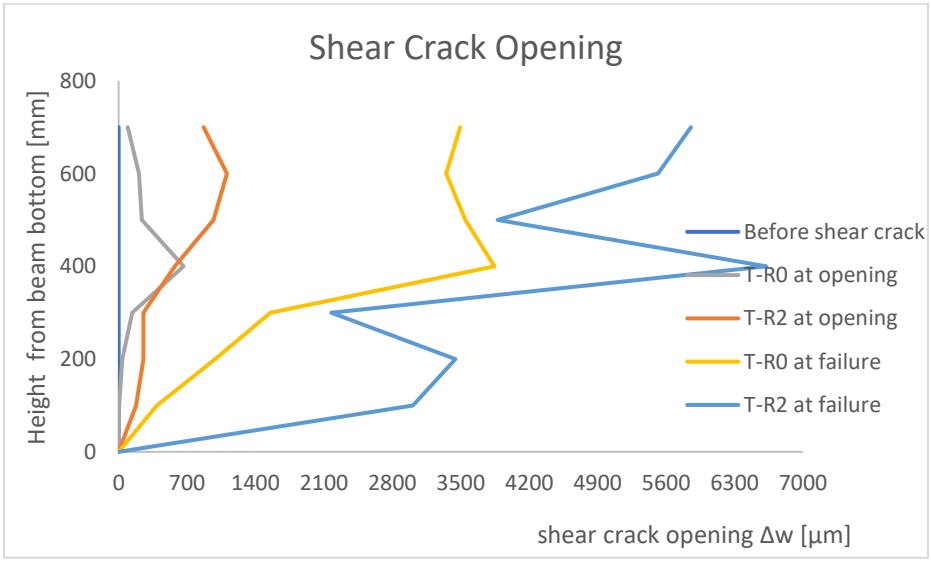

Figure 5.32 Shear tension crack opening in beam T-R0 & T-R2

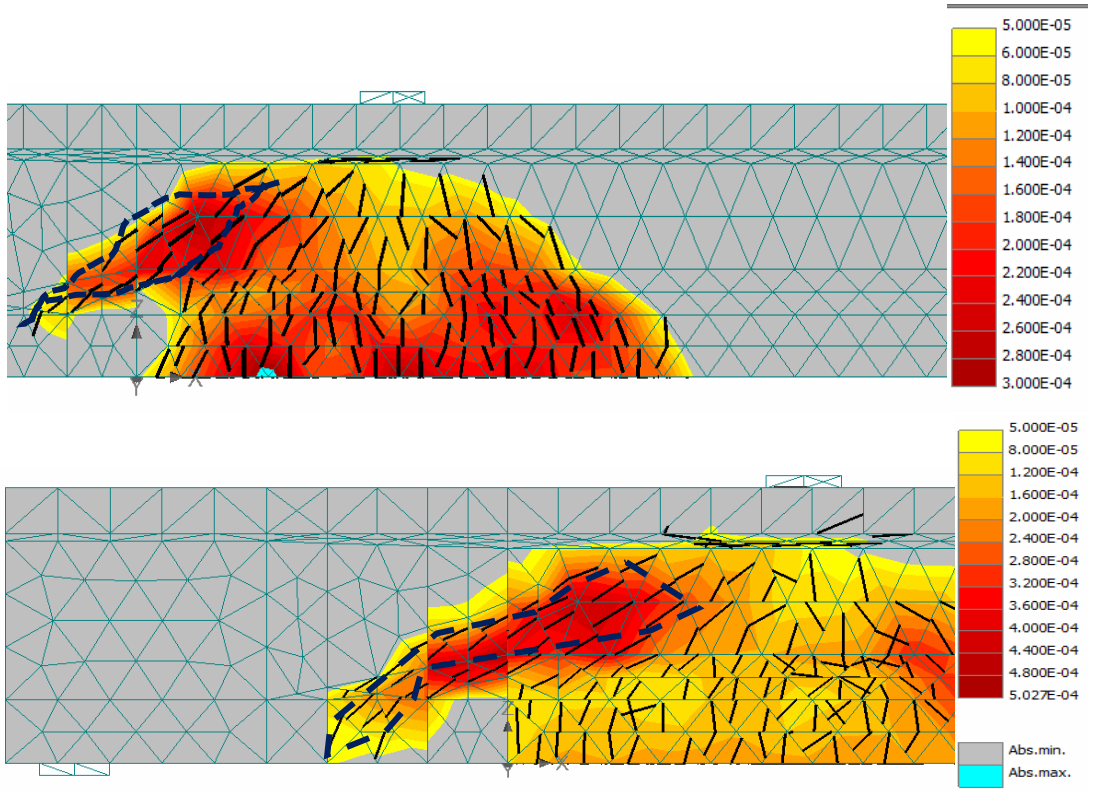

Figure 5.33 Crack width at the onset of shear tension crack in T-R0 (top) & T-R2 (bottom) (m).

Due to the absence of stirrups and reduction in fracture energy and shear crack stiffness factor, the crack width of the shear tension crack at opening is higher than it is in beam T-R0.

5.4.2 Failure Mode.

The final failure mode is once again by concrete compression in the top flange accompanied by formation of several flexural shear cracks. Even the reduction in the fracture energy and shear crack stiffness does not seem to induce a shear tension failure.

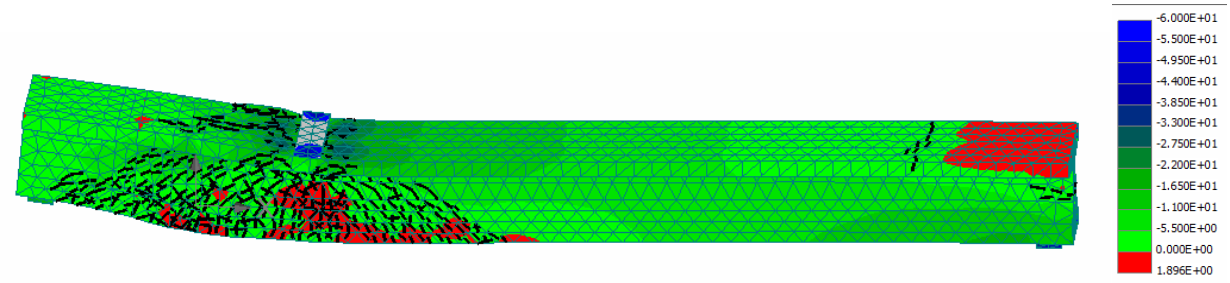

Figure 5.34 Normal stresses σxx in concrete at failure in T-R2 (MPa).

Both the longitudinal reinforcement and prestressing tendons have not reached their yield strength yet (Figure 5.35 and 5.36).

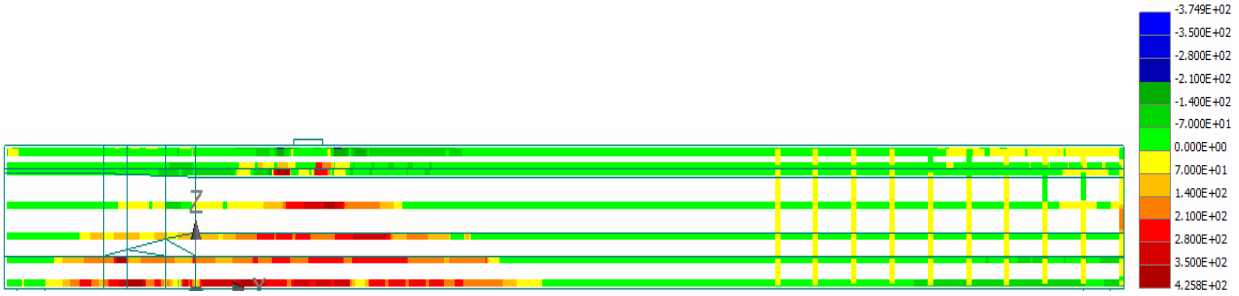

Figure 5.35 Normal stresses σxx in longitudinal steel at failure in T-R2 (MPa).

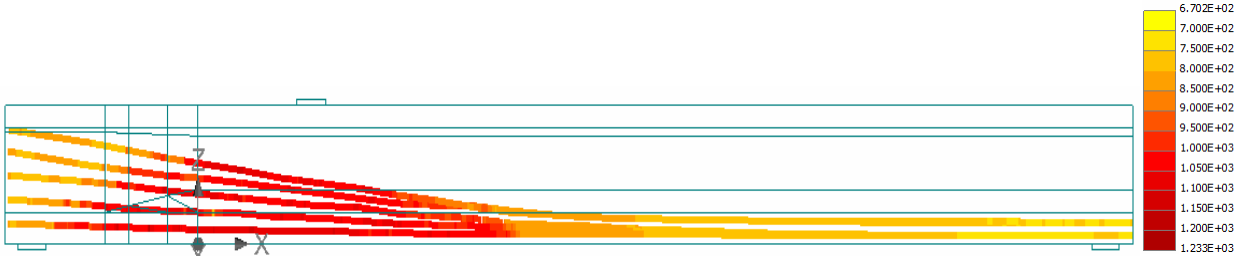

Figure 5.36 Normal stresses σxx in prestressing tendons at failure in T-R2 (MPa).

In the next step, 3 inclined prestressing cables crossing the shear span are removed from the beam in the model and tested. This is done to investigate whether absence of the prestressing tendons will cause localization of the shear tension crack without further crack propagation. The beam without the 3 cables and stirrups is denoted as T-R3.

5.5 Reference beam T-R3.

The effect of removing the 3 prestressing tendons on the failure mode of the T beam without stirrups is tested in this section.

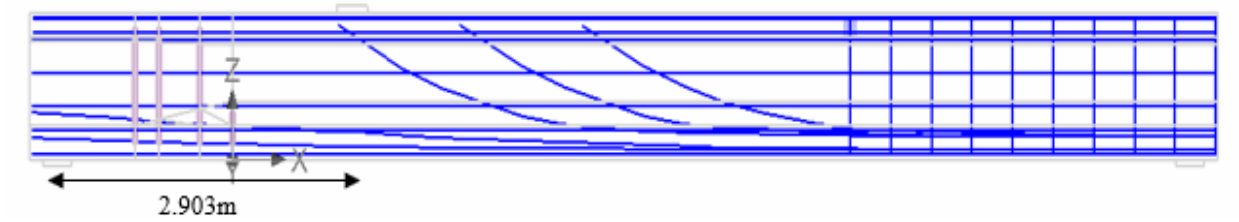

Figure 5.37 T beam without stirrups and inclined prestressing cables.

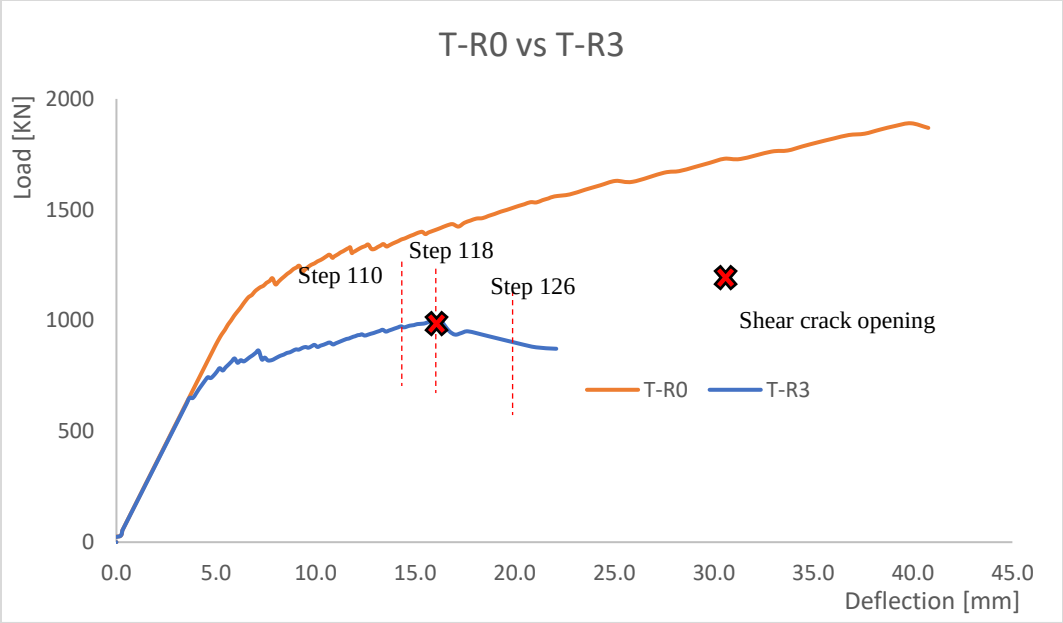

Figure 5.38 Load-deflection curve for beam T-R3.

The peak load in the load-deflection curve corresponds to 1009 kN. Therefore, the shear capacity V_u of the beam T-R3 is 746 kN and the maximum deflection is 22 mm. This is the lowest strength and ductility among all the beams tested.

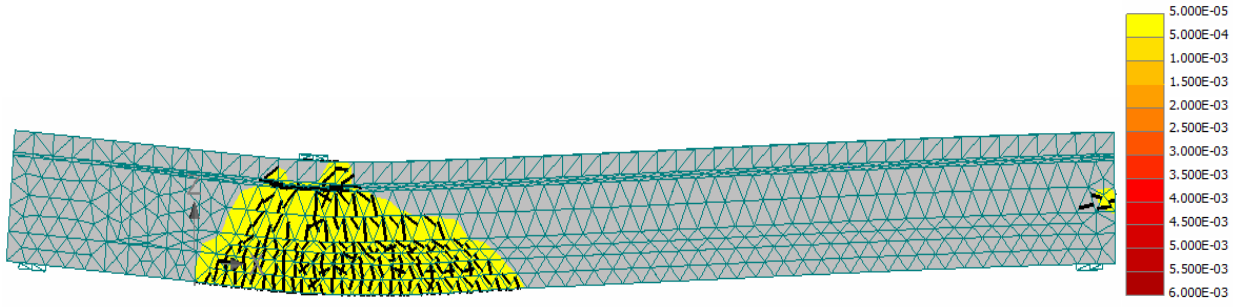

Figure 5.39 Crack pattern of T-R3 at load = 976 KN.

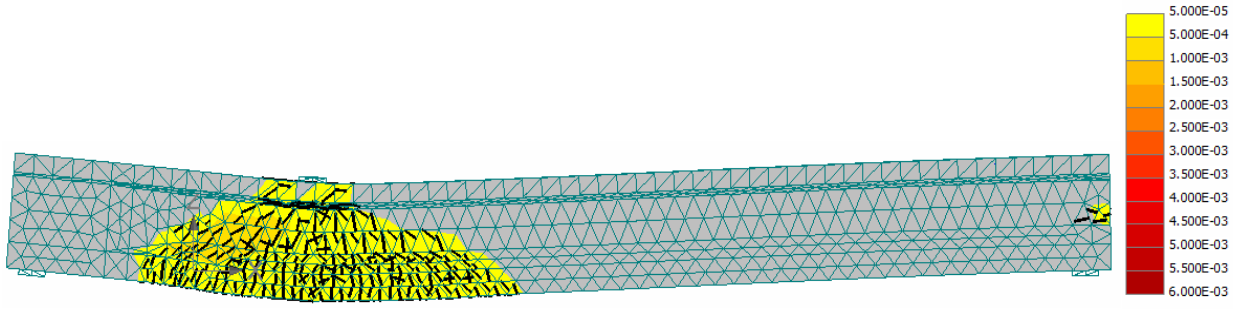

Figure 5.40 Crack pattern of T-R3 at load = 1009 kN (Peak load).

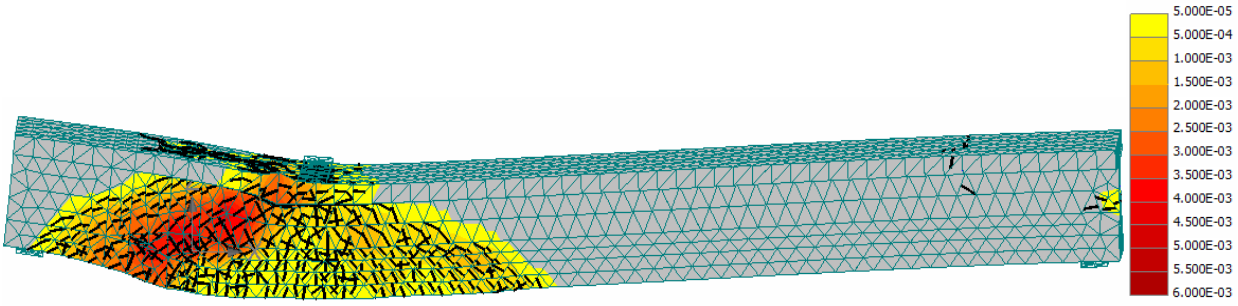

Figure 5.41 Crack pattern of T-R3 at failure.

The shear tension crack opens at load 1009 kN (V_{cr} = 746 kN) and localizes immediately leading to opening of the shear tension crack with a width of close to 4.0 mm at failure. This is a typical brittle shear failure. The effect of removing prestressing cables is clear here. Not only does the shear tension crack open at a lower load level compared to the previous beams but the shear crack also localizes immediately without further crack propagation leading to failure of the beam.

5.5.1 Shear Crack Opening

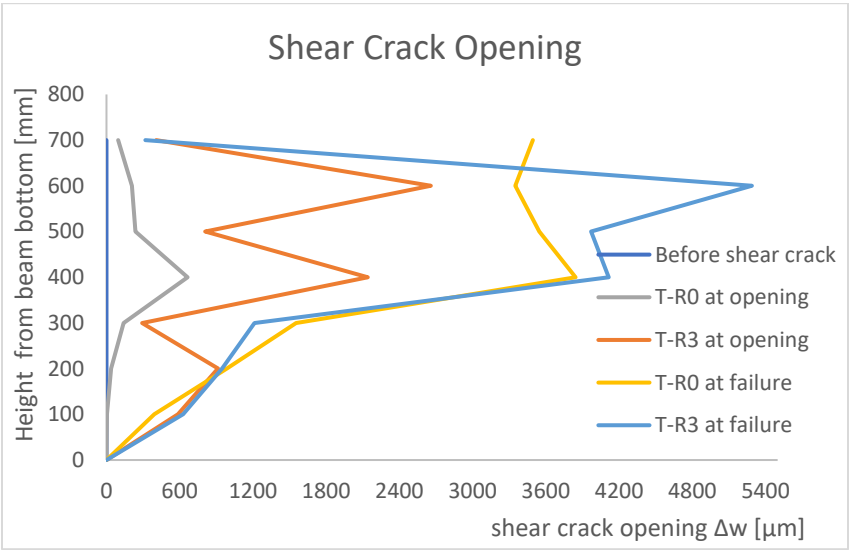

Figure 5.42 Shear crack opening in T-R0 and T-R3.

Due to the absence of both stirrups and inclined prestressing the crack width of the shear tension crack is larger in beam T-R3 than in any other reference beam. At a height of 600 mm from the bottom fiber level (close to centroidal axis - 618 mm) the crack width is larger than 2.0 mm even at the opening of the crack.

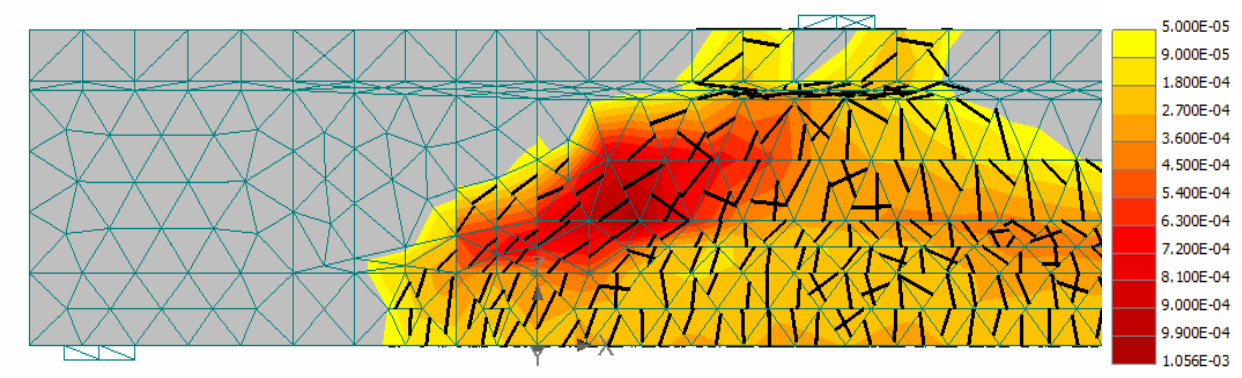

Figure 5.43 Crack width at the onset of shear tension crack in T-R3 (m).

Another important observation is the angle of inclination of the shear tension crack. Due to absence of the axial compressive force from the prestressing cables, the angle of inclination of the shear crack is greater than 45 degrees. (The compressive forces from prestressing reduce the angle of inclination to less than 45 degrees. This is particularly beneficial in beams with stirrups as lower the angle of inclination means more stirrups cross the cracks and therefore an increase shear capacity.)

5.5.2 Failure Mode.

As seen earlier, the T beam without stirrups and inclined prestressing cables develop a shear tension failure mode immediately after cracking. This is a brittle shear failure mode (see Figure 5.41).

5.6 Mechanism of shear transfer.

Shear in cracked prestressed concrete beam is transferred by 5 main mechanisms as shown in the Figure 5.44 In this section the results obtained for 3 reference beams (T-R0, T-R1,T-R3) are explained by estimating the contributions of mainly the stirrups and the prestressing cables.

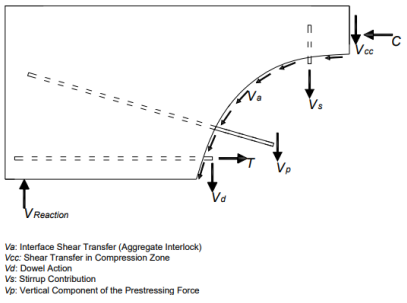

Figure 5.44 Mechanism of shear transfer in cracked prestressed beam [43]

The shear reinforcements act as transverse ties and help in resisting the shear force by redistribution of stresses. This prevents localization of the shear tension crack leading to brittle failure. The stirrups distribute the deformation in many small cracks rather than a single large

crack. The small cracks help in activating the interface aggregate interlock which further contributes to the shear carrying capacity of the concrete.

Apart from stirrups, the longitudinal reinforcements also contribute to the shear resistance by dowel action. Dowel action is the mechanism by which longitudinal steel bends around a shear crack leading to a vertical tensile force that resists a part of the shear force.

Prestressing tendons help in carrying the shear force by action of the vertical component of the prestressing force in the tendons. When a shear crack opens, the prestressing tendons act as inclined stirrups, thereby, helping in redistribution of shear cracks. Since the tendons are bonded to concrete, the stresses in the tendons increase upon opening of a shear crack. This prevents localization of a single large shear crack and many more cracks at different locations are formed on increasing the load. The increase of steel stress in the tendons give rise to increase in the prestressing forces in the tendons. The vertical components of these forces carry a part of the shear force resulting from the support reaction.

In this section, the contribution of the stirrups and the prestressing cables to the shear resistance of the post-tensioned T beams is estimated.

5.6.1 Reference beam T-R0

The stresses in both stirrups and tendons are measured at points where they cross the shear cracks. 5 stirrups and 3 tendons cross the region where shear cracking occurs. The increase in stresses in both stirrups and tendons after opening of the crack until the ultimate load capacity has been reached is evaluated. The transverse tensile force in the stirrups and the vertical component of the prestressing force resulting from the stress increase are calculated. From this, the contribution of both the stirrups and tendons to the shear resistance of the beam can be estimated.

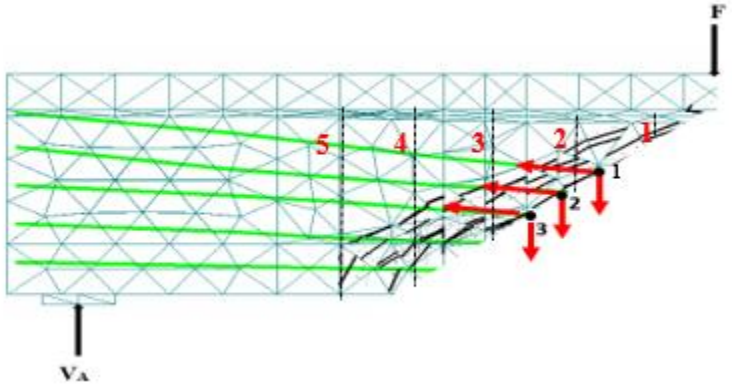

Figure 5.45 Cross-section cracked in shear in beam T-R0.

1. Contribution of stirrups to the shear resistance.

The increase in steel stress in stirrups at the onset of the shear tension crack is estimated for 5 stirrups crossing the crack. Since the shear crack is inclined, the point where the steel stress is measured differs in each of the 5 stirrups.

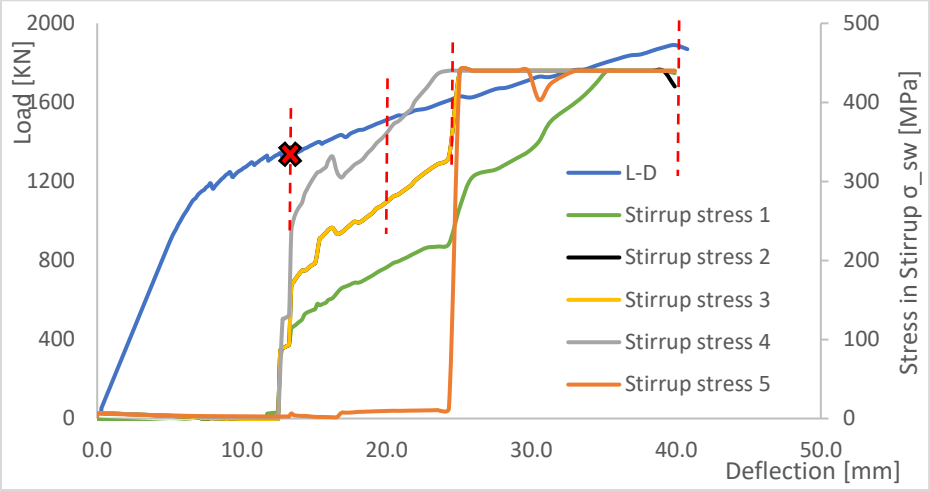

Figure 5.46 Load-deflection-stirrup stress in T-R0.

The inclined shear crack originates at load level 1343 KN. The ultimate load capacity is 1890 KN. There is an increase of 547 KN in load capacity after the shear crack has occurred. The resulting increase in shear force from the support ΔV_A is equal to 404.8 KN. The increase in steel stress in stirrups after shear cracking can be seen in the graph (Figure 5.46).

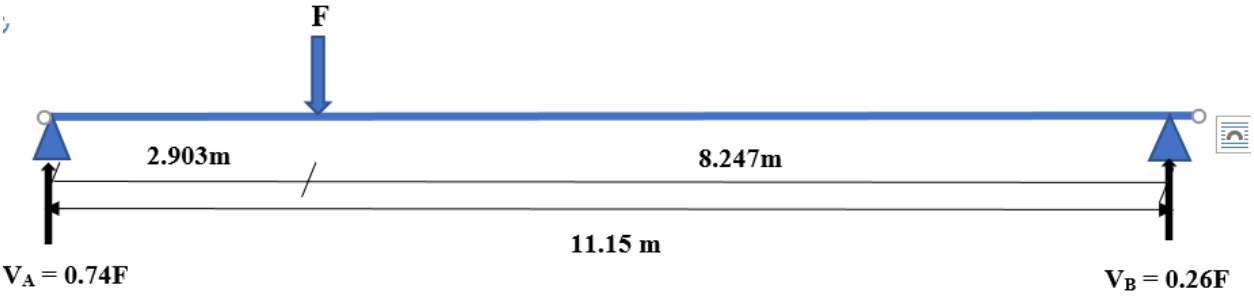

The evolution of stresses in stirrups is shown against the crack pattern in the beam at different load intervals (Figure 5.47).

Before the shear crack occurs, the stresses in the stirrups are zero. Immediately after the opening of shear cracks, the stress in stirrups 1, 2 & 3 start to increase. The crack opens near the centroidal axis level. Therefore, the stress in stirrup 3 is higher at the location of the shear crack opening (centroidal axis level). As the load increases, more cracks are formed at different locations in the beams and the stresses continue to increase in stirrup 4 and 5 as well. Ultimately the stirrups yield on reaching their strength of 440 MPa. The increase of stress from 0 MPa to 440 MPa results in a

transvers tensile load that resists the shear force. This force is denoted as V_{sw}. It is calculated by multiplying the increase in stress $\Delta\sigma_{sw}$ by area of the shear reinforcement A_{sw}.

$V_{sw} = \Delta\sigma_s \times A_{sw} = 440 \times 78.55 = 34.6$ KN. For 5 stirrups, total $V_{sw} = 173$ KN. This is nearly 43% of the total increase in shear force ΔV_A (404.8 KN).

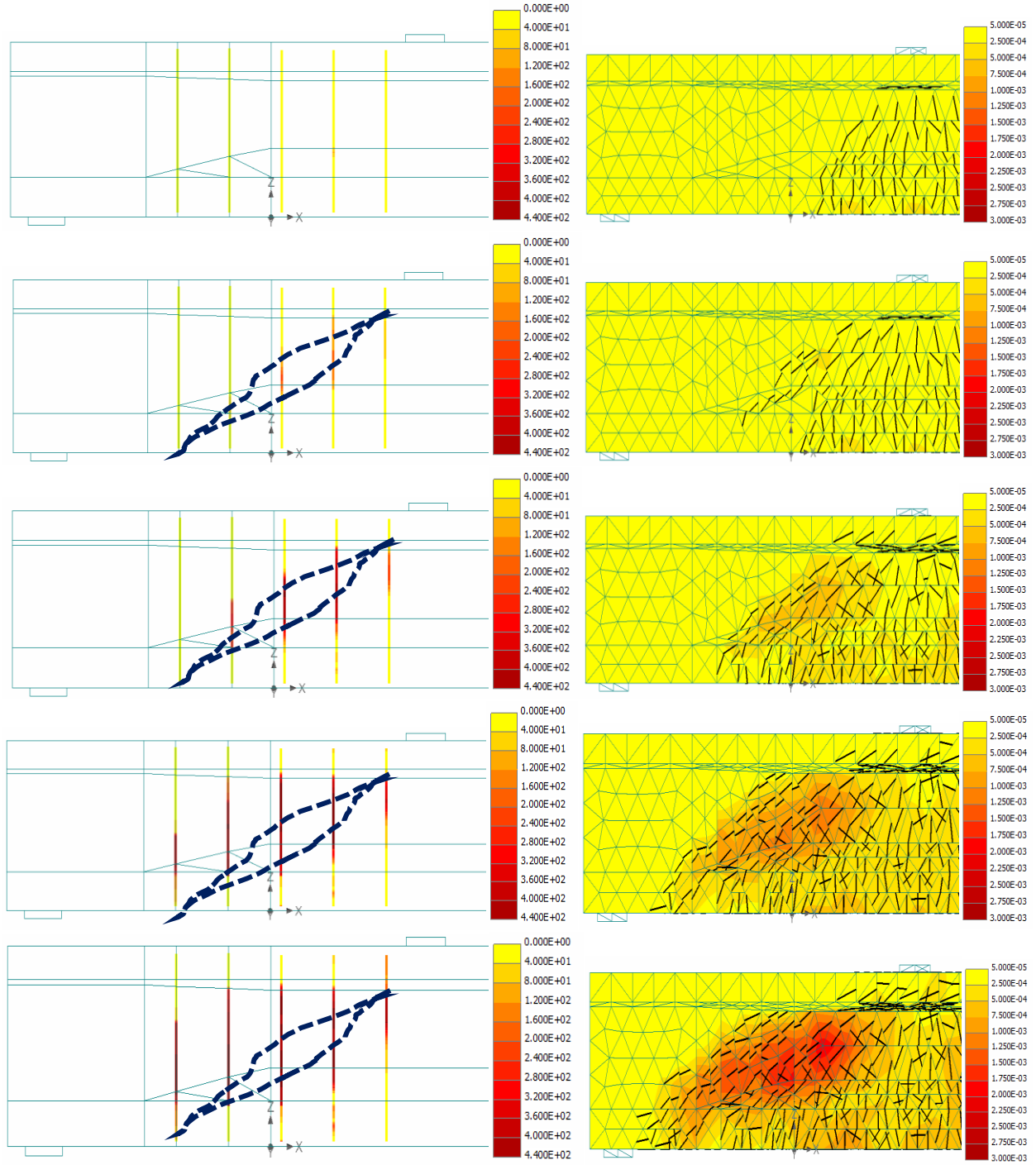

Figure 5.47 Evolution of stirrup stresses (MPa) (left) & Crack width (m)(right) in beam T-R0.

2. Contribution of the prestressing tendons to the shear resistance.

Like the stirrups, the stresses in the 3 tendons crossing the shear span are measured. The vertical component resulting from the increase in tendon stress is calculated for each tendon.

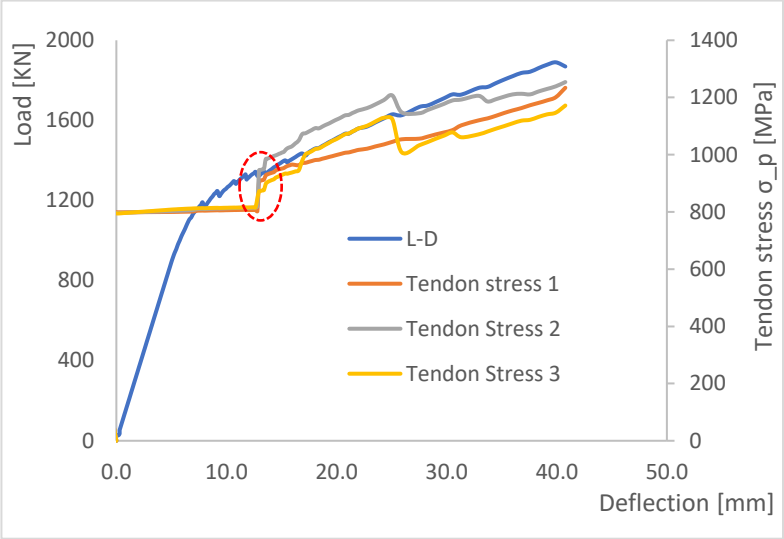

Figure 5.48 Load-deflection-tendon stress in beam T-R0.

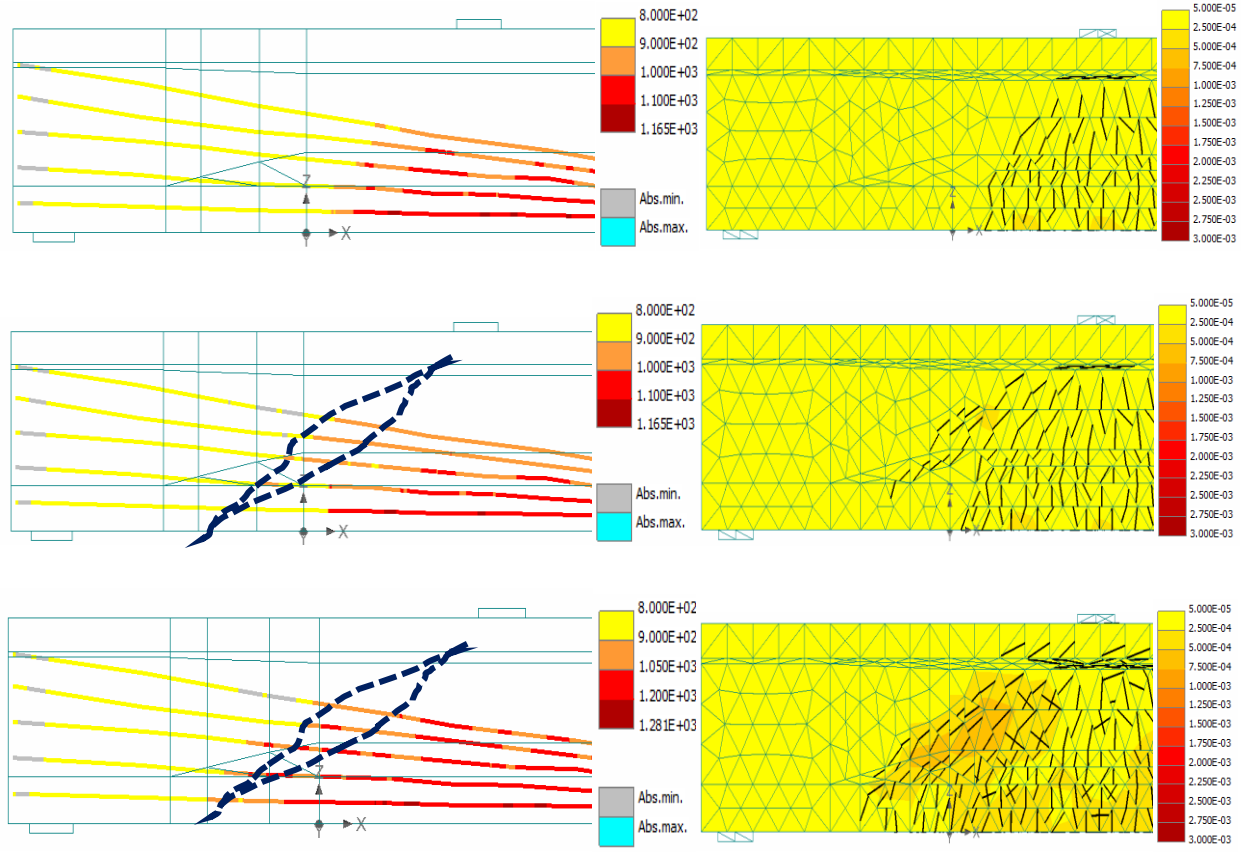

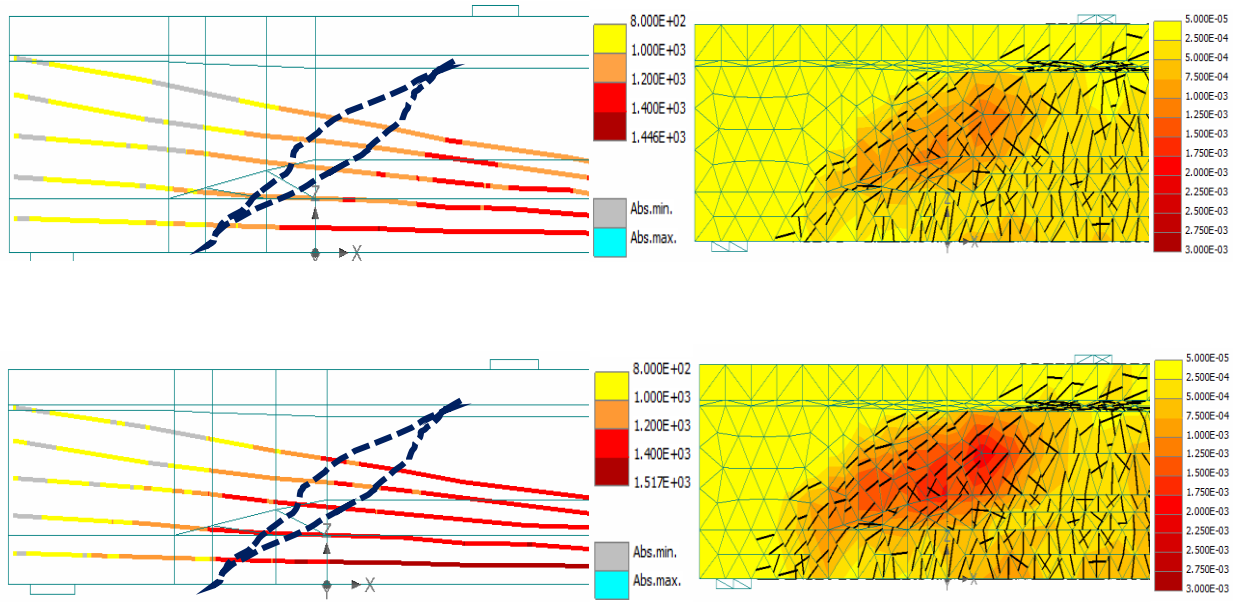

Figure 5.49 Evolution of tendons stresses (MPa) (left) & crack width (m)(right) in T-R0.

The stresses in the tendons increase at the onset of the inclined shear crack. This is evident in the plots for tendon stresses shown in Figure (5.49).

The increase in tendon stress post shear cracking is concentrated around the crack opening. Another important observation is the decreasing stress measured along the points. This is a result of the crack formation at locations different from the points of measurement. The cracks at other locations on cracking, release the stress in the previously formed crack. Ultimately the cracking reaches a widening phase and the stress begins to increase in the already formed cracks thus increasing their width. As seen previously the beam fails by compression in the top flange.

Table 5-2 Contribution of tendons to shear capacity in T-R0.

Load (KN)	Stress in Cable 1 (MPa)	Stress in Cable 2 (MPa)	Stress in Cable 3 (MPa)
1343	817	814	825
1890	1270	1210	1230
$\Delta F = 547$	$\Delta\sigma_{P1} = 454$	$\Delta\sigma_{P2} = 391$	$\Delta\sigma_{P3} = 404$
$\Delta P = \sigma_P.A_P$	$\Delta P_1 = 210$ (kN)	$\Delta P_2 = 181$ (kN)	$\Delta P_3 = 186$ (kN)

$A_P = 462$ mm^2.

Increase in shear force due to ΔF, $\Delta V_A = 0.74.\ \Delta F = 404.8$ KN

$\Delta V_P = \Delta P_1\alpha_1 + \Delta P_2\alpha_2 + \Delta P_3\alpha_3$ – α is the angle of inclination of the tendons, $\alpha_1 = 7.6°$, $\alpha_2 = 5.7°$and $\alpha_3 = 4.4°$

$\Delta V_P = 27.8+18+14.3 = 60$ KN.

$\Delta V_P/\Delta V_A = 0.148$ The 3 cables contribute to 14.8 % of the increase in the shear force. This is the contribution of the 3 cables to the increase in shear resistance post cracking.

The additional contribution from the other 4 tendons crossing the shear span is also calculated and the total contribution from the 4 cables is equal to 30 KN. The 7 tendons have a total force in the vertical direction of 60+30 = 90 KN. This is roughly 22 % of the total increase in shear force post cracking in the beam.

Summary.

The beam T-R0 (with shear reinforcement) has a shear capacity of 1399 kN (load capacity = 1890 kN). An inclined shear crack is formed at load level 1343 KN i.e., V_{cr} = 994 kN. The rest of the load capacity is obtained by the action of other mechanisms as mentioned before.

Post shear cracking the stirrups and prestressing tendons contribute to approximately 7% of the total increase in shear capacity. The remaining shear force should be carried by the other mechanisms such as the interface aggregate interlock, shear transfer by uncracked concrete and dowel action of longitudinal reinforcement.

For the ultimate shear resistance, the contribution of concrete and the vertical component of the initial prestressing force is 994 kN (until cracking), which is 71 % of the resistance. The contribution of the stirrups to the shear strength of the beam is 12.5% (173 kN). The prestressing cables contribute 6.4% i.e., 90 KN of the total resistance of the beam. The remaining 10% is contributed by the combined action of aggregate interlock, uncracked concrete in the compressive zone and dowel action of longitudinal reinforcement.

5.6.2 Reference Beam T-R2.

Contribution of prestressing tendons to the shear resistance.

Unlike the beam with shear reinforcements, the increase in shear capacity of the beam post shear cracking is mainly due to the action of prestressing cables in the beam without shear reinforcement. The cables act as inclined reinforcements redistributing stresses that facilitates formation of smaller cracks at different locations rather than localization of a single large crack after the opening of the inclined shear crack.

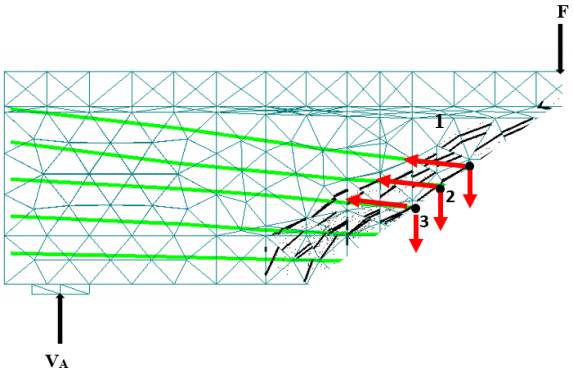

Figure 5.50 Cross-section cracked in shear in beam T-R2.

To estimate the contribution of the vertical component of the prestressing force, 3 prestressing tendons crossing the cracked region are chosen. The steel stress in each tendon is measured at a

single point (node) crossing the cracks for the tendon. The steel stress is plotted against the load for all the 3 tendons and the increase in steel stresses is observed (Figure 5.51).

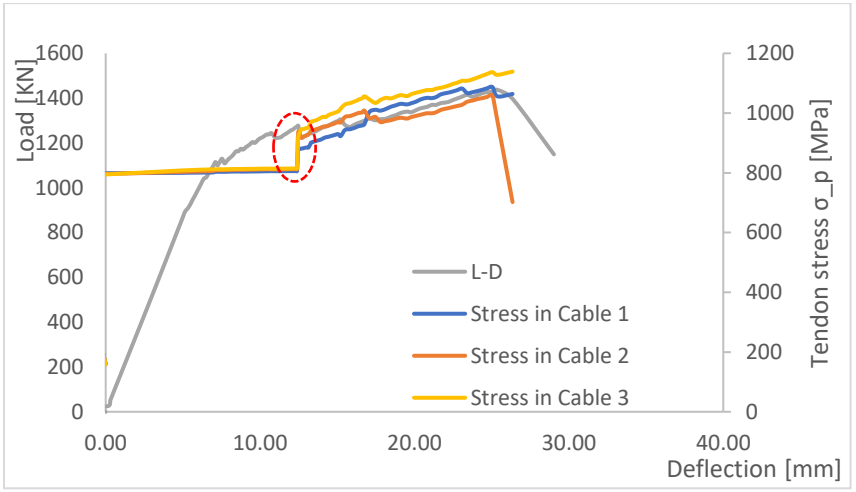

Figure 5.51 Load-deflection-tendon stress for beam T-R2.

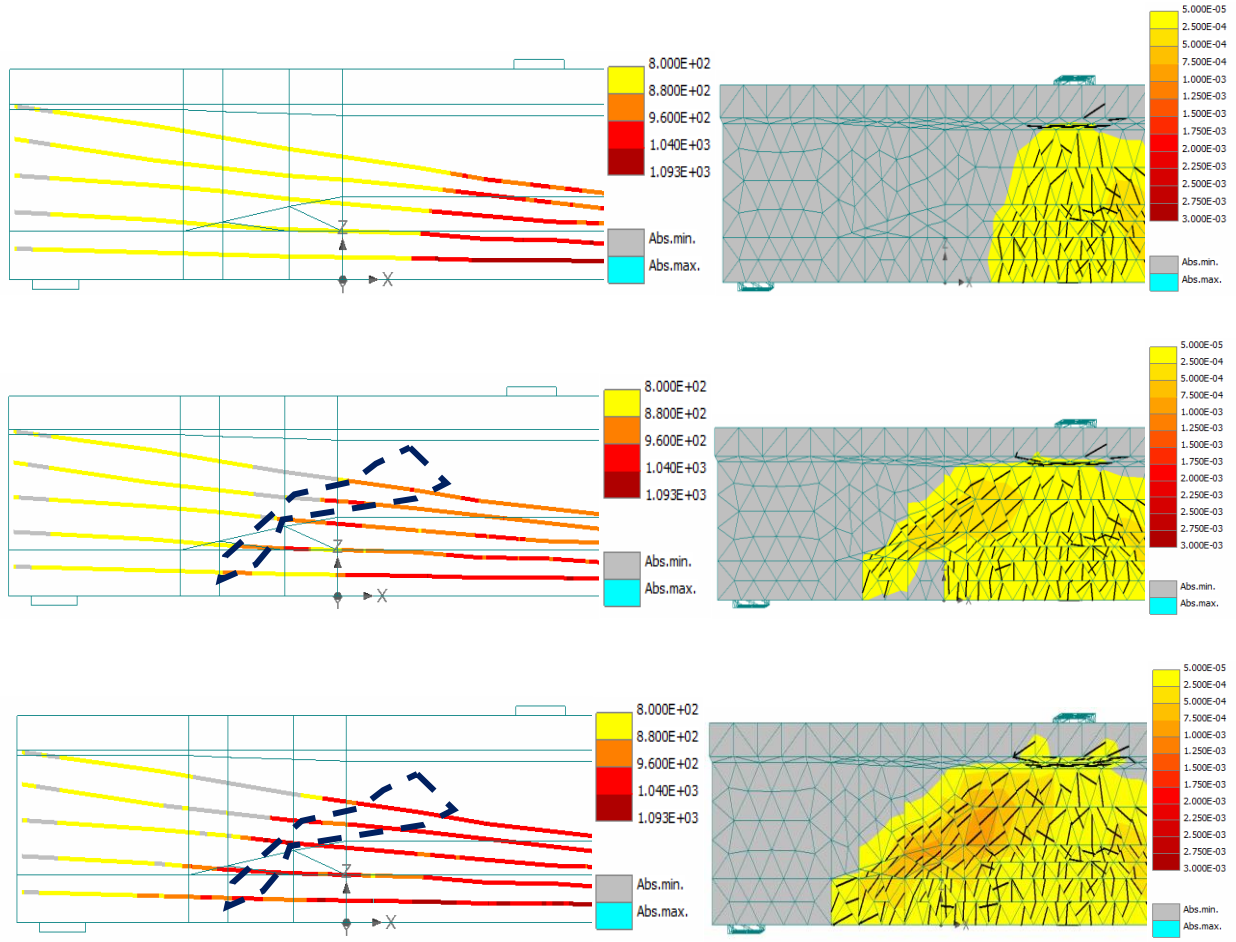

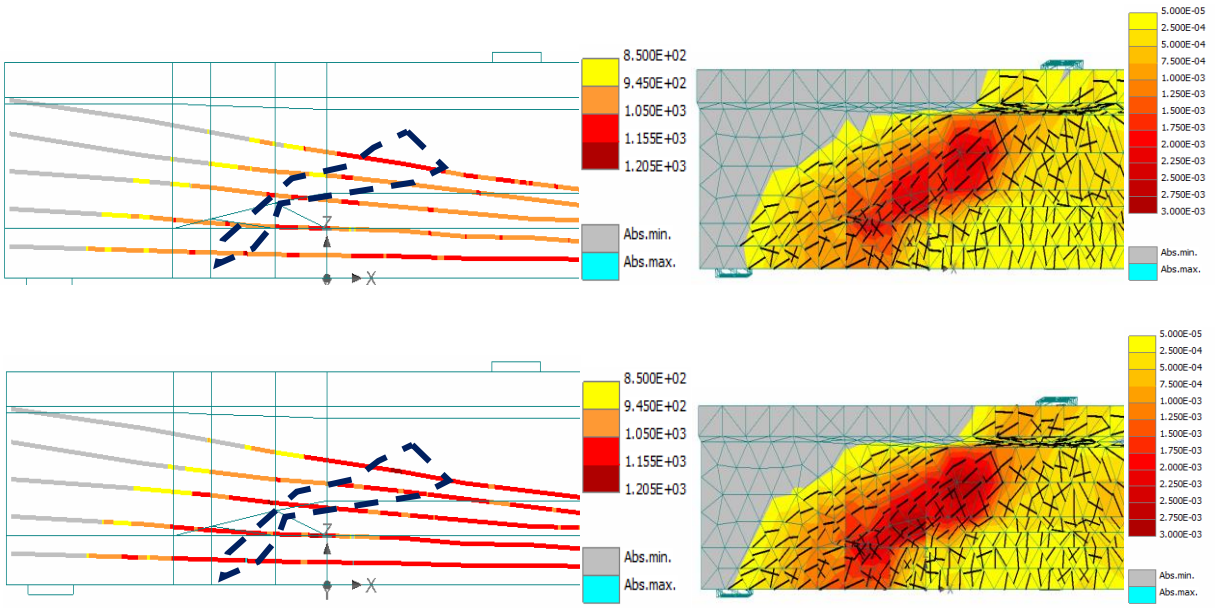

Figure 5.52 Evolution of tendon stresses (left)(MPa) & crack width (right)(m)

The inclined shear crack originates at load level 1277 KN. The ultimate load capacity is 1430 KN. There is an increase of 153 KN in capacity after the shear crack has occurred. While it is observed that the stress in tendons increase at a significantly higher rate after the opening of shear crack. (Figure 5.51 and 5.52) This confirms the contribution of the tendons to redistribution of the shear stresses and therefore to the ultimate capacity. The contribution of the tendons is estimated by calculating the increase in prestressing load after the shear crack has opened.

Table 5-3 Contribution of tendons to shear capacity in T-R2.

Load (KN)	Stress in Cable 1 (MPa)	Stress in Cable 2 (MPa)	Stress in Cable 3 (MPa)
1277	816	811.6	821.5
1430	1185	1008	1037
$\Delta F = 153$	$\Delta\sigma_{P1} = 369$	$\Delta\sigma_{P2} = 196.4$	$\Delta\sigma_{P3} = 215.5$
$\Delta P = \sigma_P.A_P$	$\Delta P_1 = 170.5$ (kN)	$\Delta P_2 = 90.7$ (kN)	$\Delta P_3 = 99.5$ (kN)

$A_P = 462\ mm^2$.

Increase in shear force due to ΔF, $\Delta V_A = 0.74$. $\Delta F = 113.3$ kN.

$\Delta V_P = \Delta P_1\alpha_1 + \Delta P_2\alpha_2 + \Delta P_3\alpha_3$ – α is the angle of inclination of the tendons.
$\Delta V_P = 22.5+9+7.6 = 39$ kN.

$\Delta V_P/\Delta V_A = 0.344$. The 3 cables contribute to 34.4 % of the increase in the shear force. This is the contribution of the 3 cables to the ultimate capacity

The remaining 4 tendons contribute to the shear resistance by the vertical component of the prestressing load. The contribution of those tendons is estimated to be 13.8 kN. Therefore, the total contribution of the prestressing cables is around 52.8 kN (39+13.8). The remaining shear force i.e., 113-52.8 = 60.2 kN can be resisted by the combination of both uncracked concrete and the dowel action of the longitudinal reinforcement.

To summarize, the prestressing cables contribute to the shear capacity of the T beam in 3 ways.

1. The axial compressive stress on the concrete resulting from prestressing, delays the opening of the shear crack. Thus, increasing its resistance.
2. The 3 cables crossing the shear crack region act as inclined shear reinforcements to redistribute the shear stresses and thus prevent localization of the shear crack leading to brittle failure.
3. The vertical component of the prestressing force in the tendons directly resist the shear force resulting from the support reaction. Thus, increasing the shear capacity of the beam.

The cables also contribute by activating the other mechanisms such as aggregate interlock, shear transfer by uncracked concrete and dowel action of the longitudinal reinforcement by preventing localization of the inclined shear crack leading to a brittle shear failure.

Summary.

The contribution of concrete and the initial prestressing force to the total shear resistance (1063 kN) of the T beam without stirrups is 89%. (945 kN). After shear cracking the prestressing cables contribute to the shear capacity by acting as inclined stirrups and redistribution the stresses. This is about 5% (52.8 kN) of the total resistance. The remaining mechanisms such as shear transfer by uncracked concrete, dowel action of longitudinal reinforcement and aggregate interlock contribute to about 6 % of the total shear resistance.

5.6.3 Reference Beam T-R3.

In the absence of both stirrups and the inclined prestressing cables, the shear force is resisted only by the concrete and the other 4 prestressing tendons. In this case there is no increase in the shear capacity post cracking and the beam fails by localization of the shear tension crack. The shear cracking force and the shear capacity are same. (V_{cr} and V_u = 746.7 kN).

5.7 Summary of results from reference beams.

In total 4 reference beams were tested. T-R0 is the beam with both stirrups and inclined prestressing cables. T-R1 and T-R2 are beam without stirrups. The difference between T-R1 and T-R2 is explained in section table 5-1. The last beam T-R3 is without stirrups and inclined prestressing cables.

Table 5-4 Overview of reference beams.

Beam	Stirrups	Inclined prestressing tendons
T-R0	✖	✖
T-R1	-	✖
T-R2	-	✖
T-R3	-	-

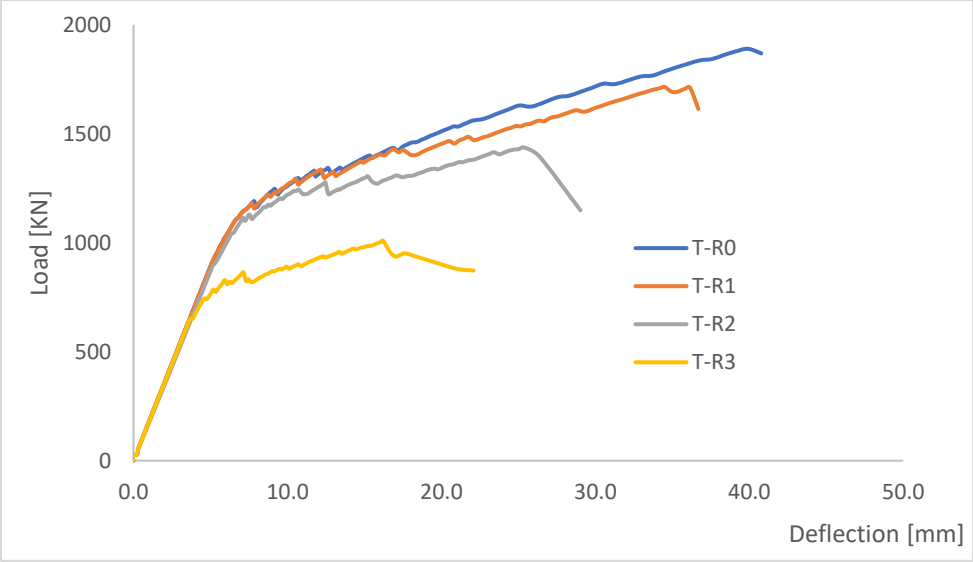

Figure 5.53 Load-deflection curves for all reference beams.

A summary of results of reference beams is presented in Table 5-5.

Table 5-5 Summary of results from reference beams.

Beam	Cracking shear load V_{cr} (kN)	Shear Capacity V_u (kN)	Max. Deflection δ_{max} (mm)	Failure Mode	Stirrups contribution V_{sw} (%)	Contribution of Vertical component of P, V_P (%)	Additional contribution of P, ΔV_P (%)
T-R0	994	1399	40.8	Shear Compression	12.5	11	6.4
T-R2	945	1063	29.03	Shear Compression	-	11	5
T-R3	746.7	746.7	22.09	Shear Tension	-	-	-

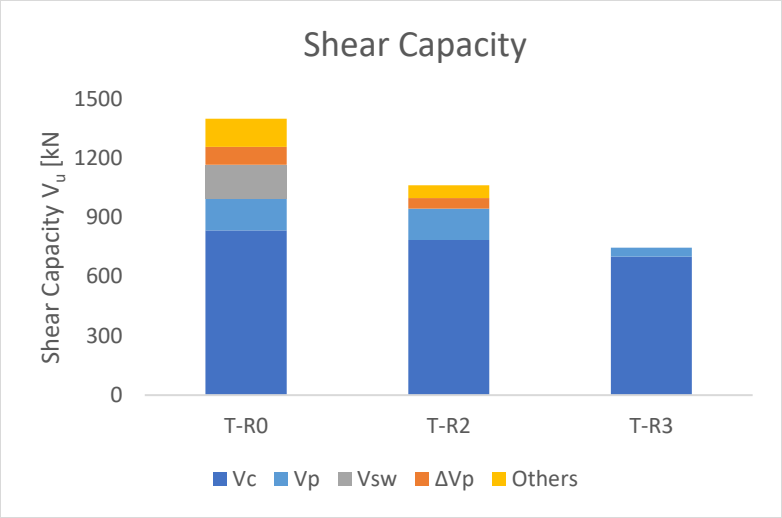

Figure 5.54 Shear capacity of reference beams showing contribution of various mechanisms.

5.1 Shear tests on post-tensioned bridge girders of existing bridges [1]

The section discusses the results of experimental tests performed on existing post-tensioned girders to determine their shear capacity. The results of the tests are compared with the results obtained from the numerical analysis of the post-tensioned T beam of Helperzoom bridge. The experimental results explained in 5.1.2 show close similarities with the results obtained from the numerical analysis performed in this research.

5.1.1 Bridge crossing the suburban railway station Sudtirolerplatz in Vienna.

Two post-tensioned T girders (SP2 and SP3) from the bridge were tested to investigate their shear behavior. Important specifications of the beams are the shear reinforcement ratio, amount of prestressing and the cross-sectional dimensions of the girders.

The girders had a shear reinforcement ratio ρ_w = 0.302%, with $\rho_{w,min}$ = 0.136%. The girder consisted of 14 bonded prestressing tendons each of diameter 26 mm. The cross-sectional dimensions and the test-up of the experiments are shown in Figure 5.55 and 5.56.

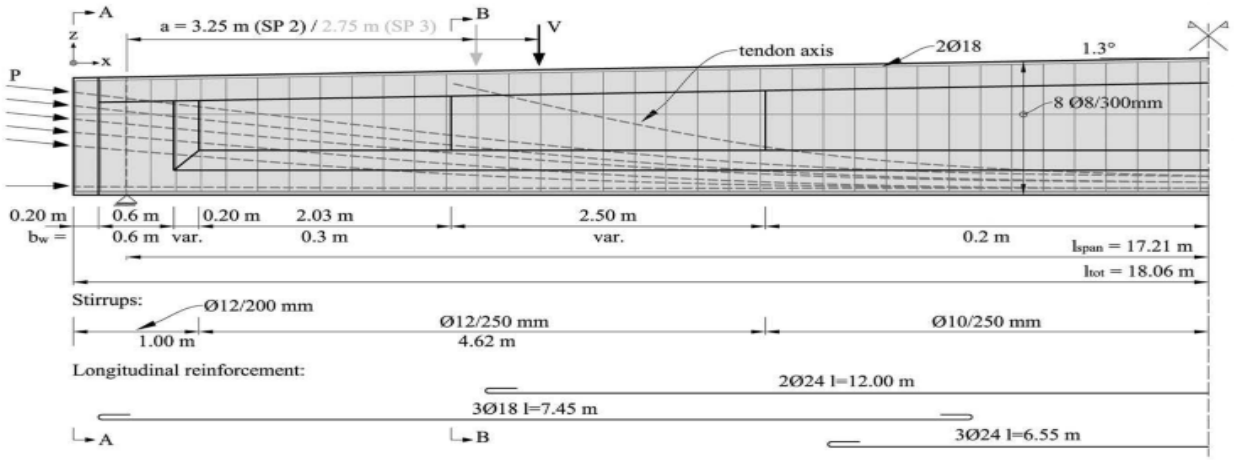

Figure 5.55 Longitudinal view of test-setup for Sudtirolerplatz bridge girder [1].

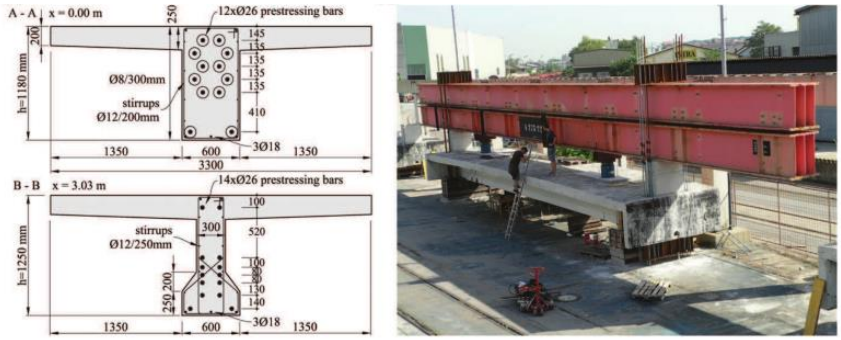

Figure 5.56 Cross section of girders (left) and open- air test set-up (right) [1]

The girder was subjected to 4-point bending load. The mean cube compressive strength, $f_{cm,cube}$ of the concrete was 70.9 MPa. The steel used for longitudinal and shear reinforcements had a yield strength f_y = 448.4 MPa and yield strength of prestressing cables f_{py} was 779.7 MPa.

Results and Discussion.

Both the beams SP2 and SP3 failed by yielding of the prestressing tendons and longitudinal steel at V_{exp} = 2283 kN and 2640 kN respectively. Since bending failure occurred before the shear failure this is the lower limit of shear capacity of the girders.

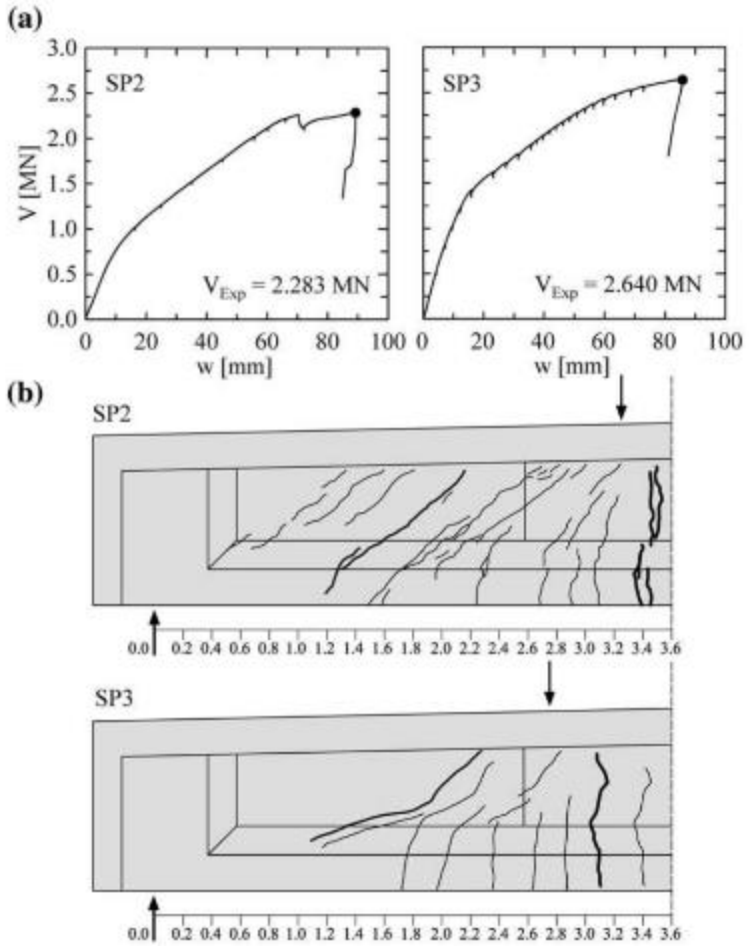

Figure 5.57 Test results for the girders from the bridge above the Südtirolerplatz railway station in Vienna: (a) shear load V versus deflection w at the point of load introduction; (b) crack pattern at failure in the region of load introduction [1].

5.1.2 Melk east overpass, Melk, Austria.

The post-tensioned T beams of the Melk east overpass bridge were tested to ascertain their shear behavior and therefore their shear capacity. The girders consisted of 12 prestressing tendons. Each tendon was composed of 16 single wires of 30 mm^2 cross-sectional area. Shear reinforcement was provided by 120 mm stirrups spaced 250 mm apart. This resulted in a ρ_w of 0.22%. The yield strength of steel used for longitudinal and shear reinforcement was 435 MPa. Yield strength (f_{py}) and ultimate strength (f_{pu}) of the prestressing wires are 1440 MPa and 1590 MPa respectively.

Two girders Pb1 and Pb2 were tested under 3-bending load with a shear span (a/d) = 3.7.
The test set-up and cross-sectional dimensions of the beams are shown in Figure 5.58.

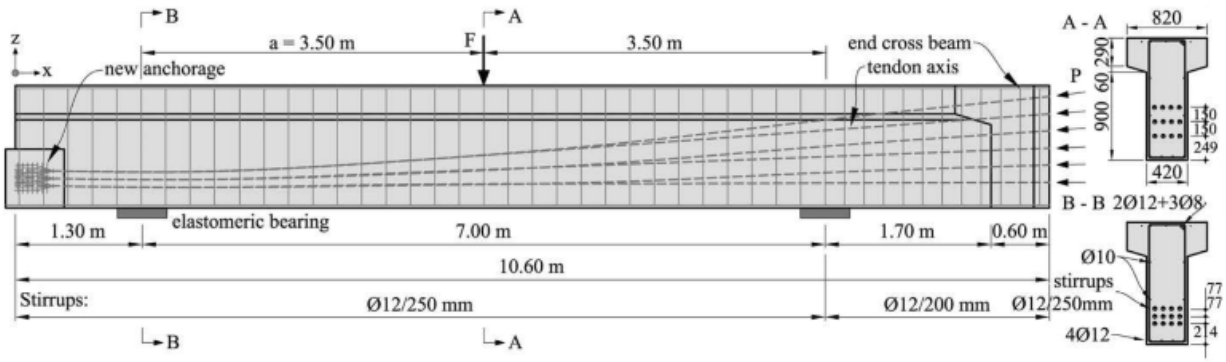

Figure 5.58 Reinforcement and tendon layout in the girders and schematic of the test setup (Melk east overpass bridge girder).

Results and Discussions.

Both the girders that failed exhibited a type of shear-tension/shear compression failure. At a certain load level ($V_{cr,exp}$) a shear-tension crack occurred in the zone of maximum shear. After the crack, the load continued to increase and resulted in formation of many more shear cracks. Just before the failure a critical flexural shear crack occurred along with horizontal cracks in the compression strut. This indicated a desirable action of indirection strut action or arching effect. The beam ultimately failed by compression of concrete in the top flange after yielding of the stirrups. Upon failure the critical flexural shear crack widened significantly reaching a width of 10 mm, leading to rupture of the stirrups in specimen Pb2. For Pb1, the test was aborted as soon at the compression failure occurred. It should be noted that although the amount shear reinforcement was low, yielding of stirrups did not result in failure of the girders [1].

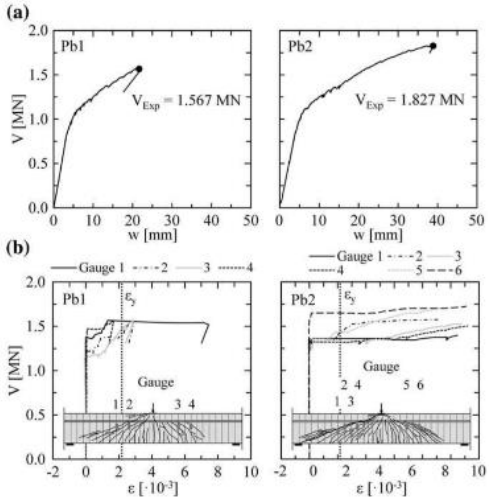

Figure 5.59 Results of test on girders from the Melk East Overpass in Melk, Austria: (a) shear force V versus mid-span deflection w and (b) strain in the stirrups [1].

Summary of results.

Post-tensioned T girders from two existing bridges were tested to investigate their shear behavior and capacity. The results of the two tests are summarized in Table 5.6.

Table 5-6 Summary of Results from two existing bridge girders.

Beam	$V_{cr,exp}$ (kN)	V_{exp} (kN)	Failure type.
SP2	980	2283	Bending
SP3	1160	2640	Bending
Pb1	1377	1567	Shear Compression
Pb2	1350	1827	Shear Compression

5.2 Comparison of results from experimental tests on existing bridge girder with results from numerical analyses on post-tensioned T beam from Helperzoom bridge.

The results obtained from the experimental tests discussed in previous section presents an opportunity to compare the results of the numerical analyses performed in this research on the reference post-tensioned T beam (T-R0).

The results of the tests on girders of Melk east overpass (Pb1 and Pb2) show a close similarity with the results obtained from the numerical analyses on the shear test of Helperzoom bridge.
The numerical simulations show that the beam T-R0 fails in a similar failure mode as beam Pb1 & Pb2 i.e., compression failure of the top flange.

Before comparing the results of the two cases, the parameters that influence the failure mode and the load capacity of the girders are presented.

The shear reinforcement ratio ρ_w in T-R0 calculated from equation 9.2.2(5) of Eurocode 2 part 1-1: Design of Concrete structures, which gives,

$$\rho_w = A_{sw} / (s \cdot b_w \cdot \sin\alpha)$$

and

$$\rho_{w,min} = (0{,}08(f_{ck})^{0,5})/f_{yk}$$

Where,
s is the spacing between stirrups in the longitudinal direction
A_{sw} is the area of shear reinforcement between the spacing
b_w is the width of beam

α is angle of inclination of stirrups with the longitudinal axis of the beam.
f_{ck} and f_{yk} are the characteristic compressive strength of concrete and yield strength of reinforcing steel respectively.

For T-R0, s =400 mm, with Ø = 10mm A_{sw} = 157.1 mm^2, b_w = 200 mm and α = 90°.

ρ_w = 0.196 % and $\rho_{w,min}$ = 0.140 %. Therefore, shear reinforcement ratio is 1.4 times the minimum shear reinforcements ratio required. The reinforcement ratio in Pb1 and Pb2 is 0.22 %. Both the girders have a comparatively low amount of shear reinforcement. The shear span ratio (a/d) used in tests is 2.9 for T-R0 and 3.7 for Pb1 and Pb2.

The compressive stresses due to prestressing σ_{cp} is calculated for the two types of girders by the equation $\sigma_{cp} = P_m/A_c$. For T-R0, P_m = 7 x 380.10^3 N and A_c = 0.517 m^2. For Pb1 and Pb2, P_m = 14 x 185.10^3 N and A_c = 0.628 m^2. From this σ_{cp} is equal to 5.14 MPa and 4.12 MPa for T-R0 and Pb1 & Pb2 respectively.

Table 5-7 Comparison of input properties for T-R0 and Pb1 & Pb2.

Beam	Concrete compressive Strength f_{cm} (MPa)	Shear reinforcement ratio ρ_w (%)	Compressive stress from prestressing σ_{cp} (MPa)	Yield strength of reinforcing steel f_y (MPa)	a/d ratio
T-R0	60	0.196	5.14	440	3.0
Pb1 & Pb2	57.5	0.22	4.12	435	3.7

In shear tests on many post-tensioned beams with a low amount of transverse reinforcement, it has been observed that failure is caused by the development of a critical flexural shear crack. This is accompanied by failure of the compression zone and rupture of stirrups [44]. This is the failure mode observed in Pb1 and Pb2 (5.8.2). Also, the reference post-tensioned T beam tested by numerical simulations fails ultimately by compression in the top flange. Here, the stirrups have reached their yield strength, but they do not undergo rupture because of the infinite ultimate strain capacity of the stirrup steel assumed in the model.

The results from the two beams namely the cracking load and the shear capacity are compared.

Table 5-8 Comparison of results from T-R0, Pb1 and Pb2.

Beam	Cracking load V_{cr} (kN)	Shear Capacity V_u (kN)	Maximum Deflection δ_{max} (mm)
T-R0	994	1376	40.8
Pb1	1377	1567	22
Pb2	1350	1827	40

The failure modes in all the three beams is the same that is by failure of the compression zone.

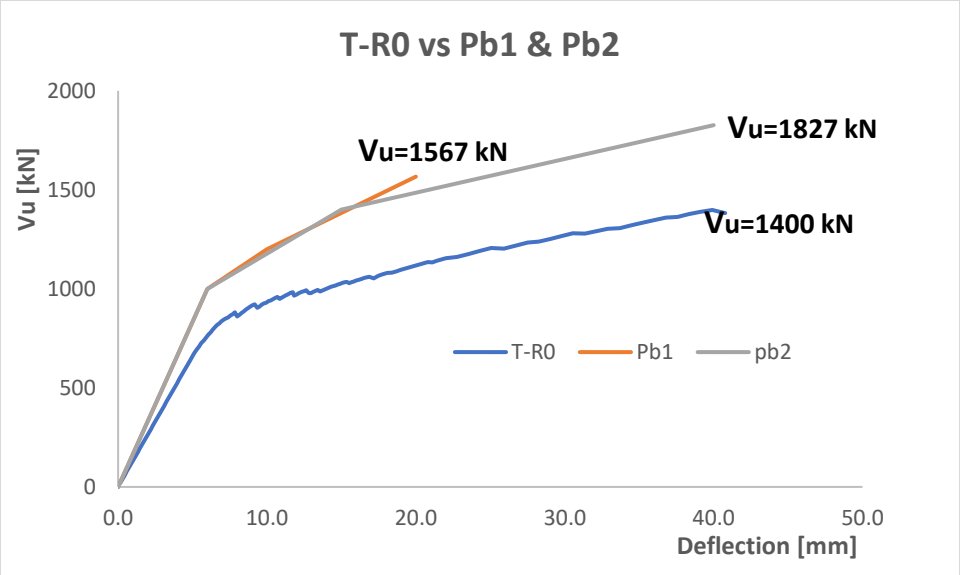

Figure 5.60 Comparison of load-deflection for T-R0 and Pb1 & Pb2.

5.3 Shear Capacity from Flexural Shear Crack Model [45]

Huber et al [45] proposed a concept for the shear assessment of post-tensioned girders of existing bridges with a low number of stirrups. Therein, it is recommended that separate verifications of the shear strength for various zones of the beam be carried out. These areas are defined according to the presence of different crack types and thus several assessment approaches corresponding to the respective shear behavior need to be used.

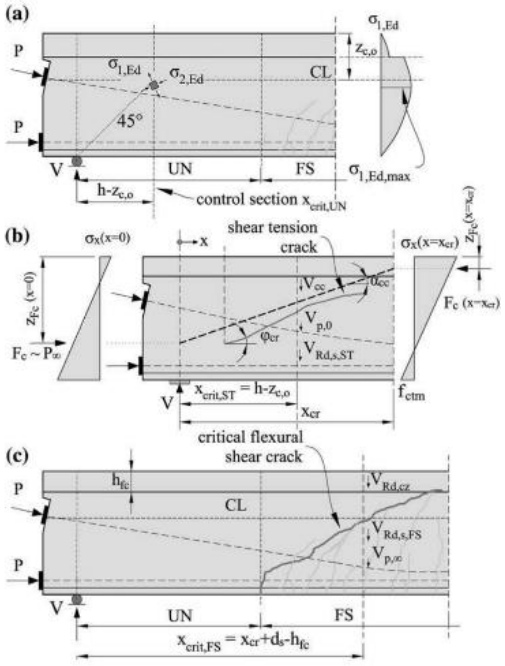

Figure 5.61 Different design scenarios for zones near an end support, characterized by different types of shear crack: (a) uncracked zone next to the end support; (b) zone with shear-tension cracks near the end support; and (c) zone with flexural-shear cracks [1].

However, in this section focus in placed on the flexural shear crack model as the model is the most suitable one to predict the shear capacity of post-tensioned beams with a low amount of shear reinforcement [1]. Also, according to the calculations based on ACI standards, the post-tensioned T beam fails in flexural shear. (Appendix 3).,

The shear capacity of the post-tensioned T beam T-R0 is calculated from the analytical model named Flexural Shear Crack model proposed by Huber et al. According to the model the shear capacity of post-tensioned beams with a low amount of shear reinforcement is given by

$$V_{Rd,FS} = V_{Rd,s,FS} + V_{P,\infty} + V_{Rd,cz}$$

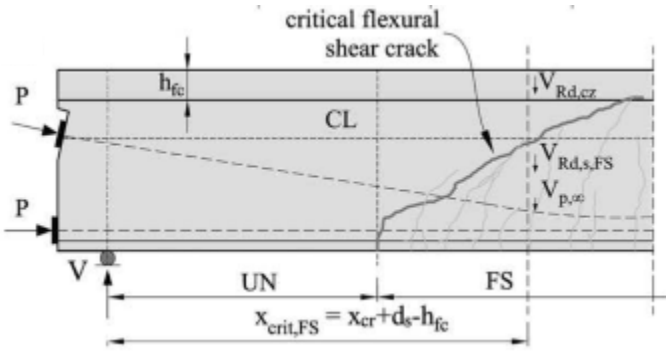

Figure 5.62 Flexural Shear Crack model [1].

Where

$V_{Rd,FS}$ is the flexural shear capacity of the post-tensioned girder.

$V_{Rd,s,FS}$ is the contribution of stirrups to the shear capacity and is given by

$$V_{Rd,s,FS} = \frac{A_{sw}}{S_w}.f_{ywd}.(d_s\text{-}c).\cot\theta_{cr}$$

A_{sw} is the area of stirrups between spacing S_w, f_{ywd} is the yield strength of reinforcing steel, $(d_s\text{-}c)$ is distance between bottom layer of longitudinal reinforcement and neutral axis and θ_{cr} is the crack angle. For simplification θ_{cr} is taken to be 26.6°.

$V_{Rd,FS}$ is the vertical component of the prestressing force in the tendons before shear cracking.

$V_{Rd,cz}$ represents the arching action in the beam as a result of prestressing.

Arching action is a beneficial shear transfer mechanism in prestressed beams with a low amount of shear reinforcement. To guarantee a favorable arching effect a certain level of prestressing is required. Based on experimental observations the additional effect of arching action $V_{Rd,\,cz}$ is only present in girders with a compressive stress due to prestressing σ_{cp} higher than equal to 2.5 MPa [46].

Arching action is given by

$$V_{Rd,cz} = \frac{2}{3}.\tau_{xz,max}.b_{v,eff}.c.ß_{cc}$$

Where $b_{v,eff} = b_w + 2.5h_{fc}$ (h_{fc} height of compression flange) is the effective width in shear, c is depth of compression zone and $ß_{cc}$ is a coefficient to take into account a favouable effect of direct strut action in deep beams ($ß_{cc} = 1.75 – 0.15a/d$ for point loads) and $\tau_{xz,max}$ is the maximum shear stress.

$$\tau_{xz,max} = \sqrt{\left(\alpha_{fc} - 0.47.\sigma_{x,cz,Ed}\right)^2 - \frac{1}{4}.\sigma_{x,cz,Ed}^2}$$

$\sigma_{x,cz,Ed}$ is the normal stress due to bending at mid-depth of compression zone and $\alpha_{fc} = (1.6 . f_{ctd} – 0.2. f_{ck}^{1/3}. f_{ctd})/ (1+0.6. f_{ctd}/f_{ck})$ is a coefficient taking into account different types of concrete.

$$V_{Rd,s,FS} = \frac{A_{sw}}{S_w}.f_{ywd}.(d_s\text{-}c).\cot\theta_{cr}$$

We know that for T-R0, S_w=400 mm, with Ø = 10mm A_{sw} = 157.1 mm^2, f_{ywd} = 440 MPa.

$(d_s\text{-}c) = 1042\text{-}450 = 592$ mm.

$V_{Rd,s,FS} = 203.5$ kN.

$V_{P,\infty} = P_{m,\infty,i} \times \alpha_{Pi} = 160$ kN

To calculate $V_{Rd,cz}$ the normal stress at mid-depth of compression zone is needed. This is obtained from the results of T-R0 in ATENA model. The critical cross-section is the location of the point load and the normal stress at this section is presented in Figure 5.54.

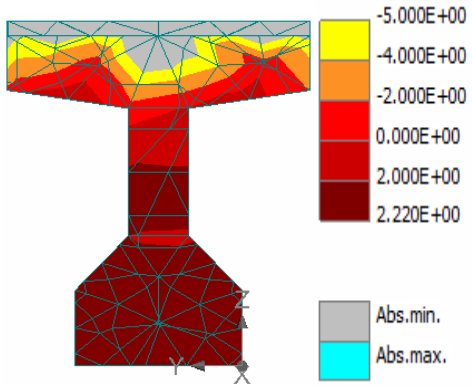

Figure 5.63 Normal stresses σ_{xx} at critical cross-section (MPa)

$\sigma_{x,cz,Ed}$ = -2.0 MPa. And we taking f_{ck} and f_{ctd} equal to 60 MPa and 4.0 MPa respectively, maximum shear stress $\tau_{xz,max}$ = 4.2 MPa

Using the above input parameters, $V_{Rd,cz}$ can be calculated.

$V_{Rd,cz}$ = 1077 kN.

The shear capacity calculated from flexural shear crack is $\mathbf{V_{Rd,FS,\ T\text{-}R0}}$ = 203+160+1077 = 1440 kN.
The shear capacity from the numerical analysis by ATENA $\mathbf{V_{u,\ ATENA,\ T\text{-}R0}}$= 1400 kN.

Similarly, the shear capacity calculated from flexural shear crack model for beam T-R1 (without stirrups) is $\mathbf{V_{Rd,FS,\ T\text{-}R1}}$ = 160+1077 = 1237 kN.
The shear capacity from the numerical analysis by ATENA $\mathbf{V_{u,\ ATENA,\ T\text{-}R1}}$ = 1267 kN.

The contribution of the arching action $V_{Rd,cz}$ to the shear capacities of T-R0 and T-R1 are 77% and 87% respectively. The contribution of the arching action to shear resistance of Pb1 and Pb2 is between 28% and 57%. The higher contribution of the arching action in T-R0 and T-R1 compared to Pb1 & Pb2 can be attributed to the higher compressive stress σ_{cp} due to prestressing in T-R0 and T-R1.

5.4 Strengthening of T beams with UHPFRC.

The exceptional material properties such as the tensile strain hardening and high durability of the UHPFRC composite offers a possible solution for strengthening of existing reinforced concrete structures. The suitability and effectiveness of strengthening with UHPFRC is investigated by strengthening the post-tensioned T beams.

3 beams with different ratios of shear reinforcements are strengthened with UHPFRC and their load-capacities and failure mechanism under 3- point bending are determined. The strengthened beams are denoted as T-U0, T-U1 & T-U3. These beams are reference beams T-R0, T-R1 & T-R3 strengthened with UHPFRC in their shear spans. The UHPFRC material is added to the web of the T-beams. A perfect bond between the web concrete and UHPFRC is assumed in the ATENA model.

The strengthened beams with the same amount of web reinforcement are compared to the non-strengthened reference beams.

5.4.1 T-R0 vs T-U0

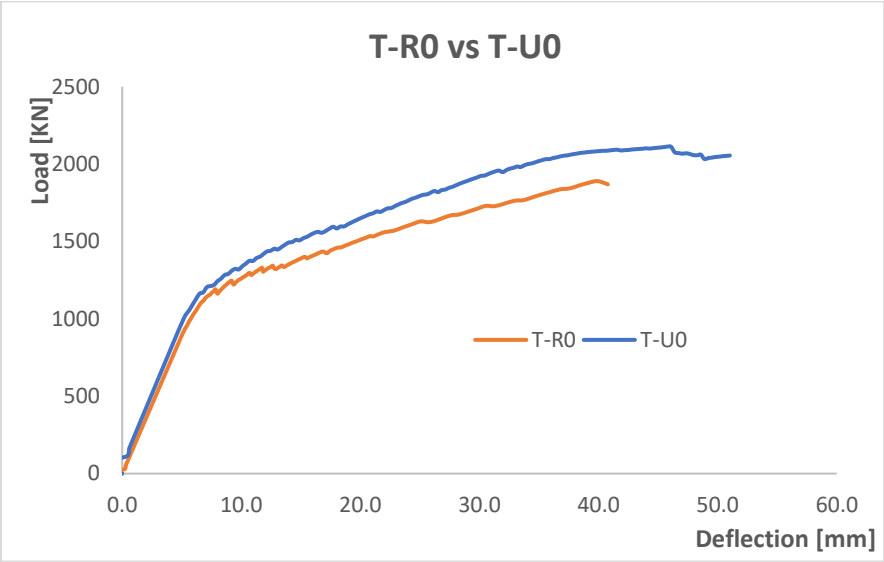

Figure 5.64 Comparison of load-deflection for T-R0 &T-U0.

The strengthened beam T-U0 has an ultimate load capacity of 2110 KN. The increase in the capacity over the reference beam T-R0 is not significant. An increase of 10% in ultimate capacity is possible with the addition of the UHPFRC composite.

The crack pattern at failure in both the beams are compared to understand the effect of the UHPFRC layer on the crack widths.

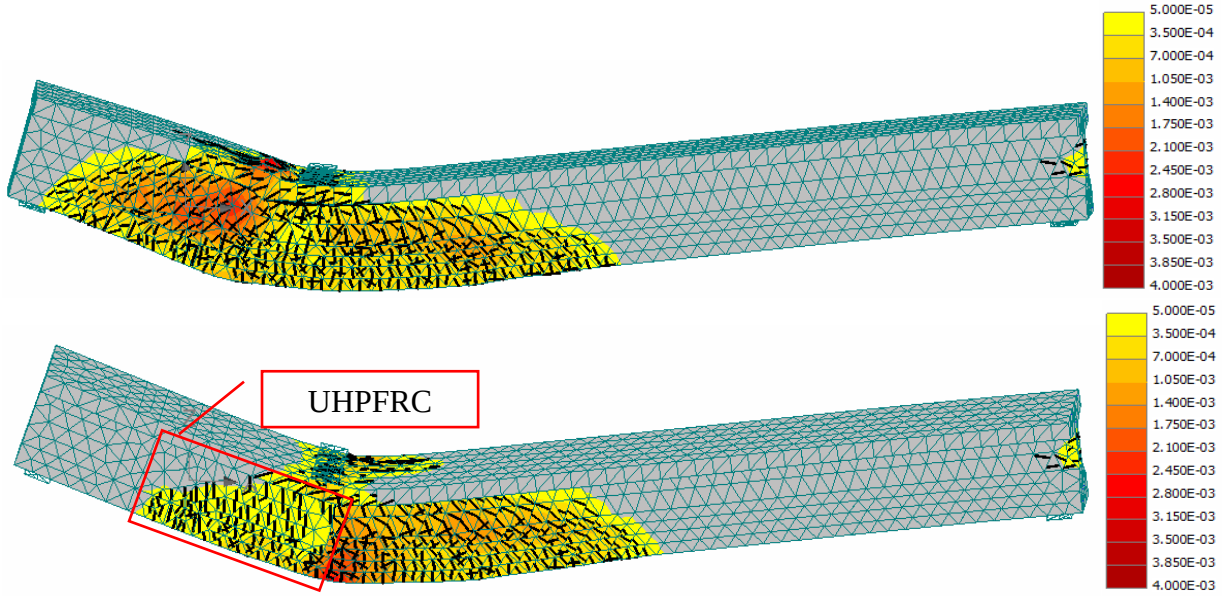

Figure 5.65 Comparison of crack patterns at failure in T-R0 and T-U0.

The effect of adding the UHPFRC layer is evident from Figure 5.65. There is no opening of the inclined shear crack, even at failure, in the region where the UHPFRC composite is added. The

reason for this is mainly the strain hardening behavior of UHPFRC in tension. Another reason is the increase in the cross-sectional width in the shear span due to the added layer. The strengthened beam ultimately fails in flexure. This can be confirmed by yielding of the longitudinal reinforcement and prestressing tendons (Figure 5.66 and 5.67). The effect of adding the UHPFRC layer can also be seen in the reduction of stresses in the transverse reinforcements in beam T-U0 as compared to the stresses in T-R0.

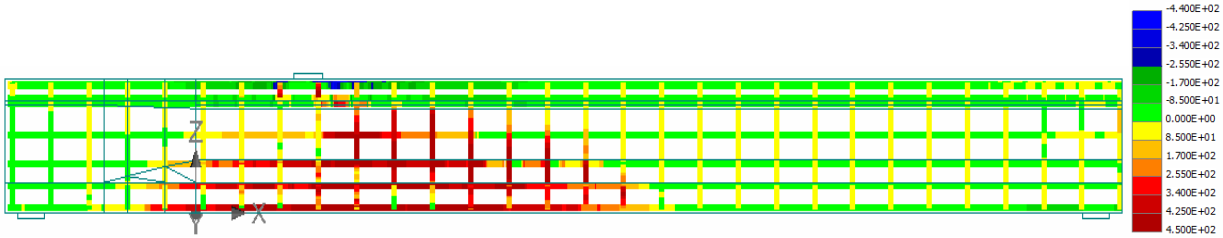

Figure 5.66 Normal stresses σxx in longitudinal and transverse steel at failure in T-U0 (MPa).

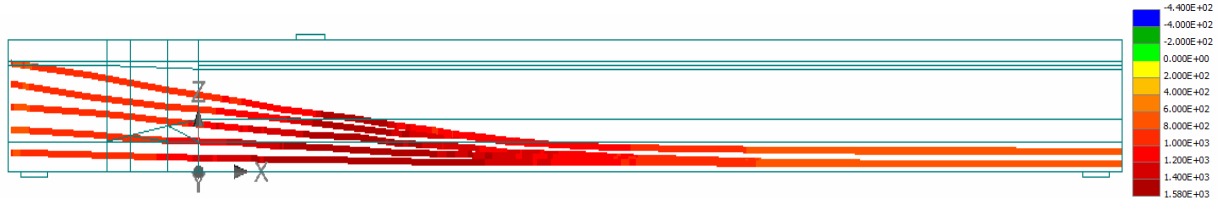

Figure 5.67 Normal stresses σxx in prestressing tendons at failure in T-U0 (MPa).

5.4.2 T-R1 vs T-U1 (without shear reinforcement).

In this case, the reference beam without stirrups (T-R1) is strengthened with UHPFRC to check for possible improvements in shear capacity and behavior.

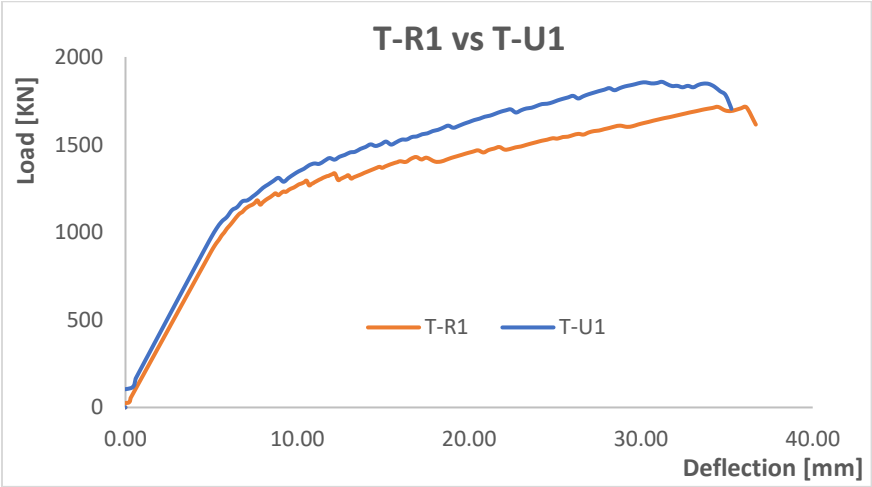

Figure 5.68 Comparison of load-deflection curves for T-R1 & T-U1.

The comparison is similar to the previous case, where there is not a significant increase in load capacity in the strengthened beam (1860 KN), i.e., an increase of 8% compared to that of the reference beam (T-R3).

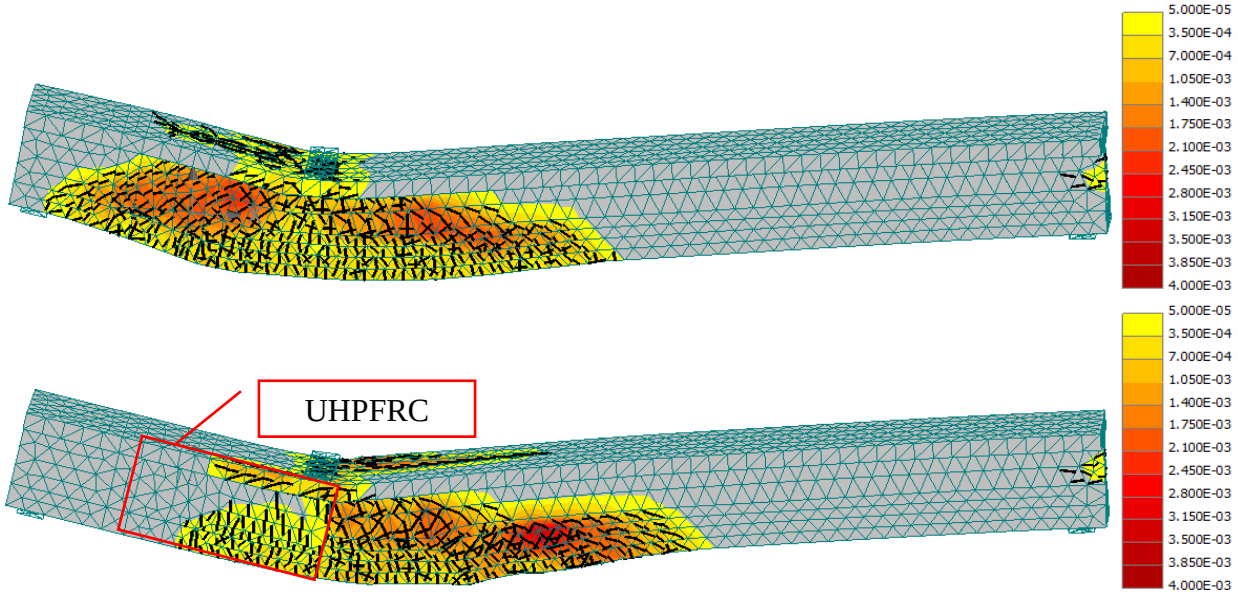

Figure 5.69 Comparison of crack patterns at failure in T-R1 and T-U1.

Here too, the opening of the inclined shear crack is prevented by the UHFRC composite. Also, the strengthened beam fails in bending by yielding of longitudinal steel (Figure 5.69). But before the yielding of prestressing steel (Figure 5.70) by crushing of concrete.

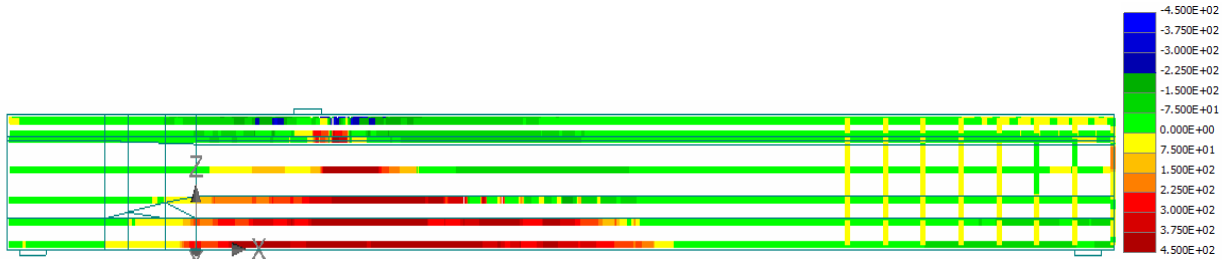

Figure 5.70 Normal stresses σxx in longitudinal steel at failure in T-U1 (MPa).

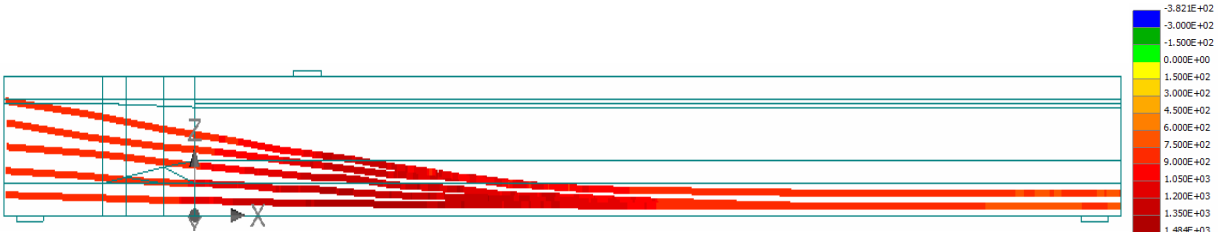

Figure 5.71 Normal stresses σxx in prestressing tendons at failure in T-U1 (MPa).

5.4.3 T-R3 vs R-U3 (without shear reinforcement and prestressing cables).

In the last comparison, the beam without the 3 prestressing cables (See figure 5.24) is strengthened with the UHPFRC composite. This beam is denoted as T-U3. The reference beam T-R3 is strengthened with the UHPFRC composite. It has already been seen in section 5.3.3 on how the prestressing influence the failure mode in the T-beam. Without the prestressing cables crossing the shear span, the T beam fails in a brittle manner by localization of the shear-flexural crack.

The effectiveness of the UHPFRC layer in preventing the brittle shear failure and the possible improvement in the ultimate load capacity is investigated in this section.

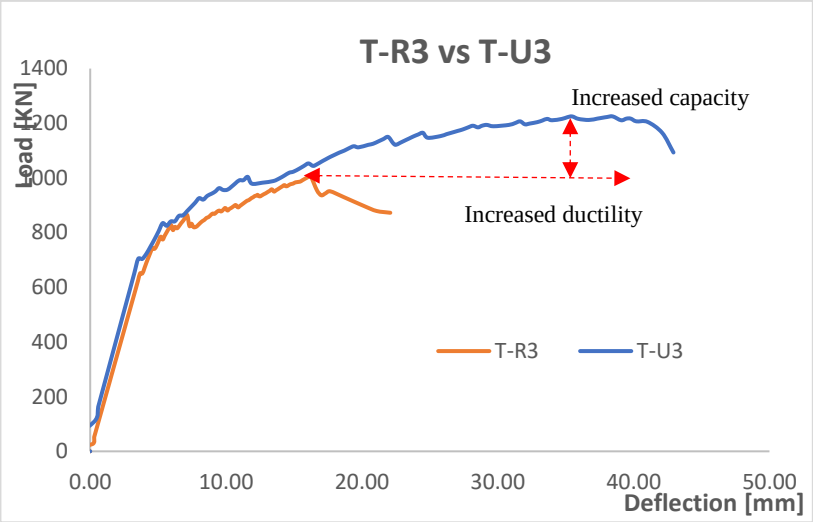

Figure 5.72 Comparison of load-deflection curves for T-R3 & T-U3.

It is quite clear from the Figure 5.72 that the strengthened beam not only shows an increase in ultimate capacity but also in ductility. The increase in the ultimate capacity is about 22% when compared to the reference beam. Also, a significant increase in ductility of 150% is achieved as a result of strengthening. This is a crucial result obtained in terms of the effectiveness of using UHPFRC as a strengthening material.

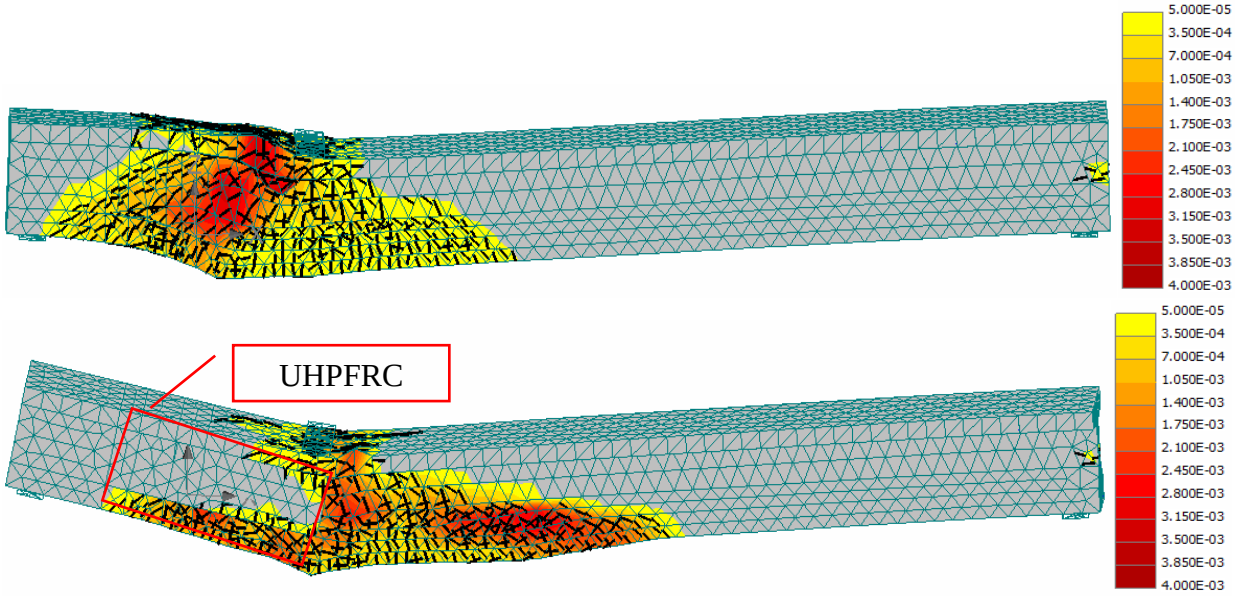

Figure 5.73 Comparison of crack patterns at failure in T-R3 and T-U3.

From the comparison of crack patterns, it is clear that the strengthened beam fails in a ductile manner in flexure without opening of an inclined shear crack. This is the obvious benefit of adding the UHPFRC material.

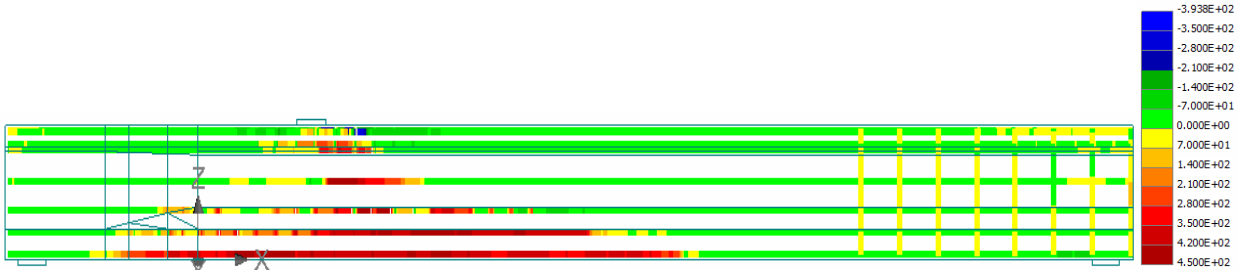

Figure 5.74 Normal stresses σxx in longitudinal steel at failure in T-U3 (MPa).

In all the three case, the UHPFRC is added to the cross-section of the T beam assuming a perfect bond between the beam and UHPFRC. The UHPFRC is bonded not only to the web region of the beam but also to both the flange (Figure 4.14). However, this type of connection is very optimistic to assume. Therefore, a simulation is carried out with UHPFRC bonded only to the web region of the T beam. This is denoted as T-U4 (Figure 5.75).

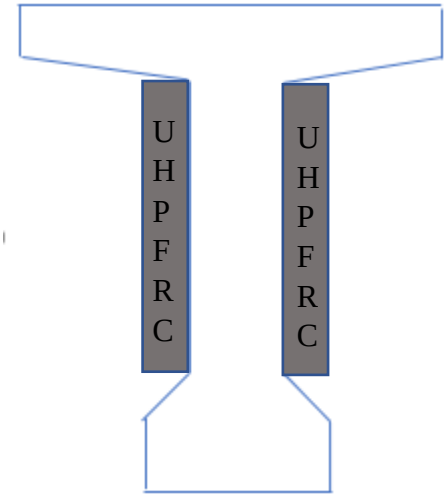

Figure 5.75 Strengthening configuration for T-U4

5.4.4 Strengthened Beam T-U4.

The UHPFRC layer is bonded only to the web region of the post-tensioned T beam and tested under 3-point bending load. This is done to investigate whether the effect of strengthening with UHPFRC differs in case the type of bonding between UHPFRC and the beam is altered from the type seen in T-U3.

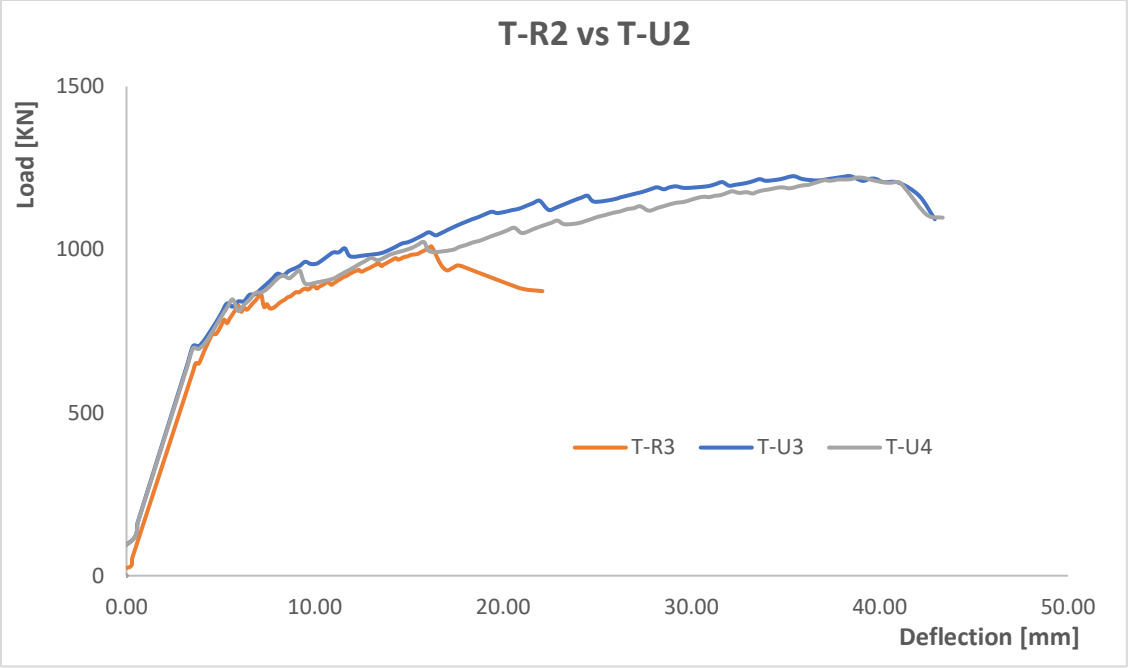

Figure 5.76 Comparison of load-deflection curve for T-U3 and T-U4.

From Figure 5.62, we can see that T-U4 has more or less has the same effect of strengthening as T-U3 even without complete bonding with the reference beam. This is an important observation has T-U4 results in a much lower usage of material albeit increasing the shear capacity of the reference beam T-R3 by the same margin as T-U3.

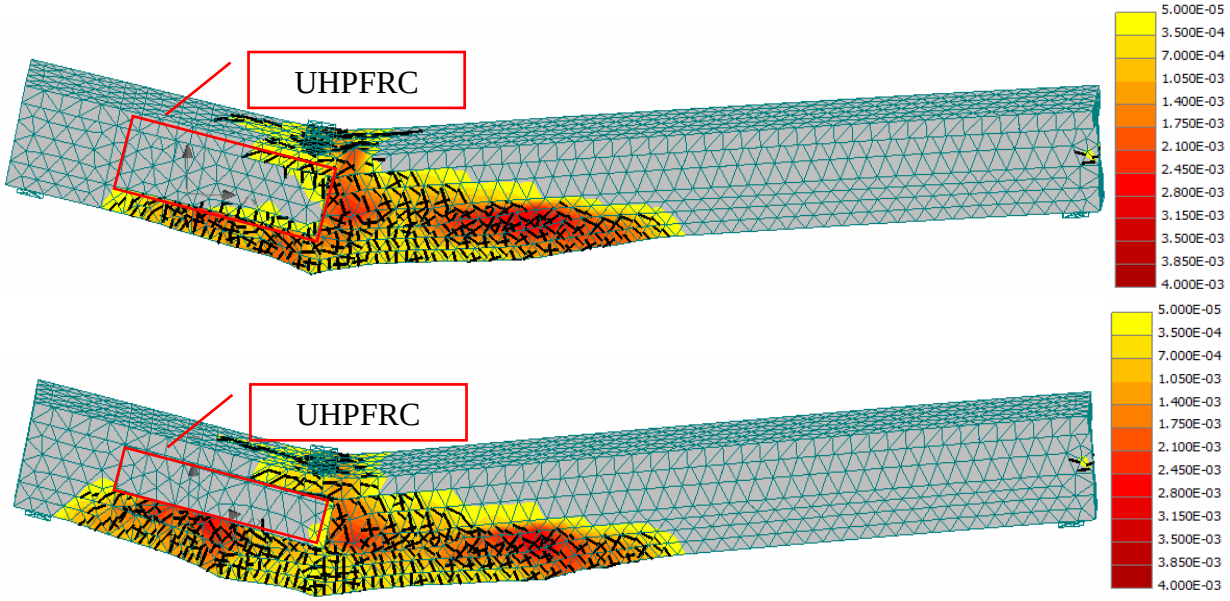

Figure 5.77 Comparison of crack patterns at failure in T-U3 and T-U4.

Table 5-9 Summary of Results.

Series	Beam	Shear crack (V_{cr}) (KN)	Shear Capacity (V_u) (KN)	Max Deflection. δ_{max} (mm)	Failure Mode	Increase in capacity (%)
Reference	T-R0	994	1400	40.8	Shear Compression	-
	T-R1	994	1267	36.7	Shear Compression	-
	T-R2	945	1064	28	Shear Compression	-
	T-R3	746	746	17.5	Shear Tension	-
Strengthened	T-U0	-	1532	50.0	Flexure	10
	T-U1	-	1368	38.0	Flexure	8
	T-U3	-	905	42.0	Flexure	22
	T-U4	-	905	42.0	Flexure	22

6 Conclusions & Recommendations.

In this research, the need for strengthening of existing concrete structures was outlined with special emphasis on shear strengthening. Shear failure represents a point of concern as a consequence of the brittleness associated with the failure. As a result, shear strengthening has been quite essential in the current age.

Although, many techniques have already been established for strengthening of concrete structures in both flexure and shear, the use of UHPFRC as a composite material offers an excellent choice due to its exceptional material properties such as the strain hardening behavior in tension and high durability.

For the purpose of investigating the impact of strengthening with UHPFRC, a post tensioned T beam supporting the Helperzoom bridge deck in Groningen, Netherlands was chosen. The post-tensioned T beam was modelled with the FEM programme ATENA and subjected to 3 point-bending tests. In the first step the reference T beam (non-strengthened) was modelled with varying parameters and tested to study the influence of such parameters on the failure mechanism and ultimate load capacity of the T beam. Later the T beam strengthened with UHPFRC was tested and the effectiveness of the UHPFRC layer was studied. In total 8 beams were modelled and tested on ATENA – 4 reference and 4 strengthened beams.

6.1 Conclusions

The following conclusions can be derived from the results obtained from the numerical simulations.

- The reference beam did not show a brittle shear failure immediately after opening of the shear tension crack. The stirrups and prestressing tendons contribute to the increase in shear capacity of the post-tensioned T beam after the shear tension crack has developed.
- The contribution of the stirrups and prestressing cables to shear capacity of the reference beam with stirrups is 12.5% and 6.4% respectively.
- The contribution of the prestressing cables to shear capacity of the reference beam without stirrups is about 5%.
- The reference beam without stirrups and 3 inclined prestressing cables crossing the shear span has the least shear capacity and ductility among all the reference beams. The beam fails in a brittle shear manner by localization of shear tension crack.
- The mechanism of failure observed in the numerical analysis of post-tensioned T beam of Helperzoom bridge shows close similarities with the failure seen in experiments performed on existing bridge girders of Melk Overpass bridge, Vienna. Both the girders fail by shear compression.

- The shear capacities of both reference beams (with and without stirrups) obtained from numerical analyses in ATENA are in close match to the capacities calculated from the Flexural Shear Crack Model proposed by Huber et.al
- The arching action in post-tensioned beams with low amount of shear reinforcement contribute significantly to the shear capacity of the beams. In T-R0 and T-R1, the contribution of the arching action to the shear resistance is 77% and 87% respectively.
- Out of the all the strengthened beams, beam T-U4 (without stirrups and 3 inclined prestressing cables) shows the maximum improvement in shear capacity (22%) and ductility (150%). The mode of failure also changes from a brittle shear failure (reference beam) to a ductile flexural failure (strengthened beam).
- The change in configuration of adding the UHPFRC – bonding UHPFRC to only the web region of the T beam showed the same effect as bonding UHPFRC to both the flange and web region of the T beam.

6.2 Recommendations

- The prestressing in the T beam is of a post-tensioned type in reality. However, the ATENA Engineering 3D model does not allow the definition of post-tensioning type of prestressing. Therefore, the model uses a pre-tensioning setting for prestressing and the prestressing force needs to be approximated by calculating the losses due to friction, wedge set and time dependent losses to arrive at a single value of the prestressing load. In the future, a way in which post-tensioning can be defined can be included in the model to avoid this approximation
- In the simulations, the prestressing tendons were modelled as reinforcements and the material properties of tendons were used to define the stress-strain relationship for reinforcements. These reinforcements which are in reality prestressing tendons were assumed to a have perfect bond with the concrete. However, it is known that the bond strength of prestressing steel is lower than that of conventional reinforcing steel [47]. This can have an effect on the redistribution of stresses and also the transfer length which influences the cracking behavior. The accuracy of model can be improved if the tendons can be defined as tendons and not reinforcements with a higher bond strength.
- The UHPFRC's strain hardening behavior is modelled solely by defining the stress-strain relationship. However other aspects such as the type of steel fibers (long or small) & orientation of the fibers have an influence on the tensile behavior of UHPFRC. These aspects need to be considered to future researches related to UHPFRC.
- The bond between the concrete in the web of the reference beams and the UHPFRC material is assumed to be perfect. However, it is almost impossible to have a perfect bond in practice. The influence of bond on the efficiency of strengthening needs to be investigated by modelling different types of bonds depending on the roughness factor of the concrete.
- The study on mesh refinement can be made to understand the influence of mesh size on the accuracy of results from the ATENA model.

7 References

[1] P. Huber, M. Vill, A. Schweighofer and J. Kollegger, "Full-scale shear tests on post-tensioned bridge girders of existing bridges," *Wiley fib,* 2017.

[2] "csengineermag.com," [Online]. Available: https://csengineermag.com/article/keys-to-success-structural-repair-and-strengthening-techniques-for-concrete-facilities/.

[3] [Online]. Available: https://theconstructor.org/structures/strengthening-concrete-structures/1576/.

[4] K. v. Breugel, *Concrete - Science and Technology,* TU Delft, 2017.

[5] M. Lukovic and D. A. Hodrijk, "Literature review on new concrete types; A start on exploring their opportunities for Dutch infrastructure," TU Delft, 2017.

[6] A. Reitsema, M. Lukovic and D. A. Hordijk, "Towards slender, innovative concrete structures for replacement of existing viaducts.," fib Symposium 2016 Performance-based Approaches for Concrete Structures., Capetown.

[7] C. Kennedy and J. C. Marlot, "Past performance and future needs for low carbon climate resilient infrastructure - an investment perspective.," *Energy Policy,* vol. 59, pp. 773-783, 2013.

[8] L. Yan and N. Chouw, "Behavior and analytical modeling of natural flax fiber reinforce polymer tube confined plain concrete and coir fibre reinforced conrete," *Journal of Composite Materials,* vol. 47, no. 17, 2013.

[9] J. R. Casas, "Frontiers in Built Environment," [Online]. Available: https://www.frontiersin.org/articles/10.3389/fbuil.2015.00003/full.

[10] M. Li, *Multi-scale design for durable repair of concrete structures.,* University of Michigan, 2009.

[11] [Online]. Available: https://www.fhwa.dot.gov/publications/research/infrastructure/structures/11030/004.cfm.

[12] K. M.J, "Analysis and Numerical analysis of shear tension critical prestressed beams.," TU Delft, 2016.

[13] [Online]. Available: https://civildigital.com/failure-modes-beams/shear-compression-failure/.

[14] A. S. D. a. E. S. E. J. O'Brien, "Reinforced and prestressed concrete design to EC2: the complete process," Spon press, 2016.

[15] "Recollect - Upper Hutt City Library Heritage Collections," [Online]. Available: http://uhcl.recollect.co.nz/nodes/view/19286.

[16] "Pinterest," [Online]. Available: https://nl.pinterest.com/pin/272819689902524890/?lp=true.

[17] Y. Kim, K. Quinn, N. Satrom, J. Garcia, W. Sun, W. M. Ghannoum and J. O. Jirsa, "Shear Strengthening of Reinforced and Prestressed Concrete Beams Using Carbon Fiber

Reinforced Polymer (CFRP) Sheets and Anchors," The University of Texas at Austin, Texas, 2012.

[18] E. Sistonen and F. Al-Neshawy, "Repair Methods of Structures," Alto University, 2016.

[19] [Online]. Available: https://csengineermag.com/article/keys-to-success-structural-repair-and-strengthening-techniques-for-concrete-facilities/.

[20] "Zimmermann Consult," [Online]. Available: www.zimmermann-consult.at/.

[21] C. Oesterlee, "Structural Response of Reinforced UHPFRC and RC Composite Members.," ÉCOLE POLYTECHNIQUE FÉDÉRALE DE LAUSANNE, 2010.

[22] "Building Trust Sika," [Online]. Available: https://gbr.sika.com/en/solutions_products/sika-markets/structural-strengthening/news/cfrp-the-alternative-to-steel-strengthening-existing-structures.html.

[23] "Epoxy Design Systems," [Online]. Available: http://www.epoxydesign.com/carbon-fiber-reinforced-polymers-cfrp/.

[24] L. Bisby, M. Green and V. Kodur, "Response to fire of concrete structures that incorporate FRP," *Progress in Structural Engineering and Materials,* vol. 7, no. 2, pp. 136-149, 2005.

[25] L. Fentao, W. Bo and W. Demin, "Failure modes of reinforced concrete beams strengthened with carbon fiber sheet in fire.," *Fire Safety Journal,* vol. 44, no. 7, pp. 941-950, 2009.

[26] E. Chatzi, E. Bruhwiler and H. Martin-Sanz, "The use of Ultra High Performance Fibre Reinforced Cement Based Composites in rehabilitation projects : a review," in *9th International Conference on Fracture Mechanics of Concrete and Concrete Structures*, Berkeley, 2016.

[27] E. Denarie, "Recommendations for the tailoring of UHPFRC recipes for rehabilitation," Deliverable Arches D06, 2009.

[28] E. Bruhwiler, "Welcome to the post-concrete era!," 2016.

[29] M. H. Al-Sherrawi and I. Hameed, "Studying the Combination Effect of Additives and Micro Steel Fibers on Cracks of Self-Healing Concrete," *University of Baghdad Engineering Journal,* vol. 22, no. 1, pp. 49-67, 2016.

[30] E. Fehling, "Design relevant properties of hardened Ultra High Performance Concrete," in *Proceedings of the international symposium on Ultra-High Performance Concrete - Heft 3*, Kassel, 2011.

[31] J. Wuest, "Structural behaviour in tension of Ultra-High Performance Fibre Reinforced Concrete in Composite Elements," Doctoral Thesis:3987 Swiss Federal Institute of Technology Lausanne (EPFL), 2007.

[32] E. Denarie and E. Bruhwiler, "Strain Hardening of Ultra-high Performance Fibre Reinforced Concrete:Deformability vs Strength Optimization," *International Journal for Restoration of Buildings and Monuments,* vol. 12, no. 6, pp. 397-410, 2011.

[33] A. Kamen, E. Denarie, H. Sadouki and E. Bruhwiler, "UHPFRC tensile creep at early age," *Materials and Structures,* vol. 42, no. 1, pp. 113-122, 2009.

[34] A. Switek-Rey, E. Denarie and E. Bruhwiler, "Early age creep and relaxation of UHPFRC under low to high tensile stresses," *CCR-Cement and Concrete Research,* vol. 86, pp. 57-69, 2016.

[35] T. Makita and E. Bruhwiler, "Tensile fatigue behaviour of UHPFRC," *Materials and Structures,* vol. 47, pp. 475-491, 2014.

[36] J. P. Charrron, E. Denarie and E. Bruhwiler, "Permeability of Ultra High Performance Fiber Reinforced Concrete (UHPFRC) under high stresses," *Materials and Structures,* vol. 40, no. 3, pp. 269-277, 2007.

[37] K. Wassmann and E. Bruhwiler, "Strengthening of RC slabs using UHPFRC – Concepts and applications," in *4th International Symposium on Ultra-High Performance Concrete and High Performance Materials*, Kassel, 2016.

[38] E. Bruhwile and E. Denarie, "Rehabilitation of concrete structures using Ultra-High Performance Fibre Reinforced Concrete.," in *Proceedings of Ultra High Performance Concrete* , Kassel, 2008.

[39] E. Fehling, M. Schmidt and S. Sturwald, "Ultra High Performance Concrete (UHPC)," Kassel, Kassel University Press, 2008, p. 901.

[40] V. A. I. ,. M. C. D. K. a. J. H. Martin Herbrand, "Strengthening of Existing Bridge Structures for Shear and Bending with Carbon Textile-Reinforced Mortar.," 2017.

[41] T. Noshiravani and E. Brühwiler, "Experimental Investigation on Reinforced Ultra-High-Performance Fibre Reinforced Composite Concrete Composite Beams subjected to combined bending and shear," *ACI Structural Journal.*

[42] V. Cervenka and J. Cervenka, *ATENA Program Documentation, Part 2-2, Manual for ATENA 3D,* Cervenka Consulting, 2017.

[43] B. Runzel, C. K. Shield and C. W. French, "Shear Capacity of Prestressed Concrete Beams," Department of Civil Engineering, University of Minnesota, Minnesota, 2007.

[44] D. K. B. F. K-H Reineck, "Extended Databases with Shear Tests on Structural Concrete Beams Without and With Stirrups for the Assessment of Shear Design Procedures [in German]," in *DeutscherAusschuss für Stahlbeton, DAfStB-Heft No. 597; 2012.*, Berlin, Germany:, 2012.

[45] H. e. a. P, "Approach for the determination of the shear strength of exist-ing post-tensioned bridge girders with a minimum amount of transverse reinforcement [in German]," in *Bauingenieur*, 2016.

[46] P. Huber, " Assessment of the Shear Strength of Existing Reinforced and Pre-stressed Concrete Bridges," TU Wien, 2016.

[47] P.-I. J. Walraven and d. C. Braam, *Prestressed Concrete - CIE 4160,* Delft University of Technology, 2015.

[48] G. P. Tilly and J. Jacobs, "Concrete repairs: Observations on performance in service and current practice," IHS BRE Press, Watford, 2007.

[49] H. M. Tanarslan, "Flexural strengthening of RC beams with ultra high performance fibre reinforced concrete laminates," *Engineering Structures,* pp. 337-348, 2017.

[50] J. H. M. VISSER and Q. F. V. ZON, "Performance and service life of repairs of concrete structures in Netherlands.," in *Concrete Repair, Rehabilitation and Retroffiting III*, London, 2012.

Appendix 1.

Girder drawings

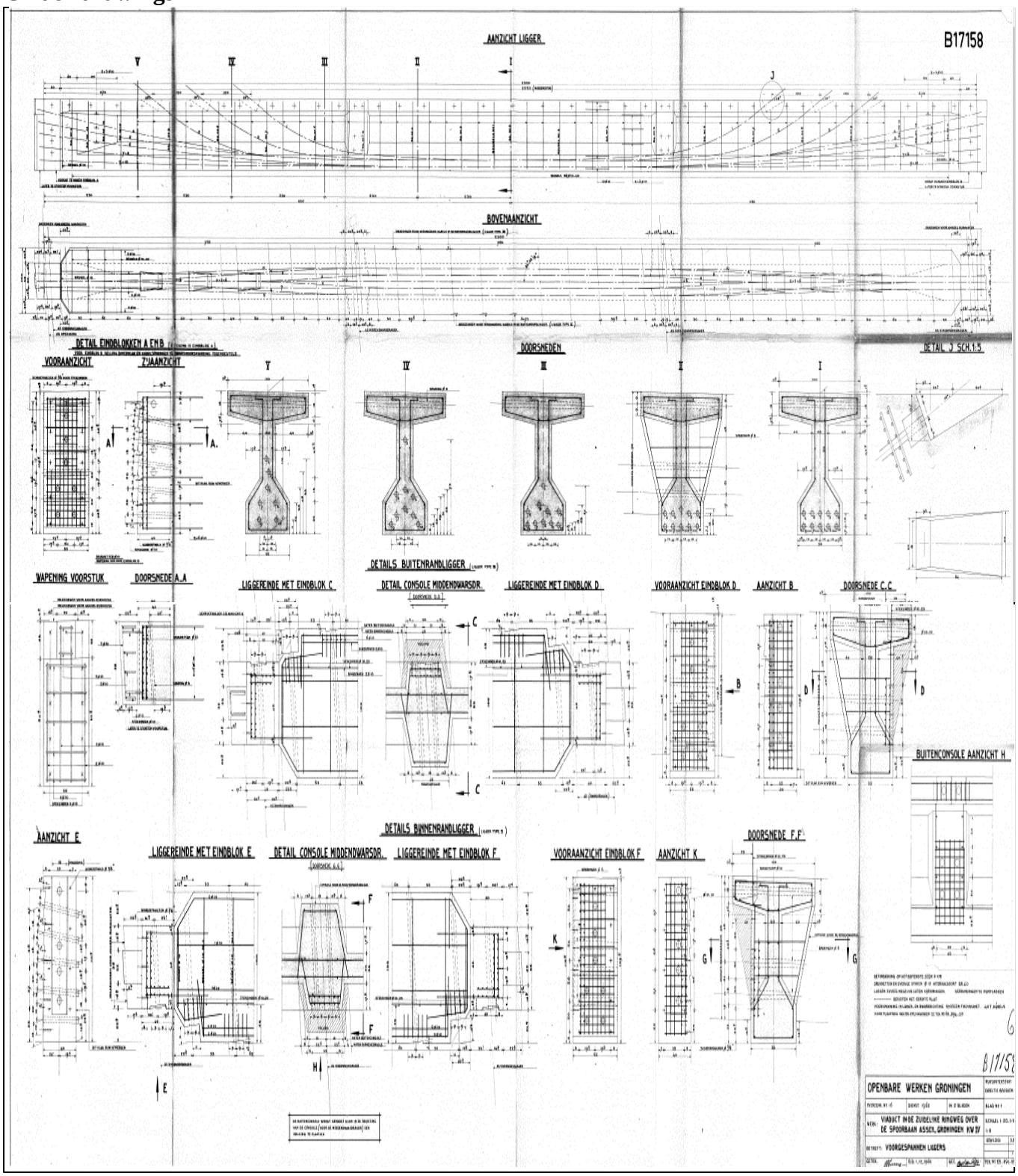

Appendix 1.

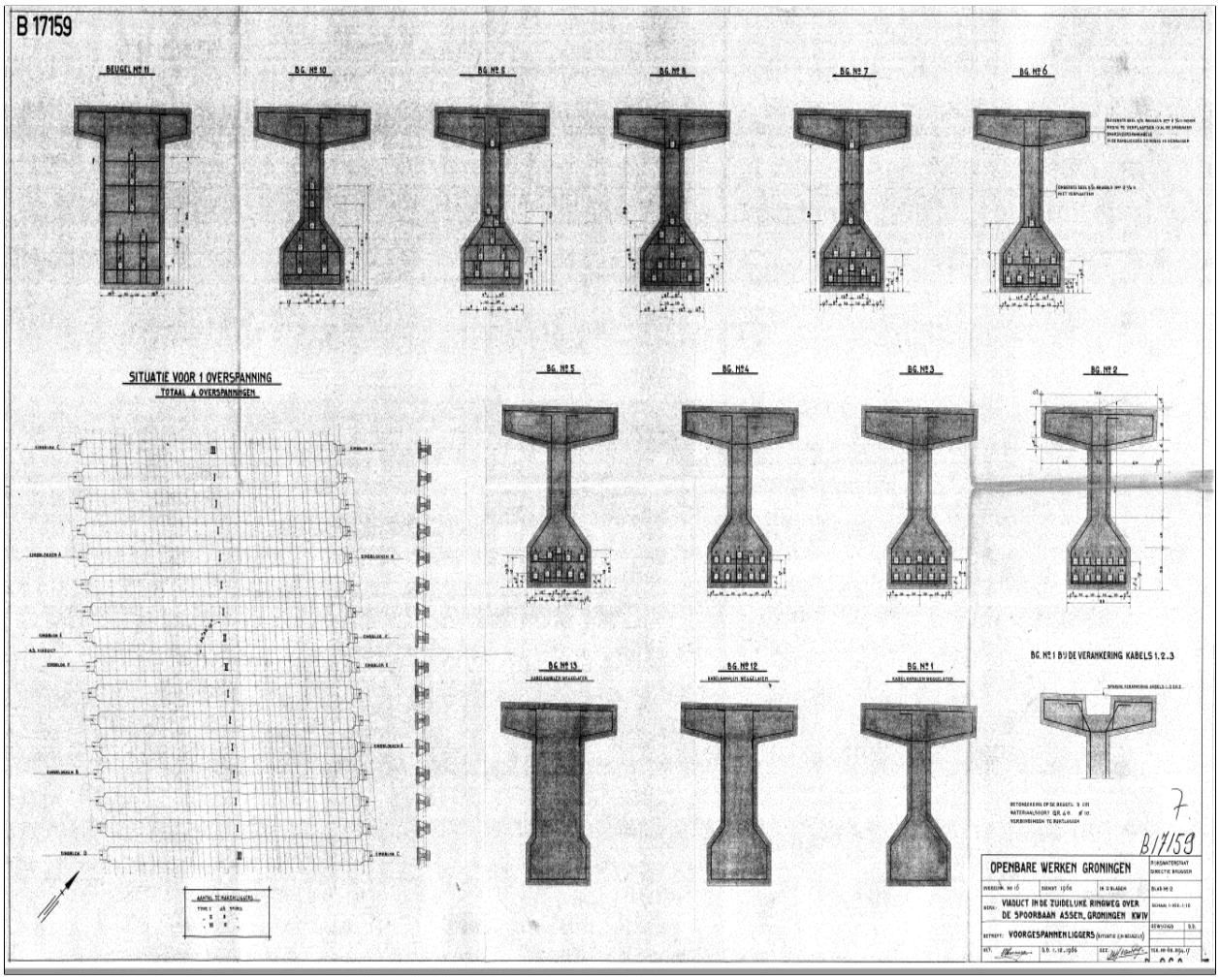
B 17159
BEUGEL Nº 11
BG. Nº 10
BG. Nº 9
BG. Nº 8
BG. Nº 7
BG. Nº 6
SITUATIE VOOR 1 OVERSPANNING
TOTAAL 4 OVERSPANNINGEN
BG. Nº 5
BG. Nº 4
BG. Nº 3
BG. Nº 2
BG. Nº 13
BG. Nº 12
BG. Nº 1
BG. Nº 1 BIJ DE VERANKERING KABELS 1.2.3
7.
B17159
OPENBARE WERKEN GRONINGEN
VIADUCT IN DE ZUIDELIJKE RINGWEG OVER DE SPOORBAAN ASSEN, GRONINGEN KWIV
VOORGESPANNEN LIGGERS

Appendix 2

1. Cross-sectional area of post-tensioned T beam (A_c) and Second Moment of Inertia (I).

The cross-sectional area and second moment of inertia for the nominal cross-section of the post-tensioned T beam is estimated using a simplified cross-section.

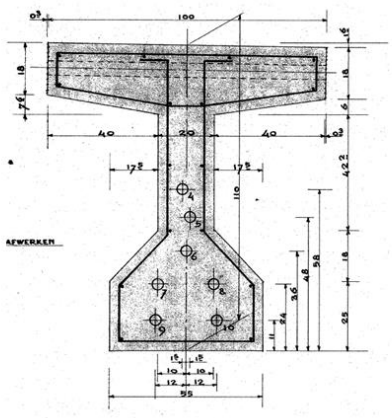

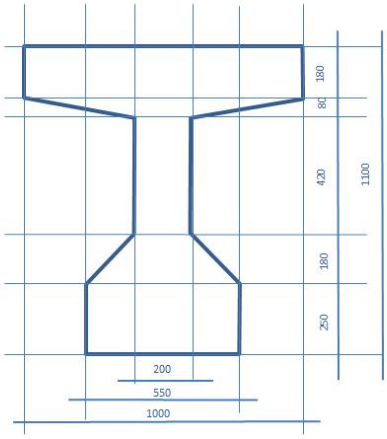

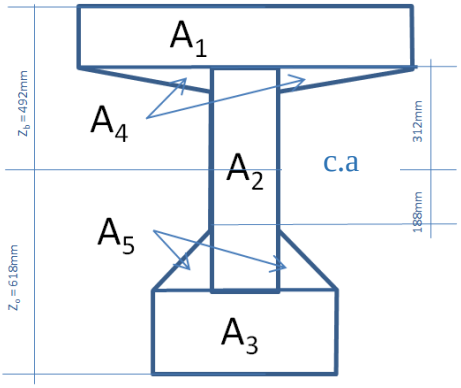

A	A (10^3 mm^2)	Z (mm)	Z_b- Z (mm)	I (10^{10} mm^4)
A_1	180	90	402	2,96
A_2	136	520	-28	0,53
A_3	137,5	985	-493	3,42
A_4	32	207	285	0,26
A_5	31,5	800	-308	0,30
Σ	517			7,47

$A_c = 517.10^3$ mm^3 and $I = 7.47.10^{10}$ mm^4.

2. Load from self-weight.

The calculation for self-weight of the T beam is simplified by assuming a constant cross-section of the beam with. (A_c=517.10^3 mm^3). The uniformly distributed load due to self-weight of beam between the span of 11.15 m is $q_g = A_c . \gamma_c = 0.517.23 = 11.9$ kN/m. The support reactions V_A & V_B due to self-weight = (11.9 x11.15)/2 = 66.3 kN.

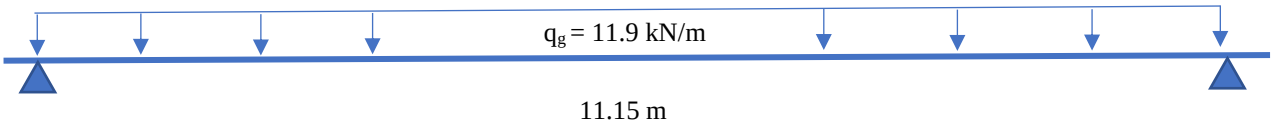

3. Load from prestress.

The prestress consists of 40tons cables from the Freyssinet system. The calculation is based on cables with Ap = 462mm2 and steel quality QP170. The prestressing steel has a yield strength f_{py}= 1570 MPa and Ultimate strength f_{pu} of 1603 MPa. The working stress is assumed to be 1084 MPa which is equal to P_{m0} = 500 kN.

Systeem	Toegepast vanaf	Groepering	Staalopp. [mm2]	Staal-kwaliteit	Max. blijvende voor-spankracht (= 55%)	Max. aanvangsvoor-spankracht (= 65%)	Opmerking
Freyssinet	1960	Kabel: 12Ø5 (d)	236	QP150	190 kN (19,4 tf)		Na 1965 is QP 150 hiervoor niet meer veel toegepast.
				QP170	216 kN (22,0 tf)		
	1960	Kabel: 12Ø7 (d)	462	QP150	374 kN (38,1 tf)		
				QP170	424 kN (43,2 tf)		
'40-tons' kabels	1966	Kabel: 12Ø7 (d)	462	QP170	424 kN (43,2 tf)	500 kN (51 tf)	Netto intrekking normale verankering = 7 mm
	1966	Kabel: 12Ø7,5 (d)	530	QP170	486 kN (49,5 tf)	574 kN (58,5 tf)	Netto intrekking normale verankering = 7 mm
	1970?	Kabel: 12Ø8 (d)	603	QP170	549 kN (56 tf)	657 kN (67 tf)	

4. Losses in Prestresses.

The losses in the prestressing force due to friction and wedge set losses need to be calculated to assign a prestressing load in the ATENA model. Also, the time dependent losses (shrinkage, creep and relaxation) are approximated to be 20% since the post-tension beam are are nearly 50 years old.

i. **Friction losses**.

The losses due to friction at different points along the longitudinal axis is estimated using the expression from the Dutch National Annex (EN 1992-1-1 eq (5.45)). The loss is calculated for one cable and all the other cables are assumed to have the same amount of losses as calculated. Cable 4 is chosen for calculation.

$$P_{max}(x) = P_{max}\, e^{-\mu(\theta + k\,x)}$$

where *x* is the distance from the position where the jack is applied (active end) to the cross-section considered. It is assumed that the coefficient of friction is μ = 0.26 and that the angular rotation caused by the Wobble effect is *k* = 0,01 rad/m. The T beam is stressed from both sides during prestressing and over-tensioning of 10% is allowed during anchoring.

P_{max} = 550 kN.

θ is the change in rotation and for a curved tendon with a parabolic profile θ = Δx/R, where x is distance along the longitudinal axis of the tendon and R is the radius of curvature of the tendon. Radius of curvature R is given by R = l^2/8f, where l is the length of the span of the tendon in the beam and f is the drape. l=23.0 m and f = 0.5 m. Therefore R = 132.25 m. The calculations are performed in excel using the expression and the friction losses are estimated.

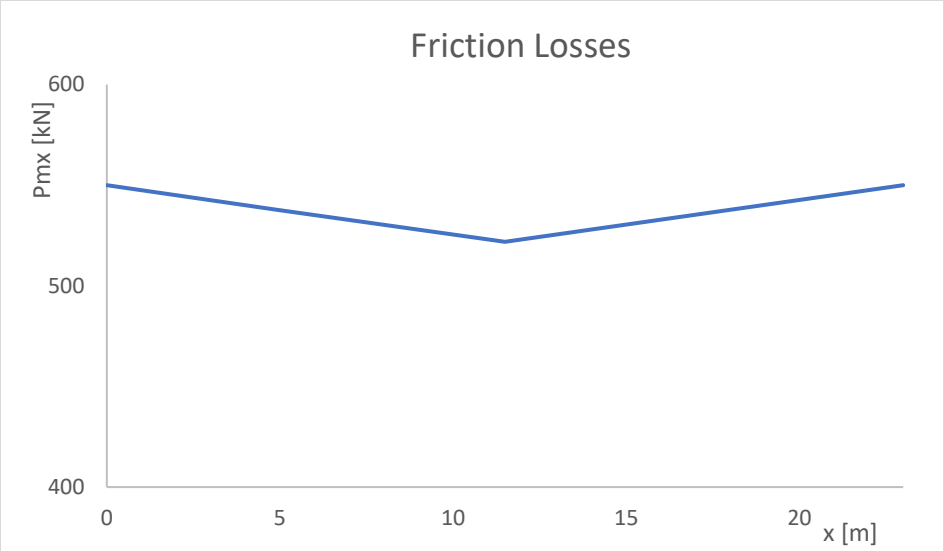

Losses due to friction.

ii. Wedge set losses.

The loss due to wedge is estimated using the expression $\Delta P_w = 2A_P \frac{\Delta\sigma_{p\mu,m}}{\Delta x} l_w.$

where $\Delta\sigma_{p\mu,m}/\Delta x$ is the mean stress reduction in the tendon caused by friction over the length l_w. (Note: Units, for example, N/mm2/mm). The slip in strands due to wedge set is given by $w = \frac{A_p.\Delta\sigma_{p\mu,m}.l_w^2}{A_p E_p \Delta x}$. The slip w is 7 mm for the given prestressing system. $\frac{\Delta\sigma_{p\mu,m}}{\Delta x} = 5.3\ MPa/m.$

From the expression l_w can be calculated and is equal to 16.45 m and $\Delta P_w = 80.5$m. This is loss at anchors on both sides of the T beam. The loss due to wedge set on one side will influence the prestressing force on the other side. However, the focus is only on the shear span of the mean i.e., between 0 and 2.903 m from the left-hand support. Therefore, the influence of wedge on the other side of beam is neglected since the l_w is 16.45m which is outside the shear span region. (from the right-hand side of the beam).

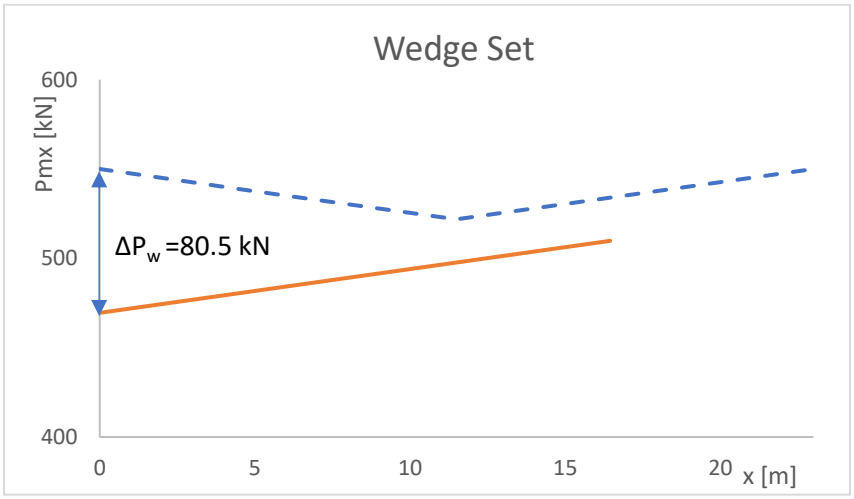

Wedge set loss.

The prestressing force at anchor position P_m (x=0) is 550-80.5 = 469.5 kN. In the ATENA a single value of prestressing load is assigned, and this load is based on the location where shear failure is expected. Shear failure/crack is expected at 1.725 m from the left-hand support. The prestressing load at this location is calculated. The inputs are the P_m (x=0) and the slope ($\frac{\Delta\sigma_{p\mu,m}}{\Delta x} = 5.3$MPa/m).

Pmo(x=1.725) = 472 kN.

iii. Time Dependent Losses.

The time dependent losses in prestressing is approximated to be 20%. This results in a working prestressing load $P_{m,\infty} = P_{mo}.0.8 = 377.6$ kN. The prestressing load to be assigned is ATENA model is **380 kN**.

5. Stresses due to self-weight and prestressing.

The stresses in concrete due to self-weight and prestressing are calculated at 2 positions. At the point of application of the bending load and at the right-hand support position.

The prestressing results in a curvature pressure which causes a negative moment (upward curvature) in the beam. The self-weight causes a positive moment (downward curvature). The stresses are calculated at the top fibre and bottom fibre of the beam.

Concrete stress at x=2.903.

At top fibre

$$\sigma c, top = +\frac{M_p Z_b}{I} - \frac{M_g Z_b}{I} - \frac{N_p}{A_c}$$

At bottom fibre

$$\sigma c, bottom = -\frac{M_p Z_o}{I} + \frac{M_g Z_o}{I} - \frac{N_p}{A_c}$$

Concrete stress at x=11.15

At top fibre

$$\sigma c, top = +\frac{M_p Z_b}{I} - \frac{N_p}{A_c}$$

At bottom fibre

$$\sigma c, bottom = -\frac{M_p Z_o}{I} - \frac{N_p}{A_c}$$

M_p is the moment due to the eccentricity of prestressing, M_g is the moment due self-weight, N_p is the compressive stress due to prestressing at the centroidal axis of the cross-section, A_c is the

cross-sectional area of the beam, I is the second moment of inertia of the beam, Z_b and Z_o are the distances of the top and bottom fibre to the centroidal axis respectively.

To calculate the moment due to eccentricity of prestressing tendons, there eccentricities with respect to the centroidal axis need to be determined first.

The cable 10 and 9 (one height), 8 and 7 (one height), 6, 5 and 4 are important for the cross sections (beam section) to be considered. Cables 3, 2 and 1 (which are anchored at the top of the flange) have no influence on the transverse force and the moment in the cuts to be considered.

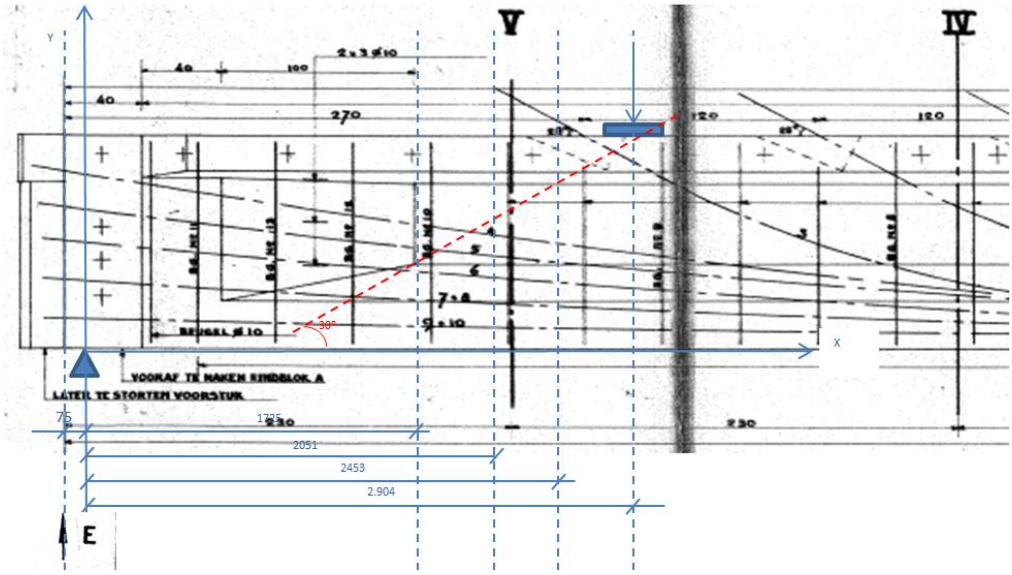

The moments and shear forces are determined by the cutting method. The location of the prestressed cables (c = cover) in the cuts 'view E', V and IV are indicated in the drawing. For the cross sections to be considered at 1.725, 2.051, 2.453 and 2.903, location is determined by linear interpolation. In this way it is easy to determine MP (with d = h - c = 1110 - c, and ep = d - zb = d - 492). In determining c, it has been taken into account that the c of cables 7 & 8 and 9 & 10 count double.

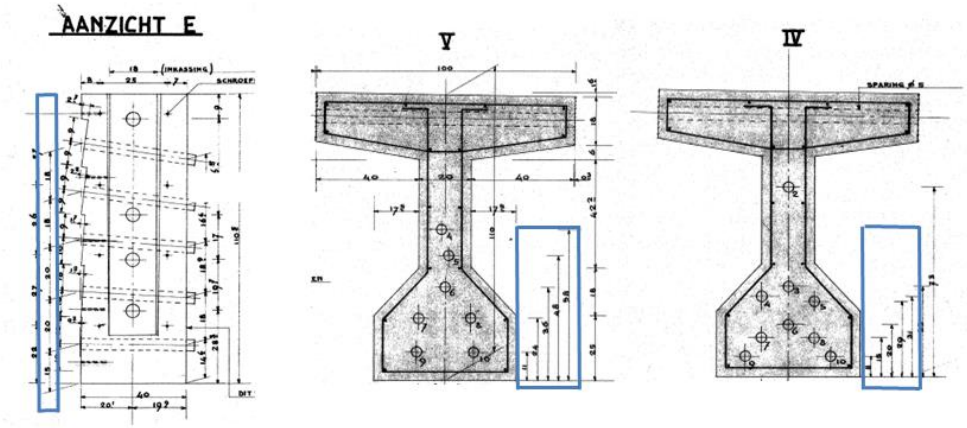

c (cut)		View E		cut V			cut IV	
X (m)	N_p	-0.075	1.725	2.051	2.3	2.453	2.903	4.6
Cable 4	380	910	659.9	614.6	580	562.0	509.2	310
Cable 5	380	730	540.5	506.2	480	467.4	430.2	290
Cable 6	380	550	406.0	379.9	360	349.4	318.1	200
Cable 7 & 8	380	350	266.6	251.5	240	234.0	216.4	150
Cable 9 & 10	380	150	119.7	114.2	110	108.0	102.1	80
$\sum N_p$ (kN)	2660							
	c =	455.7	339.9	318.9	302.9	294.7	270.6	180.0
	d =	654.3	770.1	791.1	807.1	815.3	839.4	930.0
	e_p =	162.3	278.1	299.1	315.1	323.3	347.4	438.0
	M_p =	431.7	739.7	795.3.0	873.9	860.0	924.0	1165

For x = 2.903, Mp = 924 kN-m, $M_g = V_A.2.903 – 11.9x2.903x0.5x2.903 = 142.5$ kN-m, $N_p = 2660$ kN, $A_c = 517.10^3$ mm and $I = 7.47.10^{10}$ mm^4, Z_o=618 mm and Z_b = 492 mm.
From this,
$\sigma_{c,\,top} = 0$ MPa
$\sigma_{c,bottom}$= -11.5 MPa (Compression).

At x = 11.15, the 3 other prestressing cables also contribute to the curvature pressure. Therefore, the curvature pressure is from the 10 prestressing cables at x =11.15. The distance d for the cables can be calculated by taking a weighted average of all the 10 cables.
d_p = (950x3+1040x7)/10 = 1013 mm. $e_p = d-Z_b = 1013-492 = 522$ mm. $N_p = 380x10 = 3800$ kN and $M_P = N_P.e_p = 1983.6$ kN-m. Also, no moment at the supports due to self-weight i.e., $M_g = 0$.
The stresses at x = 11.15 m can be calculated using the above values.
$\sigma_{c,\,top}$ = +5.65 MPa
$\sigma_{c,bottom}$ = -23.75 MPa (Compression).

Appendix 3

1. **Moment Capacity Calculation.**

The bending moment capacity of the post-tensioned T girder is calculated by cross-sectional analysis to determine the bending moment resistance M_{Rd} at the section x=2.903 where the maximum bending moment due to point load will occur.

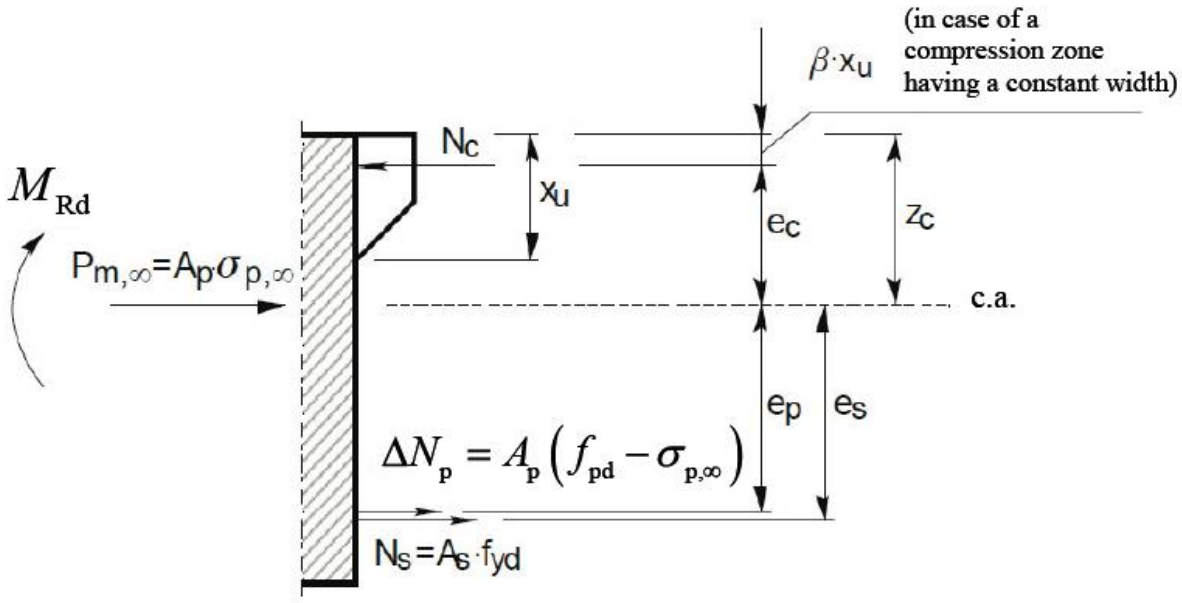

In order to calculate the bending moment resistance, the effective depths d_s and d_p of longitudinal reinforcement and prestressing tendons and the depth of compression zone x_u need to be determined.

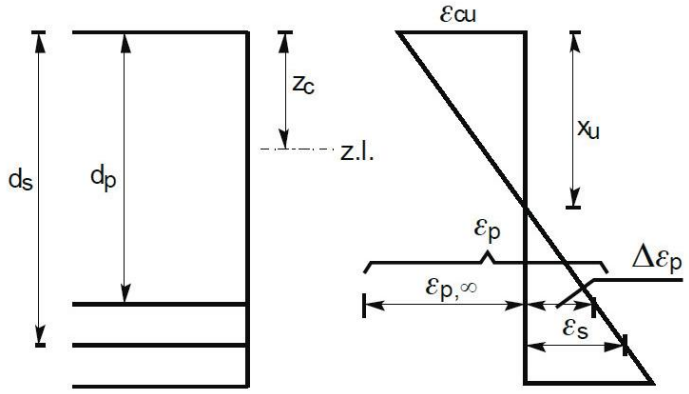

Appendix 3

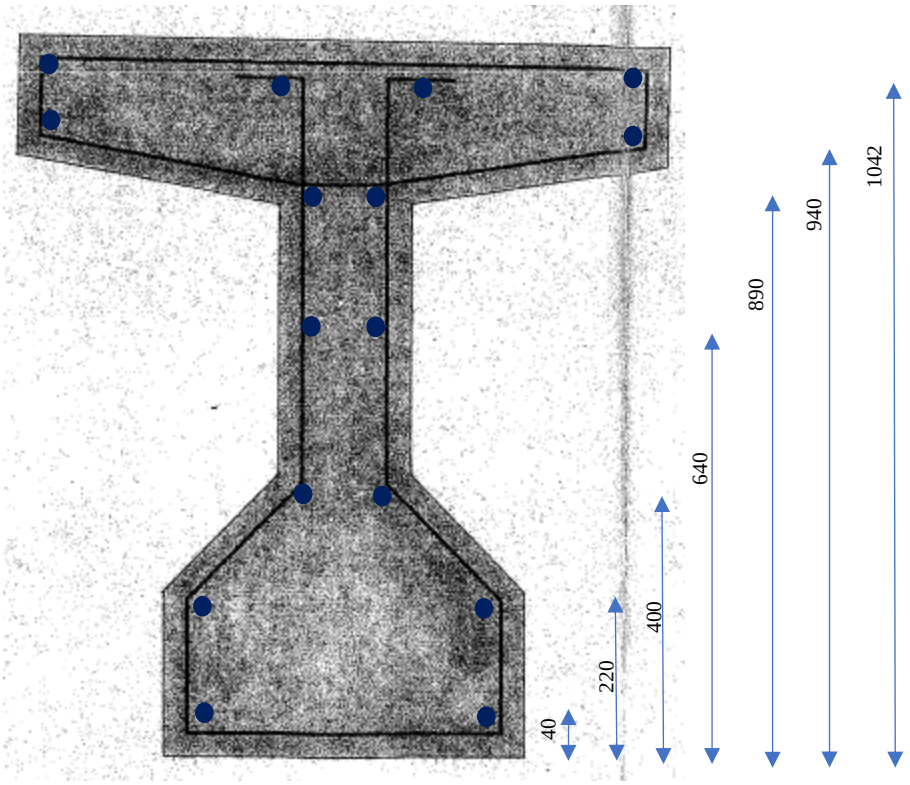

$$h - d_s = \frac{2A_s(40 + 220 + 400 + 640 + 890 + 940) + 4A_s(1042)}{16A_s}$$

d_s =440.25 mm
d_P = 975.5 mm (at x=2.903)

To determine the depth of compression zone x_u horizontal equilibrium of forces can be used.
Σ H=0:
$N_c=P_{m\infty}+N_s+\Delta N_P$
$\alpha.f_c.b.x_u = P_{m\infty}+A_sf_y+A_P(f_{pd}-\sigma_{pm\infty})$
Assuming the compression zone is in the top flange b = 1000 mm and for normal strength concrete α=0.75.
f_c = 60 MPa, $P_{m\infty}$= 2660 kN, A_s = 1256.8 mm^2, A_p = 7x462 = 3234 mm^2, $\sigma_{pm\infty}$ = 822.5 MPa, f_y=440 MPa

f_{pd} is the stress in prestressing steel at ULS. To begin the calculation f_{pd} can be taken as 0.95.f_{pu}. With f_{pu} =1603 MPa, f_{pd}=1522.85 MPa. From this the depth of compression zone can be obtained using the equilibrium condition.
$0.75x60x1000x_u=2660.10^3+1256.8x440+3234(1522.85-822.5)$
x_u =121.7 (Height of top flange is equal to 180 mm. The compression zone is indeed in the top flange).
But it should be checked whether the assumption that f_{pd} =0.95f_{pu} is correct. This is done by determining the increase in strain $\Delta\varepsilon_p$ in the prestressing steel at ULS.

$$\Delta\varepsilon_p = \frac{(d_p - x_u)}{x_u}.x_{cu}$$

Similarly, for longitudinal reinforcement the stress in steel at ULS ε_s can be expressed as

$$\varepsilon_s = \frac{(d_s - x_u)}{x_u}.x_{cu}$$

x_{cu} is the strain in concrete at ULS which is equal to 3.5‰

$\Delta\varepsilon_p$ = 24‰ and ε_s =9‰.

$\varepsilon_{p,total} = \varepsilon_{pm\infty} + \Delta\varepsilon_p$

$\varepsilon_{pm\infty} = \sigma_{pm\infty}/E_p$= 4‰ with E_p = 200 GPa

$\varepsilon_{p,total}$ = 4 + 24 = 28 ‰.

From this the stress in prestressing steel at ULS σ_{pd} can obtained using the stress strain relation of the prestressing steel.

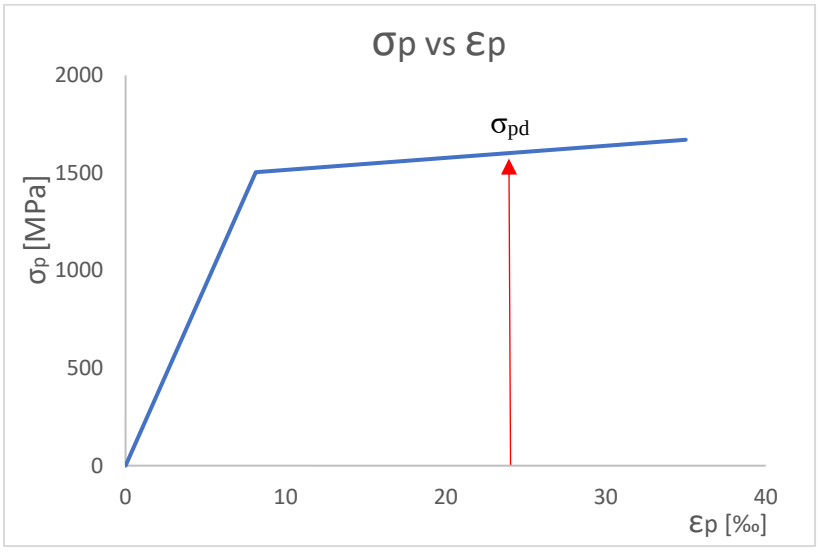

$$\sigma_{pd} = 1503 + \frac{(24-8)}{(35-8)}(1670 - 1503)$$

σ_{pd} = 1602 MPa.

1602 > 1522.85.

Repeat the calculation for x_u using f_{pd} = 1602 MPa. New x_u = 127.4 mm (Still in top flange).

Moment Resistance M_{Rd},

M_{Rd} can be calculated by taking moment equilibrium around a point in the cross-section. Taking moment equilibrium at position where the concrete compressive force acts.

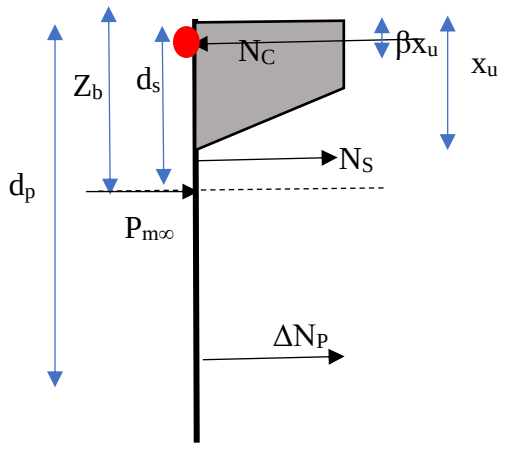

$M_{Rd} = \Delta N_P(d_p - \beta x_u) + P_{m\infty}(Z_b - \beta x_u) + N_s(d_s - \beta x_u)$
With β = 0.39 for normal strength concrete.
M_{Rd}=3724 kN-m

From the moment resistance, the bending load capacity $F_{bending}$ can be determined using simple calculations.

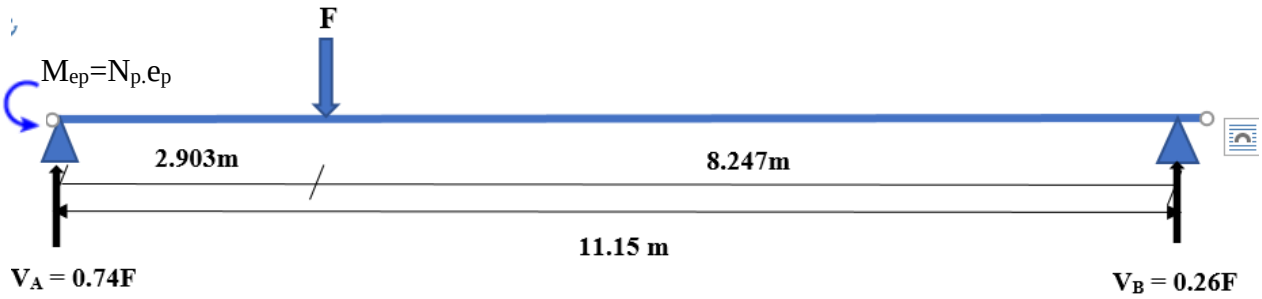

V_A.2.903 – M_{ep}= $M_{Rd,}$
M_{ep} is the concentrated moment due to eccentricity of the anchor position.
e_p is the tendon eccentricity with respect to the centroidal axis of the beam and is equal to 162.3 mm.
0.74$F_{bending}$2.903 – 2660x0.1623 = 3724.

$F_{bending}$ = 1935 kN is the flexural capacity of the post tensioned T beam.

2. Shear Capacity as per ACI Standards.

The Shear capacity of the post-tensioned T beam is calculated according to ACI standards.

Shear Capacity V_{Rd} = V_c + V_s, where V_c is the shear capacity of concrete and V_s is the shear capacity of the stirrups.

$$V_c = \min(V_{ci}, V_{cw})$$

Where V_{ci} is flexural shear capacity and given by

$$V_{ci} = 0.0498\sqrt{f_c}b_w d + \frac{V_u M_{ct}}{M_u}$$
$$V_{ci} \geq 0.141\sqrt{f_c}b_w d$$
$$M_{ct} = (\frac{I}{y_t})(0.498\sqrt{f_c} + f_{pe})$$

And V_{cw} is the capacity in shear tension given by

$$V_{cw} = \left(0.291\sqrt{f_c} + 0.3f_{pc}\right)b_w d_p + V_p$$

f_c is the concrete compressive strength, b_w is the thickness of the web, d is the effective depth, V_u is the shear force at a section, M_{ct} is the cracking moment resistance, M_u is the ultimate moment resistance, y_t is the distance to the centroidal axis from the extreme fibre in tension, f_{pe} is the compressive stress in concrete due to effective prestress force only (after allowance for all prestress losses) at extreme fiber of section where tensile stress is caused by externally applied loads.

f_{pc} is the compressive stress in concrete (after allowance for all prestress losses) at centroid of cross section resisting externally applied loads and V_p is the vertical component of the effective prestressing force.

To calculate the flexural shear capacity M_{ct} is to be calculated first.

$$M_{ct} = \left(\frac{1}{y_t}\right)\left(0.498\sqrt{f_c} + f_{pe}\right)$$

$$f_{pe} = -\frac{M_p Z_o}{I} - \frac{N_p}{A_c}$$

This needs to be calculated at the x = 1.725 m on the beam axis. At x= 1.725 M_p = 740 kN-m, N_p = 2660 kN, Z_o = 618 mm, I = 7.47.10^{10} mm^4, A_c = 517.10^3 mm^2.

f_{pe} = -11.3 MPa.

With f_c = 60 MPa, M_{ct} = 1832 kN-m.

Finally, V_{ci} = 1196 kN.

The capacity of the concrete in shear tension V_{cw} is also calculated

f_{pc} is calculated by considering the ultimate strength of the prestressing tendons $f_{pu,}$ which is equal to 1670 MPa and cross-sectional area A_c at x =1.725 m which is equal to 700.10^3 mm^2.

f_{pc} = 7.7 MPa and V_p = 160 kN.

The shear tension capacity of the concrete, V_{cw} = 1750 kN.

Therefore, $V_{ci} < V_{cw}$ and the **beam will fail in flexural shear** (the contribution of the stirrups will the be same for both failure modes).